NTNU

Norwegian University of
Science and Technology

Automated Optimization and Design of Mooring Systems for Deep Water

Kristine Ekeli Klingan

Marine Technology
Submission date: June 2016
Supervisor: Kjell Larsen, IMT

Norwegian University of Science and Technology
Department of Marine Technology

NTNU Trondheim
Norges teknisk-naturvitenskapelige universitet
Institutt for marin teknikk

MASTER THESIS SPRING 2016

for

Stud. tech. Kristine Ekeli Klingan

Automated Optimization and Design of Mooring Systems for Deep Water

Automatisert optimalisering og design av forankringssystemer for dypt vann

Background

The purpose of the mooring system is to keep a floating vessel safely at a required position. It normally consists of 8-16 mooring lines of heavy chain, steel wire ropes and/or synthetic polyester ropes connected to a seabed anchor.

During the past years, the requirements to the mooring and station keeping systems of mobile and permanent units have become more complex;
- The industry is moving into new frontiers (ultra-deep water down to 3000m depth and into arctic areas).
- There are more operations adjacent to other installations (floatel operations and tender support vessel operations).
- The new mobile units are becoming larger and many units are at the end of their lifetime.
- There are too many anchor line failures.

The overall objective of this thesis is to assess and perform automated optimization for ULS design of deep water mooring systems. The same "DEMO2000" semisubmersible unit as studied during the project work in the autumn 2015 shall be used as the floating structure.

Analysis methods for estimating ultimate mooring line tension and vessel offset can be divided into frequency domain (FD) methods and time domain (TD) methods. When using TD methods, all non-linearities in the dynamic system (stiffness and damping) and in the excitation may be taken into account. The result of TD simulations are time series of selected responses that must be carefully analysed by relevant statistical methods in order to establish a reliable estimate of the characteristic load effect. Simulations in the time domain shall be used as the basic method for the automated optimization.

Scope of Work

1) Review relevant literature for mooring systems and in particular time domain simulation of mooring systems and describe the theory related to coupled and separated analysis methodology. Describe the relevant simulation tools available in SIMA and how SIMA can effectively be utilized.

2) Establish and verify a time domain simulation model for the production semisubmersible in SIMA for use in SIMO and RIFLEX.

3) Theory related to automated optimization shall be studied and described based on relevant literature and papers. A recipe on how automated optimization can be performed when using the SIMA workbench shall be described.

4) Mooring systems based on steel components like chain and steel wire rope as well as a system based on chain and synthetic ropes (polyester) shall be optimized and compared. Sensitivity studies shall be carried out as agreed with the supervisor.

5) Quantify and compare the load effects of the selected mooring systems by comparing results from quasi-static analysis using SIMO with results from dynamic analysis using RIFLEX. The time domain results shall also be compared with results from frequency domain using MIMOSA

6) Conclusions and recommendations for further work.

General information

The work shall build on the project work report “Design and Optimization for Mooring Systems for Deep Water”. All necessary input files related to the “DEMO2000 semi” for the simulation case is assumed to be provided by Statoil/Marintek.

The work scope may prove to be larger than initially anticipated. Subject to approval from the supervisor, topics may be reduced in extent.

In the project the candidate shall present her personal contribution to the resolution of problems within the scope of work.

Theories and conclusions should be based on mathematical derivations and/or logic reasoning identifying the various steps in the deduction.

The candidate should utilise the existing possibilities for obtaining relevant literature.

Thesis report

The thesis report should be organised in a rational manner to give a clear exposition of results, assessments, and conclusions. The text should be brief and to the point, with a clear language. Telegraphic language should be avoided.

The report shall be written in English and edited as a research report including literature survey, description of relevant mathematical models together with numerical simulation results, discussion, conclusions and proposal for further work. List of symbols and acronyms, references and (optional) appendices shall also be included. All figures, tables and equations shall be numerated.

The original contribution of the candidate and material taken from other sources shall be clearly defined. Work from other sources shall be properly referenced using an acknowledged referencing system.

The report shall be submitted in two copies:

- Signed by the candidate
- The text defining the scope included
- In bound volume(s)
- Drawings and/or computer prints which cannot be bound should be organised in a separate folder.

Ownership

NTNU has according to the present rules the ownership of the project results. Any use of the project results has to be approved by NTNU (or external partner when this applies). The department has the right to use the results as if the work was carried out by a NTNU employee, if nothing else has been agreed in advance.

Thesis supervisor**:**

Prof. II Kjell Larsen, NTNU/Statoil

Co-supervisor : Vegard Aksnes, Sintef Marintek

Deadline: June 10th, 2016

Trondheim, June, 2016

Kjell Larsen (date and signature) : June 8th 2016 Kjell Larsen

Kristine Ekeli Klingan (date and signature): June 8th 2016 Kristine Klingan

Preface

This master thesis concludes the degree of Master of Science in marine technology at the Norwegian University of Science and Technology (NTNU). The thesis has been carried out in cooperation with Statoil and Marintek in the spring of 2016.

The topic is station keeping systems, with focus on use of automated optimization algorithms in the design process. The idea to this master thesis was provided by Professor II Kjell Larsen. The thesis work involves an optimization algorithm implemented in the simulation software SIMA developed by Marintek. This optimization algorithm is not yet commercialized, and the work done in this master thesis can be seen as a part of a pilot study.

The readers of this report are assumed to have some prior knowledge about hydrodynamics and marine structures in general. Concerning station keeping systems and automated optimization, the basic concepts are presented in the report.

Trondheim, 2016-06-10

Kristine Ekeli Klingan

Acknowledgment

I would like to thank Professor II Kjell Larsen, who has been my supervisor during the thesis work. He has taken great interest in teaching the theoretical background and scheduled weekly meetings. His enthusiasm has been a great inspiration throughout the whole thesis period. Statoil is acknowledged through Kjell Larsen for providing input files for the semisubmersible DEMO2000 and its mooring system.

I would also like to thank my co-supervisor Vegard Aksnes at Marintek for assisting with setting up the optimization problem in SIMA, and answering all questions related to the optimization algorithm throughout the thesis period. I also thank Pål Levold at Marintek for answering optimization related questions during Vegard Aksnes' leave of absence.

I also wish to thank the teaching assistant in SIMA, Xiaopeng Wu, for answering questions and assisting with SIMO and RIFLEX.

Lastly, I would like to thank Christine Krugerud and Jan Vidar Ulveseter for valuable discussions and insights throughout the thesis period, and my fellow students at office C1.076 for providing a good working environment.

K.E.K.

Abstract

This master thesis focuses on automated optimization of mooring systems at deep water. The optimization work is based on the mooring system of the deep draft semisubmersible DEMO2000 developed by Statoil. This is a semisubmersible with mooring system designed for 1500 m water depth. The automated optimization algorithm implemented in the simulation software SIMA, developed by Marintek, is used for the optimization. This automated optimization algorithm is not yet commercialized, and the work performed in this thesis can be seen as part of a pilot study.

Mathematically, optimization of a mooring system is the minimization of a cost function subjected to constraints on its variables. Hence, automated optimization algorithms refer to the application of mathematical search algorithms in this optimization process. A collection of optimization algorithms is available. SIMA however, uses a subsequential quadratic programming method algorithm called NLPQLP.

The optimization is carried out for a maximum design condition based on metocean data form the Heidrun field. The environment is applied in-line propagating from Northeast with a combination of wind, waves and current in accordance with the requirements for the Norwegian continental shelf.

The optimization problem for this thesis is defined based on a cost function, variables and constraints. The mooring line is constructed of three segments, for each of these segments the diameter and length is defined as variables. In addition, the pretension of the mooring line is set as a variable. This allows the anchor positions to change during the optimization. The cost function is based on the price of each mooring line segment, which again depends on length and diameter. Two constraints are included in the optimization. The first constraint concerns the safety factor of the most loaded mooring line, while the second restricts the maximum offset of the semisubmersible in the direction of the environmental loading. The optimization problem is formulated in terms of workflows in SIMA workbench, and the optimization is carried out in the time domain using SIMO.

Three optimization cases are defined. The first case is the base case that requires a safety factor of 2.2 and a maximum offset of 150 m. The second case requires a safety factor of 1.8 and a maximum offset of 150 m, while the third case requires a safety factor of 2.2 and a maximum offset of 75 m.

Two different mooring systems, based on the mooring system provided by Statoil, are optimized separately for all three cases. One mooring system is constructed of polyester rope and chain, while the other is constructed of steel wire rope and chain. The results of the optimization cases and relevant sensitivity studies show that the cost may be reduced significantly by use of the automated optimization algorithm.

For the polyester rope and chain mooring system, the constraint concerning safety factor is observed to dominate the optimization. The difference in cost for the first and third case is therefore small, while the cost for the second case is significantly lower. The second case does also provide the lowest cost for the steel wire rope and chain mooring system. However, both constraints influence the optimization of this system. The third case is therefore observed to result in much higher cost compared to the two other cases. Compared to the initial system the cost of the polyester rope and chain mooring system for the base case is reduced by 29.4 %, while the cost of the steel wire rope and chain mooring system for the base case is reduced by 19.3 % compared to the initial mooring system of this type. However, the polyester rope and chain mooring system is observed to provide the lowest cost.

As the optimization algorithm only consider the cost of the mooring system, the maximum and minimum values of the variables need to be chosen carefully. Both optimized mooring system tend to have unrealistic low pretension, which indicates that the minimum value for the pretension was too low. The chain segments are also very short for the optimized systems, as chain is the most expensive mooring line material included. Polyester rope and steel wire rope is therefore close to having contact with seafloor for the optimized mooring systems at maximum offset.

Dynamic analyzes of the tension in the most loaded line for both mooring systems are performed using RIFLEX. The top end motions calculated in SIMO are for these analyzes imported to RIFLEX. Analyzes of the mooring system in the frequency domain using MIMOSA is also performed. For the polyester rope and chain mooring system only small differences are observed for the quasi-static and dynamic analysis results. The dynamic effects are neglectable for this system as the elongation of the mooring line dominates the stiffness. The differences in the results of the analysis performed in time domain and in frequency domain is also very small, indicating that the linearization performed in the frequency domain analysis have close to no impact on the top end tension. For the steel wire rope and chain mooring system, large dynamic effects are observed. This is as expected as mooring lines in a catenary system will have a lot of lateral movement. The large water span will also influence these effects. Differences are also observed in the results from the calculation in the frequency domain and the time domain. Hence, the linearization in the frequency domain will affect the top tension remarkably.

Sammendrag

Denne masteroppgaven omhandler automatisert optimalisering av forankringssystemer på dypt vann. Optimaliseringsarbeidet er her basert på forankringssystemet til dypflyteren DEMO2000 utviklet av Statoil, som er designet for 1500 m vanndyp. Den automatiserte optimaliseringsalgoritmen implementert i analyseverktøyet SIMA, utviklet av Marintek, er brukt for å utføre optimaliseringen. Denne optimaliseringsalgoritmen er ikke kommersialisert av Marintek, og arbeidet utført i denne masteroppgaven kan derfor anses som del av et pilotprosjekt.

Matematisk vil optimalisering av forankringssystemer innebære å minimalisere en kostnadsfunksjon hvor variablene er utsatt for restriksjoner. Automatiserte optimaliseringsalgoritmer refererer derfor til bruk av matematiske søkealgoritmer i optimaliseringsprosessen. En rekke optimaliseringsalgoritmer er tilgjengelige. SIMA bruker en optimaliseringsalgoritme kalt NLPQLP.

Optimaliseringen i denne masteroppgaven er utført for et ekstremvær basert på data fra Heidrunfeltet. Dette ekstremværet er påført fra nordvest, inn på linene, med en kombinasjon av vind, bølger og strømning som samsvarer med kravene stilt for den norske kontinentalsokkelen.

Optimaliseringsproblemet er definert i form av en kostnadsfunksjon, variabler og restriksjoner. Hver forankringsline består av tre segmenter, hvor diameteren og lengden til hvert segment er definert som variabler. I tillegg er forspenningen i forankringslinen definert som variabel. Dermed kan posisjonen til ankrene endres underveis i optimaliseringen. Kostnadsfunksjonen er basert på kostnaden til hvert enkelt segment, som igjen vil avhenge av diameter og lengde av segmentet. To restriksjoner er definert i optimaliseringen. Den første omhandler sikkerhetsfaktoren til den mest belastede forankringslinen, mens den andre setter begrensning på den maksimale forflytningen av flyteren. Optimaliseringsproblemet er implementert i SIMA og utført i tidsplanet ved bruk av SIMO.

Tre optimaliseringscaser er definert. Den første casen, hovedcasen, krever en sikkerhetsfaktor på 2.2 og maksimal forflytning på 150 m. Den andre casen krever en sikkerhetsfaktor på 1.8 og maksimal forflytning på 150 m, mens den tredje krever en sikkerhetsfaktor på 2.2 og maksimal forflytning på 75 m.

To forankringssystemer er studert, begge basert på forankringssystemet tildelt fra Statoil. Disse forankringssystemene er optimalisert hver for seg for alle casene. Det ene forankringssystemet er satt sammen av polyestertau og kjetting, mens det andre er satt sammen av ståltau og kjetting. Resultatene viser at optimaliseringsalgoritmen kan redusere kostnaden til disse systemene drastisk.

Restriksjonen til sikkerhetsfaktoren dominerer optimaliseringen av polyestertau og kjetting systemet. Forskjellen

i kostnad for den første og tredje casen er derfor relativt liten, mens kostnaden for den andre casen er mye lavere. Den andre casen gir også den laveste kostnaden for ståltau og kjetting systemet. For dette systemet styrer begge restriksjonene optimaliseringen. Den tredje casen gir mye høyere kostnad sammenlignet med de to andre casene. Det optimaliserte polyestertau og kjetting systemet har en kostnad 29.4 % lavere enn det opprinnelige systemet av denne typen, mens kostnaden til ståltau og kjetting systemet er redusert med 19.3 % sammenlignet med det opprinnelige systemet av denne typen. Polyestertau og kjetting gir den rimeligste løsningen.

Optimaliseringsalgoritmen betrakter kun kostnaden til forankringssystemet. Øvre og nedre verdi for variablene må derfor velges nøye. Optimaliseringen utført for begge systemer i denne oppgaven gir veldig lave verdier for forspenning, noe som indikerer at nedre grense for forspenningen var noe lav i optimaliseringsoppsettet. Kjettingsegmentene i de optimaliserte systemene er korte, da kjetting er et kostbart materiale. Marginen for kontakt med havbunn for polyestertau og ståltau er derfor liten ved maksimal forflytning av flyteren.

Dynamisk analyse av strekket for den mest belastede linen for begge forankringssystemene er utført i RIFLEX. Bevegelsen beregnet i SIMO er her importert til RIFLEX. Analyser i frekvensplanet ved bruk av MIMOSA er også utført. Kun små forskjeller er observert for de kvasistatiske og dynamiske analysene for polyestertau og kjetting systemet. De dynamiske effektene er her neglisjerbare da stivheten til systemet er styrt av linens forlengelse. Det er også kun små forskjeller på analysene utført i tidsplanet og frekvensplanet. Dette indikerer at lineariseringene utført i frekvensplanet påvirker strekket lite. Analysene av ståltau og kjetting systemet viser at de dynamiske effektene har stor påvirkning her. Dette er som forventet da forankringslinene i dette systemet vil oppleve sideveis bevegelser. Den store vanndypden vil også innvirke på de dynamiske effektene. Forskjeller er også observert i resultatene for analyser utført i tidsplanet og frekvensplanet. Lineariseringen utført i frekvensplanet vil derfor påvirke strekket i stor grad for dette systemet.

Notation

Symbols

H_s	Significant wave height
T_p	Peak wave period
$U_{1hour,10m}$	Mean wave speed, over 1 hour averaging period 10 m above sea level
V_c	Surface current speed
M	Frequency-dependent mass matrix
A	Frequency-dependent added mass matrix
x	Position vector
C	Frequency-dependent potential damping matrix
D_l	Linear damping matrix
D_q	Quadratic damping matrix
K	Non-linear stiffness matrix
Q	Excitation force vector
k_T	Total stiffness
k_G	Geometric stiffness
k_E	Elastic stiffness
T	Top end tension
E	Elastic modulus
A	Cross section area
L	Length of mooring line
q_{wi}	Wind forces
q_{cu}	Current forces
q_{wa}	Wave forces
$H^{(1)}(\omega)$	First order transfer function
ζ	Harmonic wave component

T_{QS}	Quasi-static top end tension
T_{dyn}	Dynamic top end tension
$\overline{x}$	Mean displacement
x_{LF}	Low frequency motion
x_{WF}	Wave frequency motion
ρ	Water density
g	Gravitational acceleration

Abbreviations

MODU	Mobile offshore drilling unit
FPSO	Floating production storage and offloading
HMPE	High modulus polyethylene
ULS	Ultimate limit state
ALS	Accidental limit state
FLS	Fatigue limit state
MBL	Minimum breaking load
SF	Safety factor
NCS	Norwegian continental shelf
ISO	International Organization for Standardization
FD	Frequency domain
TD	Time domain
WF	Wave frequency
LF	Low frequency
FEM	Finite element method
SQP	Subsequential quadratic programming
HSE	Health, safety and environment
DAF	Dynamic amplification factor

Contents

List of Figures

List of Tables

Chapter 1

Introduction

1.1 Background

A mooring system is applied in order to keep a floating vessel safely at a required position. The configuration of a mooring system depends on both the water depth and the environmental loads at the location. Typically, a mooring system consists of 8-16 mooring lines constructed of chain, steel wire rope and/or synthetic fiber ropes connected to anchors at the seabed.

The complexity of requirements to mooring systems of mobile and permanent units has increased the last years as a consequence of several factors:

- New frontiers in the industry are explored, including ultra-deep water and arctic areas
- Operations adjacent to other installations become more common
- Mobile units are becoming larger, and many units are at the end of their lifetime
- A large amount of mooring line failures occur

As a consequence of this advance in the design of mooring systems, more complicated rules and a tendency to increase utilization, the engineering process for mooring systems has become more complicated and cumbersome. Automated optimization algorithms, referring to the application of mathematical search algorithms in the optimization process, may in the optimization of a mooring system contribute with considerable gains (I. J. Fylling, 2013).

1.2 Objectives

The scope of work form the following main objectives for this master thesis:

1. Present time domain simulation of mooring systems and describe the theory related to the coupled and separated analysis methodology. Present the relevant simulation tools available in SIMA, and describe how SIMA effectively can be utilized.
2. Establish and verify a time domain simulation model for a production semisubmersible in SIMA for use in SIMO and RIFLEX.
3. Present theory related to automated optimization, and describe how automated optimization can be performed when using SIMA workbench.
4. Optimization shall be carried out for two different mooring systems, one based on steel components

like chain and steel wire rope and one based on chain an synthetic ropes. Relevant sensitivity studies shall be carried out. The results for these optimizations shall be compared.
5. The load effects of the selected mooring systems shall be quantified and compared using results from quasi-static analysis performed in SIMO and results from dynamic analysis performed in RIFLEX.
6. Conclusions and recommendations for further work shall be presented.

1.3 Literature Survey

The general mooring system theory in this master thesis is to a large extent based on rules and regulations, and lecture notes in the course *TMR4225 Marine Operations*. The course material from *TMR4225 Marine Operations* cover a large amount of, and briefly described, the basic mooring system theory presented in this master thesis. The rules and regulations provided a more detailed description of these topics.

The optimization theory is mainly based on papers by Klaus Schittkowski and Ivar J. Fylling, and SIMA User's Manual. Papers by Klaus Schittkowski have been used to cover the general optimization theory, while papers by Ivar J. Fylling describe automated optimization applied on mooring systems. SIMA User's Manual specifies how optimization is performed in SIMO.

Several other papers have also been visited in order to cover all topics described in this master thesis.

1.4 Limitations

The optimization is limited to only consider the segment diameters, segment lengths and the pretension of the mooring lines. Cost of other hardware components is here excluded as a simplification. Installation cost is not emphasized for the optimization, only a brief discussion regarding this aspect is included.

The time domain analysis performed in RIFLEX is based on the separated approach. There are some shortcomings of this approach compared to the coupled approach, especially for deep water.

For the comparison of the top end tension of the most loaded mooring line, only one realization of the time domain analysis is studied. This affects the comparison of the time domain and frequency domain results.

1.5 Approach

The first objective is met through a literature study of the listed references. Theory for mooring systems presented in the course *TMR4225 Marine Operations* has generally been an important source. Relevant papers in addition to different rules and regulations have also been studied. The theory manual of SIMO has carefully been read in order to describe the time domain analysis.

The second objective was met by importing the simulation model used in the project thesis into SIMA. The model data concerning hydrostatic stiffness, natural periods, damping and excitation forces was evaluated. The results from SIMO were also compared to the results from the software MIMOSA, used in the project thesis, as part of the verification.

The third objective, concerning automated optimization algorithms, are studied and described based on relevant papers. The description of how to perform optimization using SIMA workbench is based on SIMA User's Manual and own experiences.

The fourth objective was approached by using the optimization algorithm included in SIMA workbench. Two mooring systems were created as initial systems for the optimization. The polyester rope and chain mooring system was based on the mooring system provided by Statoil, and the steel wire rope and chain mooring system was created in cooperation with the supervisor. Guidance from Marintek was here provided in order to carry out the optimization correctly.

The fifth objective was carried out by converting the mooring system from SIMO into RIFLEX. The motions of the semisubmersible calculated in SIMO were imported into RIFLEX, and separated analyzes were performed for the selected mooring systems. The dynamic mooring line tensions calculated in RIFLEX were compared to the quasi-static mooring line tensions calculated in SIMO. A comparison of quasi-static and dynamic mooring line tensions calculated in MIMOSA was also included.

The last objective has been met by evaluating the work performed in this master thesis.

1.6 Structure of the Report

The rest of the report is organized as follows:

Chapter 2 gives an introduction to station keeping systems. Main hardware components in terms of mooring line materials and anchoring types are presented. The chapter is included from the project thesis as it is relevant for the work performed in the master thesis.

Chapter 3 presents the design considerations for a mooring system. The design limit states defined in rules and regulations, with corresponding acceptance criteria, are here described. Environmental criteria in terms of maximum design condition and maximum operation condition are also presented in this chapter. The chapter is included from the project thesis as it is relevant for the work performed in the master thesis.

Chapter 4 focuses on time domain simulation of mooring systems. The equation of motion is here presented, and the terms in the equation are described. Coupled and separated analysis methodology is presented and described. Mooring line response in terms of quasi-static and dynamic analysis is also presented here. The last part of this chapter describes relevant simulation tools in SIMA.

Chapter 5 focuses on the concept of automated optimization algorithms. The specification of the optimization problem for mooring systems is here described in terms of objective function, variables and constraints. The last part of the chapter describes how automated optimization could be performed in SIMA workbench.

Chapter 6 presents the model used for the simulations performed in this master thesis. The design environment for the simulations is also presented in this here.

Chapter 7 contains the optimization case. The optimization problem is here defined in terms of objective function, variables and constraints. The arrangement of the optimization in SIMA workbench is also presented here. The optimization results are presented, compared and discussed in this chapter.

Chapter 8 presents dynamic analysis of the most loaded mooring line performed in RIFLEX. A comparison of the top end tension of the most loaded mooring line calculated in SIMO, RIFLEX and MIMOSA is here carried out.

Chapter 9 gives the conclusions of this master thesis. Recommendation of further work is also presented here.

Chapter 2

Station Keeping Systems

In marine operations, an important aspect is to ensure a precise position and motion control of a floating structure. This is desirable in order to for instance maintain integrity of risers and umbilicals, and to maintain safe distance to other structures. Different types of station keeping principles are used in order to withstand the environmental forces on the floating structure arising from wind, waves and current (O. M. Faltinsen, 1990).

The main categories of station keeping systems are (K. Larsen, 2015):

- Moored system - positioning by use of mooring lines
- Thruster-assisted mooring system - positioning by use of mooring lines, thrusters and propellers
- Dynamic positioning system - positioning by use of thrusters and propellers

These systems are used for different designs and optimization, depending on cost and accuracy requirements. This master thesis focuses on moored systems.

2.1 Station Keeping Principles

The main purpose of a mooring system is to limit the horizontal offset. The system is composed of a number of mooring lines that are oriented in a desired configuration and attached to the floating structure in the upper end. The lower end of the mooring lines are attached to the sea bed with anchors (O. M. Faltinsen, 1990).

Generally, mooring systems can be divided into two categories; permanent and mobile mooring systems. Permanent moorings are normally used for production operations with longer design lives. These systems are typically designed for one specific location and purpose, and are normally applicable for production and storage units. Mobile mooring systems are designed for use at several different locations throughout its lifetime, where the stay at each location can vary from a few days to five years (DNV GL, 2012). Examples of mobile moorings include moorings for mobile offshore drilling units (MODU) and for tenders moored next to another structure, such as floatels, drilling tender and service vessels.

The station keeping system of a vessel is typically either a turret mooring or a spread mooring. Turret mooring is commonly used for ship shaped vessels, while spread moorings are mostly used for semisubmersibles

and spars (API Recommended Practice, 2005).

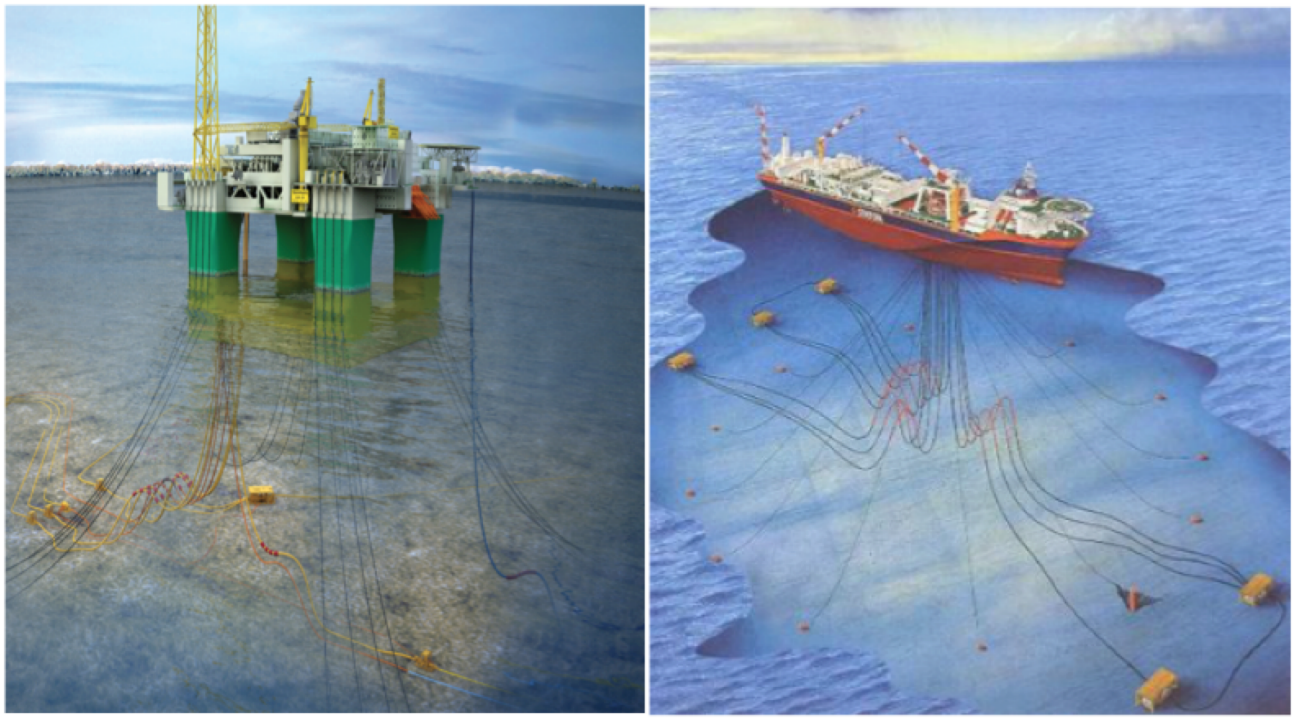

(a) Catenary moored semisubmersible (Aker Solutions)

(b) Turret moored FPSO (K. Larsen, 2015)

Figure 2.1: Spread and turret mooring.

A spread mooring system consists of groups of mooring lines terminated at the corners of the moored structure, ensuring a stable heading. Figure 2.1(a) presents a catenary spread moored semisubmersible. As both semisubmersibles and spars are relatively insensitive to the direction of the environmental force, a spread mooring system can be designed to hold the structure at position regardless of the direction of the environment (API Recommended Practice, 2005).

Turret moorings are primarily used for ships, as the turret moored Norne floating production storage and offloading (FPSO) unit presented in Figure 2.1(b). These mooring systems allow the vessel to weathervane, which is necessary in order to minimize the environmental loads on the ship by heading into the prevailing weather. The turret mooring system consists of a turret with several mooring lines attached, allowing the vessel to rotate about the mooring lines. The turret can be mounted externally in vessel bow or stern, or internally within the vessel. The chain table can be placed above or below the waterline.

2.2 Mooring Hardware Components

Mooring hardware components include the mooring line, mooring line components and anchor. The mooring line in terms of chain, steel wire rope and polyester is presented in the following. A brief introduction of the mooring line components and anchor types is also included.

2.2.1 Mooring Line

Mooring lines may be made up of chain, wire rope, synthetic rope, or a combination of these. Different combinations of line type, size, and location and size of clump weights or buoys are utilized in order to achieve given requirements for the mooring performance (API Recommended Practice, 2005).

Chain

Chain is the most commonly used material for mooring lines, and is available in different diameters and grades. The chain provides large weight and high stiffness, in addition to good abrasion characteristics (Vryhof Anchors, 2015).

There are primary two different designs of chain; studless and studlink chain. The studlink chain is commonly used for floating structures that is reset numerous times during their lifetime. The stud provides stability to the link, resulting in a chain that is strong, reliable and relatively easy to handle (S. Chakrabarti, 2005).

The studless chain is commonly used for permanent moored structures. Removing the stud reduces the weight per unit of strength and increases the chain fatigue life. However, this type of chain is more expensive and less convenient to handle (S. Chakrabarti, 2005).

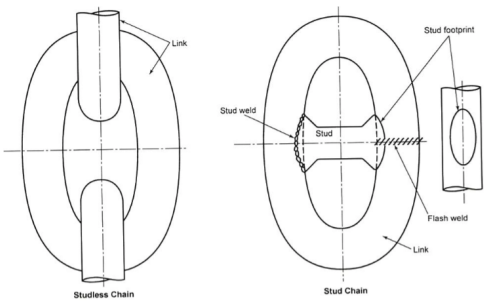

Figure 2.2: Studlink and studless chain (API Recommended Practice, 2005).

Figure 2.2 presents a schematic of studlink and studless chain, respectively. The specifications of the chain properties are important for the design of the mooring system. Different grades of chain are available on the marked, where chain of grade 4 is the highest grade available (S. Chakrabarti, 2005).

Steel Wire Rope

Steel wire rope has a lower weight than chain, but approximately the same breaking strength and higher elasticity (Vryhof Anchors, 2015).

The wire rope constructions consist of multiple wire strands wound in a helical pattern around a center core to form a rope. Figure 2.3 presents various constructions of wire rope (API Recommended Practice, 2005).

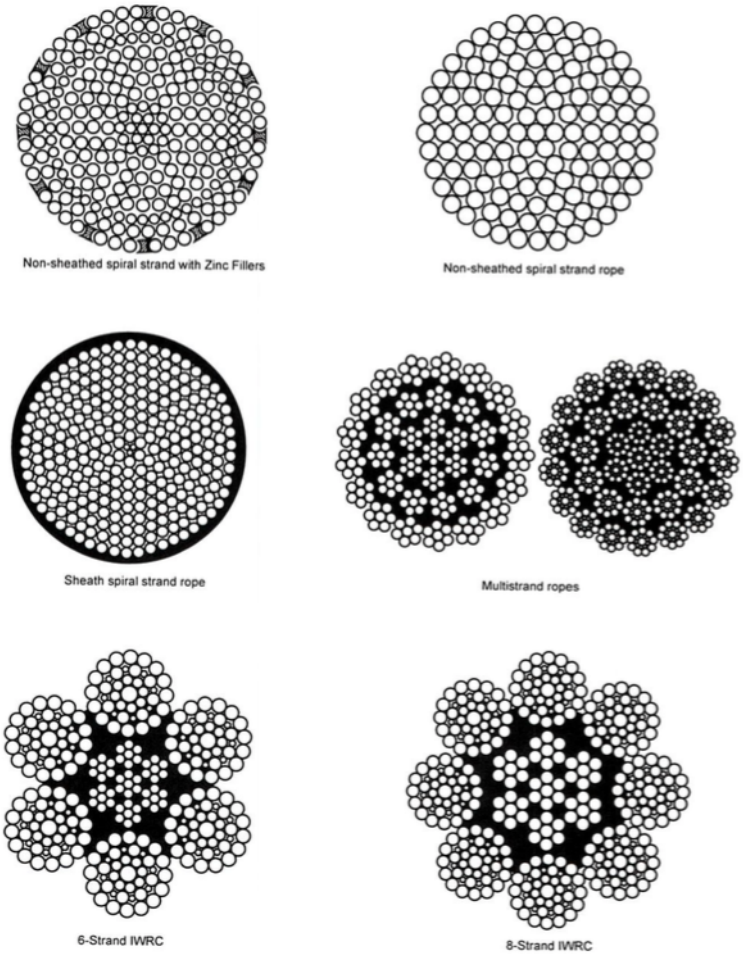

Figure 2.3: Typical wire rope constructions (API Recommended Practice, 2005).

As six-strand wire rope is easy to handle and is, along with studlink chain, commonly used in temporary mooring, for example for a MODU. The six-strand ropes are the most common type of multi-strand ropes used in the offshore industry. To achieve higher strength the wires have staggered sizes (S. Chakrabarti, 2005).

The number of strands and wires in each stand, core design and lay of strands is critical for the required strength and bending fatigue considerations of the wire rope (API Recommended Practice, 2005). The multi-strand wire ropes may contain either a fiber or metallic core. This core provides support to the outer wires, especially in a drum, and may in some applications absorb shock loading. Metallic core ropes can be divided into two types; independent wire rope core and wire-strand core. Independent wire rope core is the most common core for heavy marine applications. The fiber core is used in lighter marine applications (S. Chakrabarti, 2005).

Single-strand ropes are commonly used in permanent mooring systems. The wires are here wound as a helix with each layer rapped in a different direction, providing torque balancing which prevent the rope from twisting as load is applied. This spiral strand is more fatigue resistant than the multi-strand wire rope. Sheathing with a polyurethane coating, adding zinc filler wires or using galvanized wires is commonly used to enhance the corrosion resistance. However, sheathing provides the best performance, provided that there is no damage to the sheath (S. Chakrabarti, 2005).

The weight of the wire rope makes it suitable for use in the water span (Vryhof Anchors, 2015).

Synthetic Fiber Ropes

Fiber ropes may be used as a segment in catenary or taut mooring systems. The differences between a fiber rope system and wire rope/chain systems include primarily the non-linear stiffness, a minimum tension requirement and that the location of the fiber rope segment needs to be away from the fairlead and the seafloor. In addition, unlike the steel components the fiber rope stiffness increases with mean load and decreases with cyclic load range and with load relief over time (API Recommended Practice, 2005).

Fiber ropes for use in permanent or temporary mooring systems normally consist of polyester, aramid, high modulus polyethylene (HMPE) or nylon. Polyester is considered as a good candidate for mooring applications due to its low cost, low stiffness which induces less dynamic tension, good fatigue properties, good strength to weight ratio and good creep resistance (API Recommended Practice, 2005).

Fiber materials as HMPE and aramid are considered suitable for applications where a small rope diameter is required or for ultra deep water mooring applications. In shallow water, nylon rope is often installed in the mooring line to absorb energy from the dynamics of the moored structure, due to its high elasticity (API Recommended Practice, 2005).

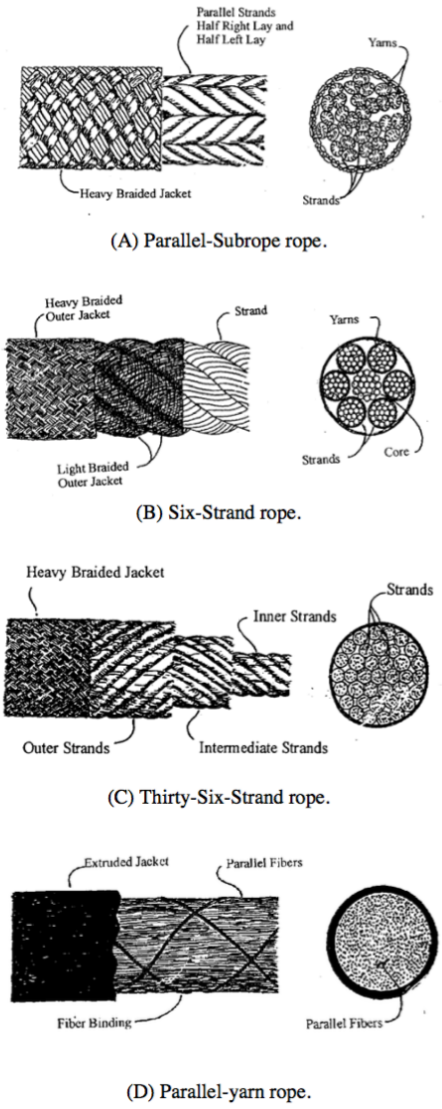

Figure 2.4: Types of synthetic fiber ropes (DNV GL, 2013).

Several different types of fiber rope construction exist, where the two most common types is wire-rope construction and parallel strand. Jacketing of the ropes is used to strengthen the resistance to abrasion. In addition, jacketing may in some cases keep the strength core strands together and protect against soil ingress, marine growth and fish bite (API Recommended Practice, 2005).

The fiber rope is typically torque balanced. However, a torque matched rope may be used in connection with

a mooring component that is not torque free, such as a six-strand wire rope (API Recommended Practice, 2005).

Factors that may limit the life of fiber ropes with respect to mooring applications include hydrolysis, heating and internal abrasion, tension-tension fatigue, axial compressive fatigue and creep rapture (API Recommended Practice, 2005).

2.2.2 Mooring Line Components

A mooring line is usually constructed of a large number of identical components of a few types.

Main mooring line components are:

- Termination hardware
- Connecting hardware
- Clump weights
- Spring buoys

Termination hardware is used to end a segment. Different types of termination hardware terminate different types of mooring line segment compositions (DNV GL, 2012).

Connecting hardware is used to connect sections of chain to one another, chain to wire rope and connect to padeyes on anchors or the vessel. Several different types of connectors are available, depending on mooring line segment composition.

Clump weights or spring buoys may be incorporated on the mooring line in order to improve its performance or cost. Clump weights may replace a portion of chain and increase the restoring force of the mooring line, while spring buoys may reduce the weight of the mooring lines supported by the hull (API Recommended Practice, 2005).

2.2.3 Anchoring Types

The choice of anchor is mainly determined by the water depth, the soil behavior and the loads the anchor needs to withstand, in addition to installation method and cost.

Figure 2.5 presents the most typical anchor types, ranged by water depth (shallow to ultra deep) and soil type (hard to soft soil).

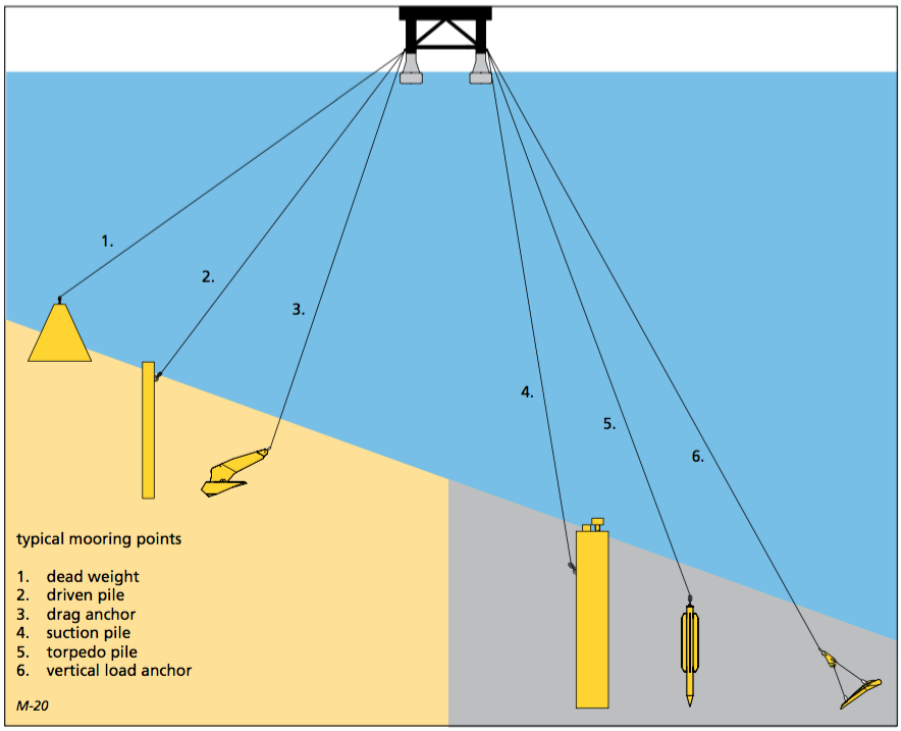

Figure 2.5: Typical anchor types ranged by water depth and soil type (Vryhof Anchors, 2015).

The main anchor types, ranged by water depth and soil type, are:

1. Dead weight anchor
2. Pile anchor
3. Drag embedment anchor
4. Suction anchor
5. Dynamically installed anchor
6. Vertical load anchor

A dead weight anchor typically consists of steel and concrete. The horizontal and vertical load capacity depends on the anchor submerged weight and the friction between soil and anchor, respectively. It may be used for small mooring systems, but is normally not used for deep water mooring systems (API Recommended Practice, 2005).

A pile anchor is a hollow steel cylinder installed by use of a pile hammer or vibrator. The anchor is able to withstand both horizontal and vertical loads. The capacity of this anchor is dependent on the friction of the soil along the pile and the lateral soil resistance (Vryhof Anchors, 2015).

Drag embedment anchors include both fluke anchors and plate anchors. Installation is performed by drag-

ging the anchor into the seabed. The anchor is well suited to withstand horizontal loads. The capacity of the anchor is dependent on size and angle of the fluke or plate, the ability to penetrate and the geotechnical conditions of the installation area (Vryhof Anchors, 2015).

The suction anchor also consists of a hollow cylinder and is similar to the pile anchor, although with a much lager diameter. The anchor withstands both horizontal and vertical loads, and the capacity of is dependent on the friction of the soil along the cylinder wall and the lateral soil resistance. These anchors can be accurately positioned and are commonly used for mooring at deep water (G. T. Houlsby and B. W. Byrne, 2004).

Dynamically installed anchors include both deep penetrating anchors and torpedo anchors, and are designed to penetrate deep into the seabed. There are no orientation requirements on the loading for this anchor (Deep Sea Anchors).

Vertical load anchors are installed in the same way as a drag embedment anchor, but the penetration depth is much larger. The anchor can withstand both horizontal and vertical loads, and is suited for deep water mooring applications (Vryhof Anchors, 2015).

Chapter 3

Design Considerations

The design consideration associated with a mooring system includes design criteria, design loads, design life, operation and maintenance considerations. In the following the design criteria with respect to the design limit states and the design loads with respect to the environmental criteria are described.

3.1 Design Limit States

The design criteria are formulated in terms of three limit states - ultimate limit state (ULS), accidental limit state (ALS) and fatigue limit state (FLS). DNV Offshore Standard (DNV GL, 2013) defines the limit states as following:

- *An ultimate limit state to ensure that the individual mooring lines have adequate strength to withstand the load effects imposed by extreme environmental actions.*
- *An accidental limit state to ensure that the mooring system has adequate capacity to withstand the failure of one mooring line, failure of one thruster or one failure in the thruster's control or power systems for unknown reasons. A single failure in the control or power systems may cause that several thrusters are not working.*
- *A fatigue limit state to ensure that the individual mooring lines have adequate capacity to withstand cyclic loading.*

Analysis of the mooring system shall be performed in accordance with these three limit states. The mooring line design for permanent mooring must satisfy all three limit states (DNV GL, 2013).

3.1.1 Ultimate and Accidental Limit State

The ULS requires that the mooring lines shall resist all known loads with a sufficient margin, and states that a design against overload of an intact mooring system in extreme weather shall be conducted.

The ALS requires that an accidental event shall not develop into progressive collapse, hence a design against overload for a damaged system in extreme weather conditions shall be performed. A damaged system is considered as a system where one or two line failures have occurred.

The ULS and ALS are both formulated as design equations at the form

$$\text{Design capacity} \geq \text{Design load} \tag{3.1}$$

which may be written as

$$\text{MBL} \geq F_{\text{MPM}} \cdot \text{SF} \tag{3.2}$$

where MBL is the minimum breaking load, F_{MPM} is the most probable maximum tension of a sea state of three hour duration in a 100-year condition and SF is the safety factor (K. Larsen, 2015).

The safety factors for the Norwegian continental shelf (NCS) are given by International Organization for Standardization (ISO). Different safety factors are applied for permanent and mobile mooring systems, as presented in Table 3.1 and 3.2. In addition, safety factors are given for three different consequence classes (ISO Standards, 2013).

	Consequence class		
	Class 3	Class 2	Class 1
Analysis	Dynamic	Dynamic	Dynamic
Intact condition	2.20	2.00	1.50
One failure	1.50	1.35	1.20
One failure, transient	1.10	1.10	1.05
Two failures	1.50	1.35	N/A
Two failures, transient	1.10	1.10	N/A

Table 3.1: Safety factors for tension in mooring lines for permanent moorings (ISO Standards, 2013).

	Consequence class		
	Class 3	Class 2	Class 1
Analysis	Dynamic	Dynamic	Dynamic
Intact condition	1.90	1.80	1.50
One failure	1.30	1.20	1.10
One failure, transient	1.10	1.10	1.05

Table 3.2: Safety factors for tension in mooring lines for mobile moorings (ISO Standards, 2013).

In Table 3.1 and 3.2, transient refers to a condition where the system is not yet stabilized after a line breakage.

The consequence classes are given as Class 1, Class 2 and Class 3. For a permanent mooring system, Class 3 refers to a system in production, where the consequences of a failure would be most severe. Class 2 refers to a system where the production is stopped, and Class 1 refers to a system where production is stopped and all risers and/or other production equipment are disconnected. Thus, a failure in Class 1 would unlikely lead to

unacceptable consequences. For production units on the NCS Class 3 is in general fulfilled, as production is desired at all times.

For a mobile mooring system, Class 3 refers to a unit in operation, for instance a drilling unit performing drilling. For Class 2 the operation is stopped, as for a drilling unit this will be the case when marine riser still is connected to the blow-out preventer while the drill string is removed. Class 1 refers to the condition when the operation is stopped, operation equipment is removed and the moored structure is moved a safe distance away from other structures. A 100-year environmental condition is generally only performed for Class 1 for a mobile mooring. Class 3 is analyzed for a maximum operational condition.

Fulfillment of ULS is required for both permanent and mobile mooring systems. However, the safety factors for mobile moorings are lower than for permanent moorings.

The ALS for permanent moorings require fulfillment for one and two mooring line failures, while only one mooring line failure is required for mobile mooring systems. In addition, also here the safety factor is somewhat lower for the mobile moorings compared with permanent moorings.

Failure of two mooring lines for permanent mooring systems are in accordance with (ISO Standards, 2013) analyzed with an environmental condition with return period of 10 years. Hence, 10-years waves, 10-years wind and 1-year current are in this case used.

3.1.2 Fatigue Limit State

The FLS requires that the safety margin against fatigue failure shall be acceptable. The mooring system shall thus be designed against fatigue failure, taking all possible sea states into account (K. Larsen, 2015).

In order to consider the FLS, a wide range of environmental conditions is needed. The following description of the properties, analysis and fatigue safety factor is based on (DNV GL, 2013).

The fatigue damage, D, in mooring line components are accumulated by cyclic loading, and summed up from the fatigue damage arising from environmental states combined to simulate the long term environment that the mooring system is exposed to

$$D = \sum_{i=1}^{n} d_i \tag{3.3}$$

where d_i is the fatigue damage to the component arising in sea state i and defined as

$$d_i = n_i \int_0^{\infty} \frac{f_{Si}(s)}{n_c(s)} ds \tag{3.4}$$

where n_i is the number of stress cycles encountered in sea state i, $f_{Si}(s)$ is the probability density of stress

cycles in sea state i and $n_c(s)$ is the number of stress cycles leading to failure. The number of stress cycles in sea state i is defined as

$$n_i = N \cdot P_i \tag{3.5}$$

where N is the total number of stress cycles during the entire lifetime and P_i is the probability of occurrence of sea state i.

The capacity of a component is described by the S-N curve

$$n_c = a_D s^{-m} \tag{3.6}$$

where a_D and m are parameters of the S-N curve dependent on the mooring line composition. Figure 3.1 presents S-N curves for different mooring line compositions.

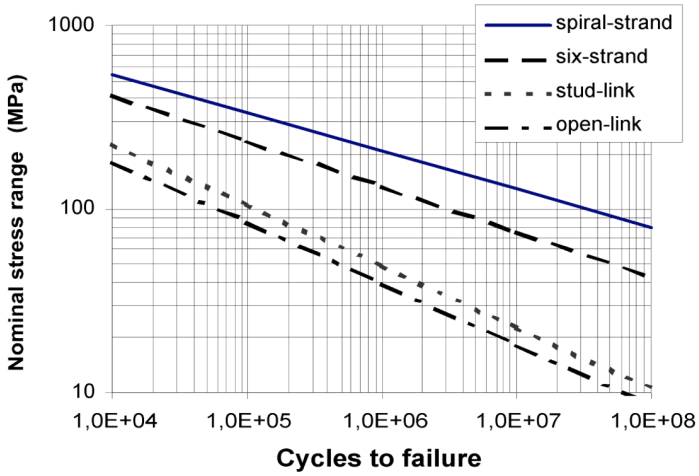

Figure 3.1: Design S-N curves (DNV GL, 2013).

Fatigue analysis is generally performed by frequency domain method, where both wave frequency tension cycles and low frequency tension cycles are taken into account. The fatigue damage in the environmental state i is determined by

$$d_i = \frac{n_i}{a_D} E[S_i^m] \tag{3.7}$$

where $E[S_i^m]$ is the expected value of the nominal stress ranges raised to the power m in environmental state i. If the low frequency content of the stress process is neglectable, a narrow-banded assumption can be applied. Fatigue damage in environmental state i then becomes

$$d_{NBi} = \frac{\nu_{0i} T_i}{a_D} (2\sqrt{2}\sigma_{Si})^m \Gamma(\frac{m}{2} + 1) \tag{3.8}$$

where σ_{Si} is the standard deviation of the stress process, $\Gamma()$ is the gamma function, υ_{0i} is the mean-up-crossing rate of the tension process and T_i is the duration of the environmental condition.

The intent of the fatigue limit state is to ensure sustainable resistance to fatigue failure of each type of component in an individual mooring line. The design equation for FLS is given as

$$1 - d_c \cdot \gamma_F \geq 0 \tag{3.9}$$

where d_c is the characteristic fatigue damage accumulated as a result of cyclic loading during the design life time, and γ_F is the single safety factor for the fatigue limit state.

In the fatigue analysis, the fatigue safety factor shall cover a range of uncertainties. For mooring lines that are not regularly inspected, the safety factor is thus given as

$$\begin{gathered} \gamma_F = 5 \quad if \quad d_F \leq 0.8 \\ \gamma_F = 5 + 3(\frac{d_f - 0.8}{0.2}) \quad if \quad d_F > 0.8 \end{gathered} \tag{3.10}$$

where d_F is the adjacent fatigue damage ratio. The ratio between the characteristic fatigue damage d_c in two adjacent lines taken as the lesser damage divided by the greater damage.

3.2 Environmental Criteria

There are mainly two classifications of environmental conditions when evaluating a mooring system; maximum design condition and maximum operation condition.

3.2.1 Maximum Design Condition

The maximum design condition is described by the combination of waves, wind and current for which the mooring system is designed. This condition is defined as extreme combinations of wind, waves and current causing an extreme load in the design environment (API Recommended Practice, 2005). The environmental effects applied for the calculations of design limit states, presented in section 3.1, should include the most severe combinations of waves, wind and current with a return period of no less than 100 years for the combination. The most severe conditions are those leading to the most extreme mooring loads. In order to determine the most unfavorable conditions, both intensity and directions of the environmental effect are of importance (DNV GL, 2013).

The environmental loads are specified in terms of (DNV GL, 2013):

- Significant wave height (H_s)
- Peak wave period (T_p)
- Wave spectrum
- Wave energy distribution
- Main wave direction
- Mean wind speed, over a 1 hour averaging period 10 m above sea level ($U_{1hour,10m}$)
- Wind spectrum function
- Wind direction
- Surface current speed (V_c)
- Current profile over depth
- Current direction

In order to obtain a 100-year design environment, different sets of conditions are investigated. In accordance with (ISO Standards, 2013), waves of a sea state with return period of 100 years should normally be used. These wave conditions shall include different combinations of significant wave heights and peak periods. In addition, the mean wind speed 10 m above the water surface with a 100-year return period and a surface current speed with a 10-year return period should be applied. Both wind and current should be based on the marginal distribution of the wind and current speeds at the specific location, respectively (DNV GL, 2013).

For all moorings at the NCS, both permanent mooring and mooring of mobile floating units, the maximum design environment with return period of 100 year is required (ISO Standards, 2013). However, for structures dominated by low frequency motions, special considerations should be made. As the low frequency motions increase with decreasing wave period, the 100-year waves may not represent the severe mooring loads. Environmental conditions consisting of lower waves with shorter periods should then also be included as these causes larger low frequency motions and thus conceivable higher mooring loads (API Recommended Practice, 2005).

3.2.2 Maximum Operation Condition

The maximum operating condition is defined as the combination of waves, wind and current in which the unit is capable of continue to work, including for instance to drill, produce, offload or maintain gangway connection. This condition shall not exceed the maximum design condition (API Recommended Practice, 2005).

Chapter 4

Time Domain Simulation

Mooring analysis is performed in order to predict the extreme responses including line tensions, anchor loads and the offset of a floating structure under the design environment. The responses are compared with allowable values, as presented in Chapter 3, to ensure adequate strength of the system against overloading and acceptable clearance to avoid interference with other structures (API Recommended Practice, 2005).

Generally, there are two different methods to predict the dynamic responses of a floating structure; frequency domain (FD) method and time domain (TD) method.

The FD method describes the stochastic process through an energy spectrum. The energy spectrum represents the energy of the stochastic process as a function of frequency. This provides a complete description of the Gaussian process' statistical properties, including standard deviation, zero up-crossing period and extreme values. Given that the spectral moments can be calculated accurately, the statistical parameters may be computed without any statistical uncertainty (C. M. Larsen, 2014). The method depends on the linear principle of superposition. All non-linearities are here eliminated, either by direct linearization or by an iterative linearization (API Recommended Practice, 2005). The FD method was covered in detail in the project thesis.

The time domain method describes the stochastic process through a realization of the response. Time histories of all main response parameters are obtained from the simulation, and the resulting time histories are processed statistically to yield the extreme values. Thus, the time domain simulation should be long enough to obtain stable statistical values (ISO Standards, 2013). The time domain method take into account all the non-linear effects, and implies recalculation of each mass term, damping term, stiffness term and load at each time step. Thus this is a complex and time consuming computation (API Recommended Practice, 2005). The TD method will be covered in detail in the following.

4.1 Equation of Motion

The vessel motions at the top end is the governing excitation mechanism for the mooring line loading, as shown in Figure 4.1.

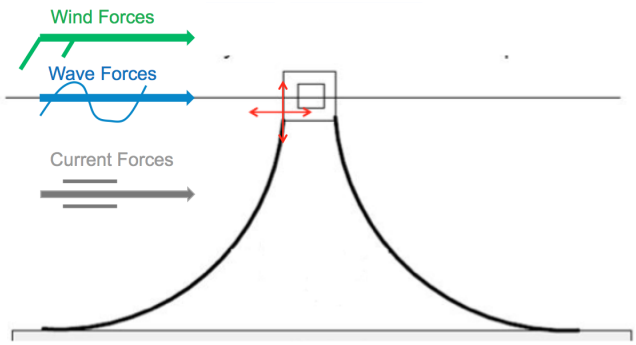

Figure 4.1: Top end motion of mooring line (K. Larsen, 2015).

Hence, it is desirable to estimate the motions in the top end of the mooring system. In order to find these motions, the motion equation in six degrees of freedom (d.o.f), presented in equation 4.1, needs to be solved

$$(M + A(\omega))\ddot{x} + C(\omega)\dot{x} + D_l\dot{x} + D_q\dot{x}|\dot{x}| + K(x)x = Q(t, x, \dot{x}) \tag{4.1}$$

where

M = frequency-dependent mass matrix
$A(\omega)$ = frequency-dependent added mass matrix
x = position vector
$C(\omega)$ = frequency-dependent potential damping matrix
D_l = linear damping matrix
D_q = quadratic damping matrix
$K(x)$ = non-linear stiffness matrix
$Q(t, x, \dot{x})$ = excitation force vector

4.1.1 Stiffness

The restoring force, $K(x)$, of the mooring system is provided by the stiffness of the mooring lines. There are two governing contributions to mooring line stiffness; geometric stiffness and elastic stiffness. The elastic stiffness arises from the elastic properties of the line, while the geometric stiffness is caused by the mooring line geometry (O. M. Faltinsen, 1990).

The total stiffness, k_T, is a play between geometric and elastic properties, and is found by equation 4.2

$$\frac{1}{k_T} = \frac{1}{k_G} + \frac{1}{k_E} \tag{4.2}$$

where k_G is geometric stiffness and k_E is elastic stiffness (K. Larsen, 2015).

Geometric Stiffness

The geometric stiffness, k_G, is caused by the change of geometry in the mooring line. This geometry change will be a result of change in external loading. For a catenary line the geometric stiffness is governing, and a detailed description of how the restoring force, in terms of tensions and horizontal offset, is provided in this case is presented below. The following is based on (O. M. Faltinsen, 1990) and (S. Chakrabarti, 2005).

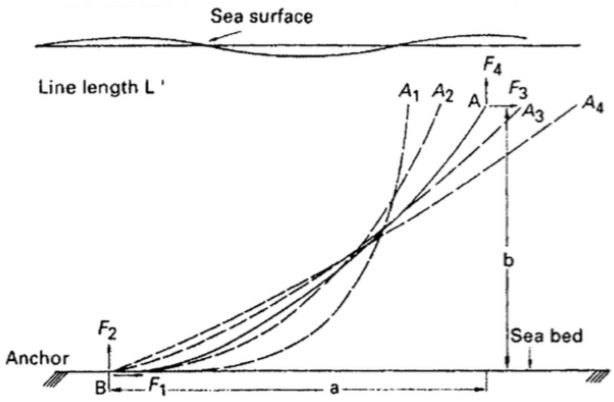

Figure 4.2: Catenary mooring line (S. Chakrabarti, 2005).

A catenary mooring line is presented in Figure 4.2. The mooring line is deployed from a floating structure at point A and anchored at the seabed at point B. A part of the catenary line will be laying on the seabed, and the horizontal distance, a, is usually 5-20 times larger than the vertical distance, b. As external forces affect the moored structure, a horizontal movement from A_1, through A_2, A_3 and A_4 occurs. This results in the part of the catenary line resting on the seabed varying from a significant length in position A_1 to none at A_4. The static cable tension is provided by the total weight in seawater of the suspended line length. The effect of lifting the catenary from the seabed, when the structure moves from A_1 to A_4, results in an increased line tension at point A. This effect, in addition to the simultaneous decrease in line angle to the horizontal, results in a restoring force on the floating structure that increases with the vessel offset in a non-linear manner.

The catenary equations can be used to describe this behavior. Figure 4.3 presents a mooring line. Using this figure, derivations of line tensions and shape of a single mooring line can be established. In the development of these equations, assumptions of a horizontal seabed and zero bending stiffness effects are made. The latter assumption is acceptable for small curvatures, which is a good approximation for chain. The dynamic effects in the line are also neglected.

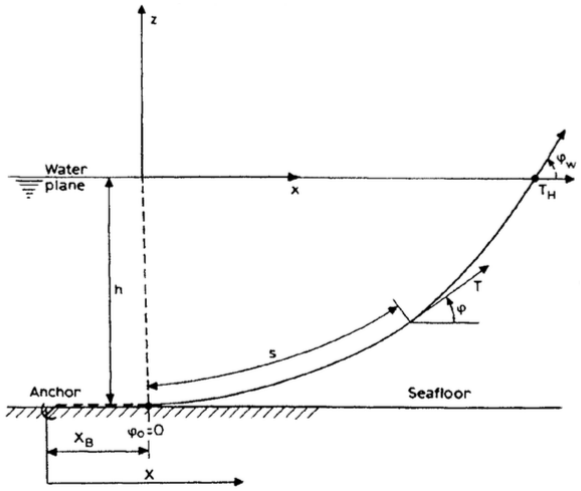

Figure 4.3: Catenary line with symbols (S. Chakrabarti, 2005).

Figure 4.4 shows a line segment. The term w is the submerged weight per unit length, T is the line tension, A is the cross-section area and E is the elastic modulus. D and F present the hydrodynamic forces acting on the line per unit length.

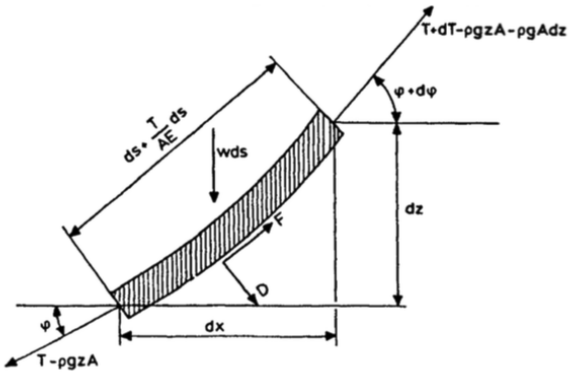

Figure 4.4: Forces acting on an element of an mooring line (S. Chakrabarti, 2005).

From figure 4.4, the in-line and transverse forces are given as:

$$dT - \rho g A dz = [w sin(\Phi) - F(\frac{T}{EA})]ds \tag{4.3}$$

$$Td\Phi - \rho g A z d\Phi = [w cos(\Phi) - D(1 + \frac{T}{EA})]ds \tag{4.4}$$

These equations are non-linear, and it is not possible to find an explicit solution. An approximation is made by neglecting the effect of the hydrodynamic forces, F and D, and the effect of elasticity. However, elasticity can be very important and needs to be considered in extreme conditions. Further information on the catenary equations can be found in (O. M. Faltinsen, 1990).

The line characteristics of a mooring line are defined as the relation between the horizontal offset and the tension at the top end of the mooring line. This may be derived from equation 4.3 and 4.4, assuming inelastic line, i.e $\frac{T}{EA} \ll 1$, and using Figure 4.5. The complete derivation can be found in (K. Larsen, 2014).

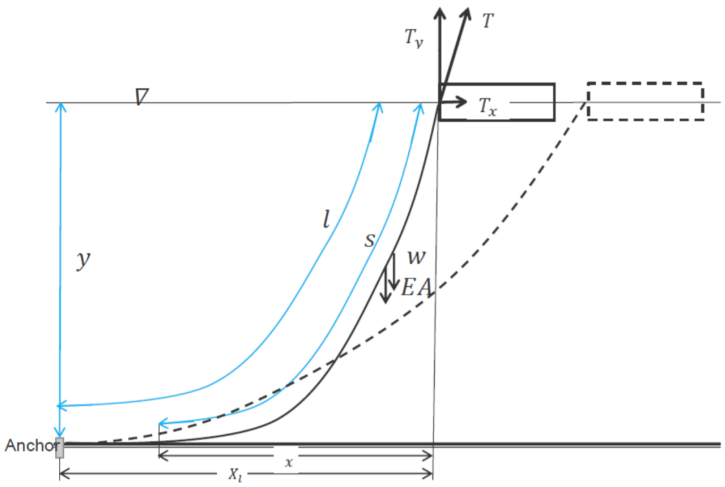

Figure 4.5: Schematic of notation defining line characteristics (K. Larsen, 2015).

The relation is presented in equation 4.5

$$X_l = l + \frac{T_x}{w} \cdot cosh^{-1}(1 + \frac{w \cdot y}{T_x}) - \sqrt{y \cdot (y + \frac{2T_x}{w})} \tag{4.5}$$

where X_l is the horizontal distance to the anchor, l is the length of the mooring line from fairlead to anchor, T_x is the horizontal tension, w is the weight in water and y is the water depth.

As described in this section, the geometric stiffness is defined by the top end tension and the horizontal offset. It is non-linear and dependent on the mooring line characteristics. Considering a mooring system this non-linear geometric stiffness is an important effect, which needs to be properly accounted for when performing a mooring analysis.

The catenary mooring system is applicable for shallow water applications. For increasing water depths, the catenary mooring system would impose very large vertical forces due to the large weight and the restoring

force provided in the horizontal direction would be too low.

Elastic Stiffness

The elastic stiffness, k_E, is caused by the elastic elongation of the line. This stiffness is linear and given by

$$k_E = \frac{EA}{L} \tag{4.6}$$

where E is the elastic modulus, A is the cross section area and L is the length of the mooring line. The mooring line will act as a mechanical spring. Hence, when pulled out from its equilibrium position a restoring force back to equilibrium position is created. This effect is important for a taut-leg system, where synthetic fiber ropes are spanning almost the whole height of the water column.

Figure 4.6 presents a schematic of a taut-leg mooring line.

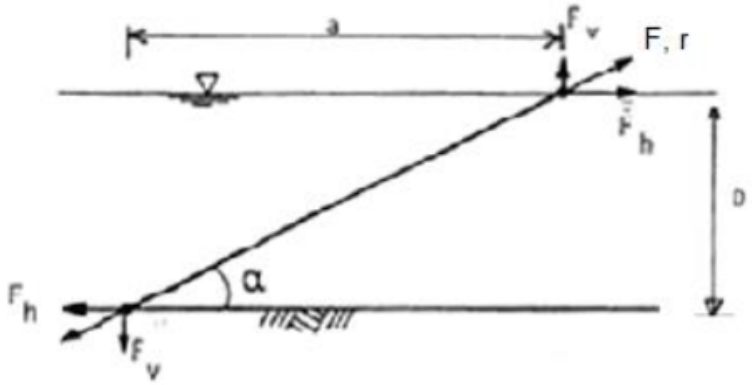

Figure 4.6: Elastic stiffness provided by line stretch (K. Larsen, 2015).

The equilibrium of the line is given as

$$F_h \cdot D = F_v \cdot a \tag{4.7}$$

The horizontal force, F_h, is thus given as

$$F_h = F_v \frac{a}{D} \tag{4.8}$$

where F_v is the vertical force, D is the depth and a is the horizontal length from attachment on seabed to attachment on vessel, as shown in Figure 4.6 (K. Larsen, 2015).

Due to the low weight, reduced floater offset, reduced seabed footprint and less complicated installation compared to a catenary mooring system, a taut-leg mooring system is preferred at deep water.

System Restoring Force

The system restoring force, $K(x)$, for the mooring system presented in Figure 4.7, gives the relationship between the mean and low frequency external loads on the vessel and its position.

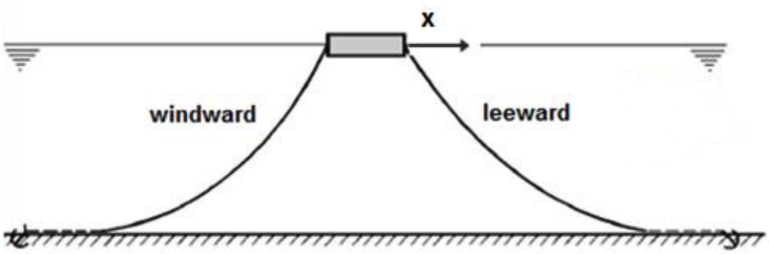

Figure 4.7: System restoring force (K. Larsen, 2015).

The horizontal system restoring force and moments are estimated by combining the contribution of stiffness for each line, as presented in equation 4.9 (O. M. Faltinsen, 1990).

$$\begin{aligned} F_1^{Restoring} &= \sum_{i=1}^{n} T_{x_i} \cdot cos\psi_i \\ F_2^{Restoring} &= \sum_{i=1}^{n} T_{x_i} \cdot sin\psi_i \\ F_6^{Restoring} &= \sum_{i=1}^{n} T_{x_i} [x_i \cdot sin\psi_i - y_i \cdot cos\psi_i] \end{aligned} \tag{4.9}$$

where T_{x_i} is the horizontal force from mooring line number i. The direction is from the attachment point of the mooring line towards the anchor. x_i and y_i are, respectively, the x- and y-coordinate of the attachment point of the mooring line to the vessel and ψ_i is the angle between the mooring line and the x-axis as seen in Figure 4.8.

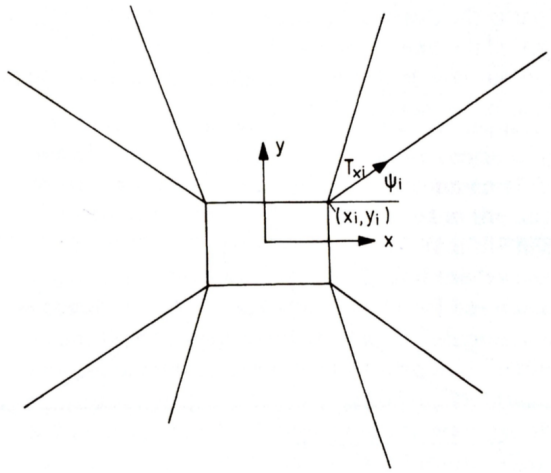

Figure 4.8: Notation for estimating horizontal system restoring force (O. M. Faltinsen, 1990).

4.1.2 Damping

The main sources of damping for a system consisting of a floater and a mooring system, assuming no thrusters or propellers, can roughly be listed as below (S. Chakrabarti, 2005)

- Wave radiation damping
- Wave viscous damping
- Wave drift damping
- Mooring line damping
- Damping due to wind
- Damping due to current

In addition to this there will be material damping in the structure itself.

Wave radiation damping results from wave making, and is determined from first order potential theory. This damping force is proportional to the wave amplitude, and is an important damping contribution to the wave frequency (WF) motions (A. Næss and T. Moan, 2013).

The viscous effects are caused by skin friction and by viscous forces due to the pressure distribution around the hull (O. M. Faltinsen, 1990). The latter effect is associated with flow separation and generation of vortices. The viscous damping is normally included in the low frequency (LF) motion calculations (API Recommended Practice, 2005).

Wave drift damping is proportional to the square of the wave amplitude, and proportional to the slowly varying velocity of the floater. The damping is caused by the change in wave drift force with floater velocity (K. Larsen, 2015). This damping contribution is important for the low frequency motion.

The top end motion will introduce dynamic lateral movement of the mooring lines. This lateral movement introduces drag forces, which creates damping forces on the mooring lines (H. Lie, Z. Gao and T. Moan, 2007). The damping contribution increases with water depth, as both the horizontal top end motion and the suspended length becomes larger (A. Næss and T. Moan, 2013).

Damping due to wind is caused by change of wind loads with floater velocity (K. Larsen, 2015). This low frequency damping contribution can be observed in equation 4.14 in section 4.1.3.

Damping due to current will also be present, which is caused by the change of current loads with floater velocity, as seen from equation 4.17 in section 4.1.3.

4.1.3 Excitation

Excitation loads from the physical environment include contributions from waves, wind and current. These loads include both components that are static and components that vary with time. The excitation forces can be expressed as in equation 4.10

$$Q(t, x, \dot{x}) = q_{wi} + q_{cu} + q_{wa} \tag{4.10}$$

where

q_{wi} = Wind forces
q_{cu} = Current forces
q_{wa} = Wave forces

These excitation forces will contribute to different excitation regimes. Table 4.1 presents the excitation forces and their contribution to mean frequency forces, wave frequency forces and low frequency forces.

	Mean	Wave frequency (5-30 s)	Low frequency (30-500 s)
Waves	Mean 2^{nd} order force	1^{st} order force	2^{nd} order difference frequency force
Wind	Mean wind speed	-	Wind gust
Current	Mean current speed	-	-

Table 4.1: The external forces divided into excitation regimes (K. Larsen, 2015).

A description of these excitation loads is presented in the following.

Wind forces

Wind is modeled as a constant velocity with an added varying velocity component with zero mean, called wind gust, as presented in Figure 4.9.

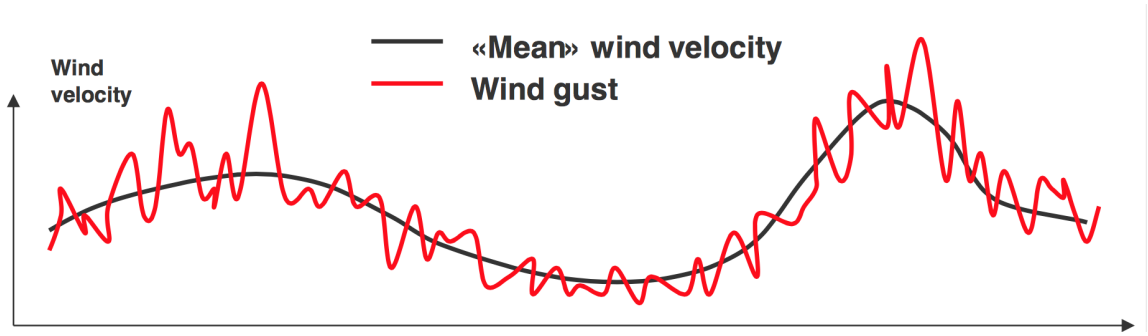

Figure 4.9: Mean wind velocity with added wind gust (K. Larsen, 2015).

The constant velocity causes the mean value of the wind, while the wind gust contributes with excitation forces for the low frequency motions (K. Larsen, 2015).

The wind force q_{wi} is given as a presented in 4.11

$$q_{wi}(t) = c_{wi}(U(t) - \dot{x})^2 \tag{4.11}$$

where the wind force coefficient, c_{wi}, is given by

$$c_{wi} = \frac{1}{2}\rho_{\text{air}} C_D A \tag{4.12}$$

where ρ_{air} is the density of air, C_D is the drag coefficient and A is the area, and the wind velocity, $U(t)$, is given by

$$U(t) = \overline{U} + u(t) \tag{4.13}$$

with $\overline{U}$ as the constant wind velocity and $u(t)$ as the time varying wind gust. $\dot{x}$ is the LF motion of the vessel.

Equation 4.11 consist of several contributions, as presented in equation 4.14

$$q_{wi}(t) \approx c_{wi}\overline{U}^2 + 2c_{wi}\overline{U}u(t) - 2c_{wi}\overline{U}\dot{x} \tag{4.14}$$

where the first term is a constant force, the second term is the excitation force for the LF motion and the third term is a damping force for the LF motion (K. Larsen, 2015).

The time varying wind component, also called the LF wind component, can as the LF wave component cause resonant surge, sway and yaw motions (API Recommended Practice, 2005). The component is modeled by a gust spectrum, where wind power density is given as a function of time. Some typical wind gust spectra is the Davenport spectrum, the Harris spectrum, the ISO spectrum and the API spectrum (K. E. Kaasen, H. Lie and K. Mo, 2012). On the NCS, the ISO spectrum is most commonly used.

Figure 4.10 presents all the four wind spectra for a mean wind velocity of 20 m/s. The figure shows that the power density for the wind gust generally decays with increasing frequency.

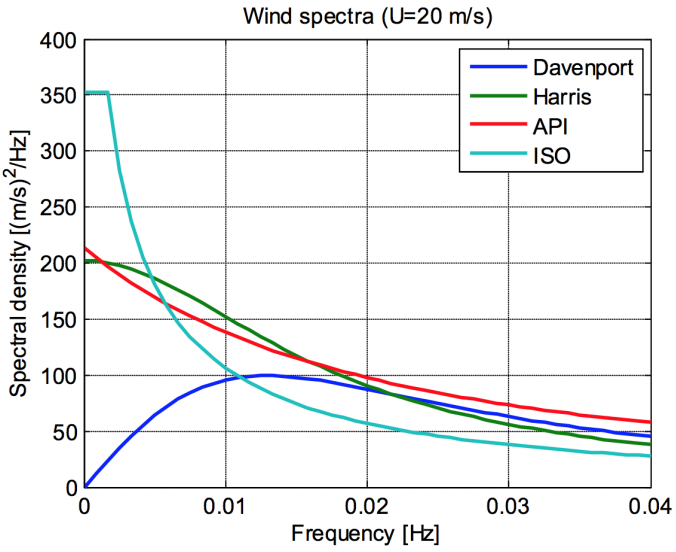

Figure 4.10: All four wind spectra for a mean velocity of 20 m/s (K. E. Kaasen, H. Lie and K. Mo, 2012).

Current forces

Equation 4.15 gives the current force on a vessel

$$q_{cu}(t) = c_{cu}|\overline{V} - \dot{x}|(\overline{V} - \dot{x}) \tag{4.15}$$

where $\overline{V}$ is the current mean velocity, $\dot{x}$ is the LF motion of the vessel and the current coefficient, c_{cu}, is given as

$$c_{cu} = \frac{1}{2}\rho C_D A \tag{4.16}$$

where ρ is density of water, C_D is the drag coefficient and A is the area. Assuming that $\overline{V}$ is larger than $\dot{x}$, equation 4.15 can be rewritten into equation 4.17

$$q_{cu}(t) = c_{cu}(\overline{V} - \dot{x})^2 = c_{cu}(\overline{V}^2 - 2\overline{V}\dot{x} + \dot{x}^2) \approx c_{cu}(\overline{V}^2 - 2\overline{V}\dot{x}) \tag{4.17}$$

where the first term is a constant force and the second term is a LF damping force (K. Larsen, 2015).

Current on the mooring lines can be accounted for by modeling a depth profile with specified current velocity vectors at given depths. However, for the motion response of the floater the current velocity at the surface is of primary interest.

Wave forces

The wave forces will have three contributions of importance for the mooring system; wave frequency-, mean value- and slowly-varying wave loads. Figure 4.11 presents the different wave components, where high frequency component refer to the WF component.

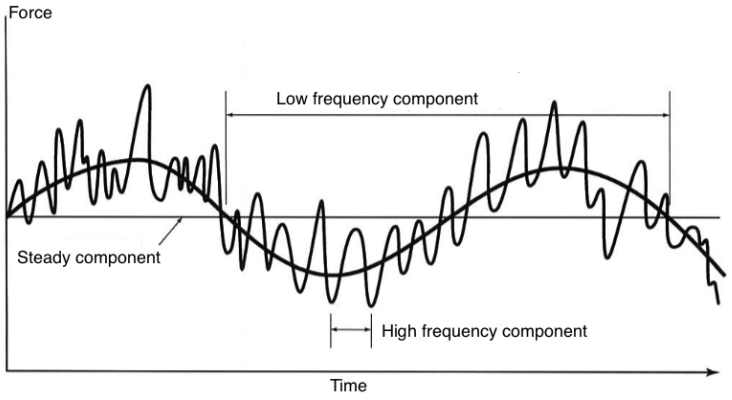

Figure 4.11: Wave force components (API Recommended Practice, 2005).

The excitation force from the waves may be written

$$q_{wa} = q_{wa}^{(1)} + q_{wa}^{(2)} \tag{4.18}$$

where $q_{wa}^{(1)}$ and $q_{wa}^{(2)}$ is the first order and second order wave loads, respectively.

The first order wave loads, known as WF loads, is proportional to the wave amplitude. These first order forces are described in the frequency domain as a transfer function between wave elevation and force

$$q_{wa}^{(1)}(\omega) = H^{(1)}(\omega)\zeta(\omega) \tag{4.19}$$

where $H^{(1)}$ is the complex first order transfer function and $\zeta(\omega)$ is the complex harmonic wave component (Marintek, 2013).

These motions represent an important contribution to the total mooring system loads, particularly in shallow water. The wave frequency motions have six degrees of freedom - surge, sway, heave, roll, pitch and yaw. Normally, these motions are considered to be independent of the mooring line stiffness for floating structures with natural periods less than 30 s (API Recommended Practice, 2005).

The second order loads, which in regular waves are proportional to the square of the wave amplitude, will have three contributions; mean forces, forces oscillating with difference frequency and sum frequencies forces. The mean and the difference frequency wave loads, the slowly varying loads, will be of importance

for the mooring system (O. M. Faltinsen, 1990). The contribution from the second order wave loads are estimated by used of Newmans approximation of the wave drift force coefficients in regular waves. A detailed description can be found in (Marintek, 2013).

The second order wave forces are in general small compared with the first order wave forces. Thus, the LF forces may typically not be of significant importance to the motions in the vertical plane (roll, pitch and heave), as large hydrostatic restoring forces are present here. However, in the horizontal plane (surge, sway and yaw) the restoring force is only present due to the mooring system. Here the motions created by the LF forces can be substantial. Particularly for frequencies near the natural frequency of the mooring. Consequently, LF surge, sway and yaw motions are important for mooring analysis (API Recommended Practice, 2005).

4.2 Time Domain Analysis Approaches

Generally, the time domain simulation is performed in a storm condition with duration of three hours. This duration is generally sufficient for obtaining reliable statistical values. The simulation is repeated several times using different seed values for generating the wave and wind time histories (API Recommended Practice, 2005).

The time histories for all the system parameters, including the displacement of the moored vessel, mooring line tensions and anchor line tensions, are available from this simulation. The resulting time histories are then processed statistically to obtain the expected extreme values (API Recommended Practice, 2005).

In general, there are two different approaches in executing a time domain analysis. The traditional approach is the separated approach, where a vessel motion analysis and a dynamic mooring analysis is carried out in two separated steps. The second is the coupled approach, where all interactions between mooring lines and vessel are modeled directly. Figure 4.12 presents a schematic of the separated and coupled approach.

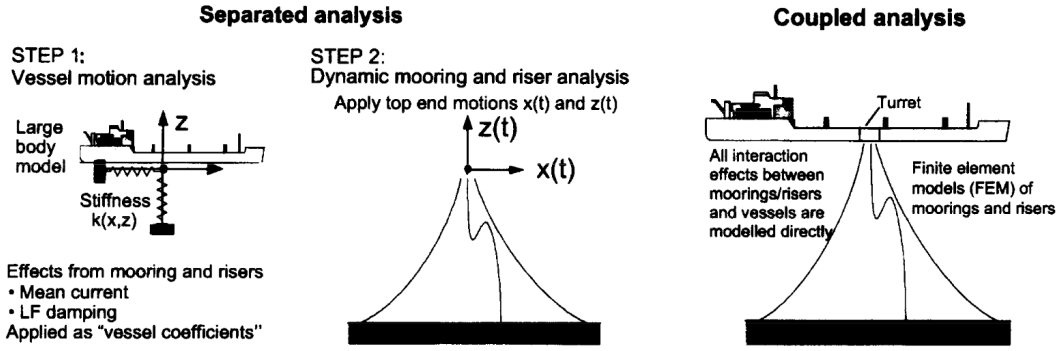

Figure 4.12: Separated (left) and coupled (right) approach (H. Ormberg, I. J. Fylling, K. Larsen and N. Sødahl, 1997).

In the following sections a description of these approaches, in addition to a comparison of them, is presented.

4.2.1 Separated Approach

In the separated approach, the response analysis is preformed using two different models - one for the floater and one for the mooring system. The procedure can be described as follow (H. Ormberg, I. J. Fylling, K. Larsen and N. Sødahl, 1997):

1. Simulation of the top end motions by the floater model
2. Simulation of the mooring tension by the mooring system model, taking the top end motion from 1. as input

For the motion response of the floater, calculated in 1., the response is often separated into WF and LF. Forces from the mooring system are applied as a non-linear position dependent force, the stiffness. Two important simplifications are usually made for the vessel model. The first simplification concerns the damping forces, which are either neglected or implemented roughly by a linear damping force acting on the vessel. This simplification influences the accuracy of the estimated LF motions. The second simplification concerns the influence of the current force on the moorings on the position dependent forces, which is neglected or included as an additional current force on the floater. These simplifications result in some inaccuracy in the restoring forces and line tensions (H. Ormberg, I. J. Fylling, K. Larsen and N. Sødahl, 1997).

4.2.2 Coupled Approach

In the coupled approach, a simultaneous analysis of floater motion and mooring line dynamics is performed. The model consists of a large volume body and finite element slender models for the mooring system. The total loads, including dynamics, from the slender body models of the mooring lines are transferred as a force into the large body model of the vessel. As a consequence, all the interaction effects, including stiffness, damping, mass and mooring line dynamics, between the moorings and the floater is modeled directly (L. Wang, 2010).

In order to execute a coupled time domain analysis, the whole motion equation needs to be solved in the time domain.

4.2.3 Comparison of Separated and Coupled Approach

The main shortcomings of a separated approach compared to a coupled approach is in (H. Ormberg, I. J. Fylling, K. Larsen and N. Sødahl, 1997) listed as:

- The mean loads on mooring lines due to current is not taken into account.
- The important damping effects from the mooring system on the low frequency motions are only accounted for in a simplified way.
- The dynamics of the mooring line will not have any influence on the wave frequency motions of the floater.

For the coupled approach, the effect of change in mean current forces on the moorings as the horizontal restoring force and mooring line tension for a given floater offset changes are accurately accounted for. Same for the damping forces from moorings. These effects can only be approximately accounted for in the separated approach. Hence, the coupled approach provides a more accurate estimate of the mean offset and LF motions (L. Wang, 2010).

In general, friction between the mooring line and the seabed and contact between floater and mooring system can not be accounted for using the separated approach. However, these effects are included in the coupled approach (L. Wang, 2010).

For shallow water, the floater motions are mainly excited and damped by fluid forces on the floater itself. An uncoupled system will therefore in this case provide a good estimate. However, for deep water the floater motions are in addition influenced by the moorings through the coupling effects. For instance, at deep water with strong current the interaction between the current forces on the submerged elements and the mean offset and LF motions becomes important. The same holds for the damping effects from the moorings on the LF motions. The effect of simplifying these contributions will increase with depth. Hence, for deep water a coupled system is preferable in order to get an accurate solution (L. Wang, 2010) (H. Ormberg, I. J. Fylling, K. Larsen and N. Sødahl, 1997).

4.3 Mooring Line Response

Response of the mooring system due to mean forces can be predicted by the static catenary equations presented in section 4.1.1. Generally, the response to low frequency motions can also be predicted by this method, as these motions have long periods. However, the response to the wave frequency motions of the structure is predicted by either quasi-static or dynamic analysis (API Recommended Practice, 2005).

4.3.1 Quasi-Static Analysis

Quasi-static analysis is simple and convenient method for determining maximum tension of mooring lines of floating structures due to wind, current and waves. Hence, it is frequently used in the initial stage of the design of mooring systems (Y. Inoue, H. Miyabe, X. Weiyi and M. Nakamura, 1991).

In the quasi-static analysis, the maximum top end tension is calculated with respect to the maximum displacement due to the WF and LF motions as presented in Figure 4.13 and equation 4.20

$$T_{QS} = T(x, z) \tag{4.20}$$

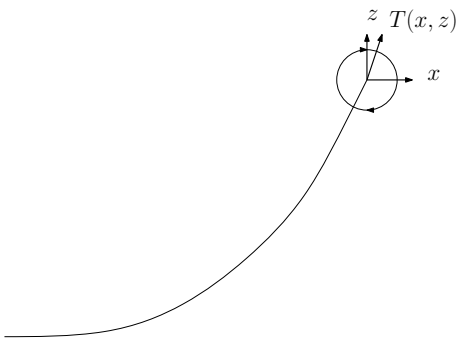

Figure 4.13: Quasi-static analysis of mooring line tension.

Hence, the dynamic wave loads are accounted for by statically offsetting the moored structure by wave induced motions. The vertical motions and dynamic effects associated with mass, damping and fluid acceleration on the mooring line is neglected (API Recommended Practice, 2005).

Quasi-static analysis of mooring line response can be applied for both frequency and time-domain simulations. However, according to DNV GL Offshore Standard (DNV GL, 2013), the analysis of a mooring system shall be based on a dynamic approach. A quasi-static analysis may only be accepted if the effects from the mooring line dynamics are demonstrated neglectable.

4.3.2 Dynamic Analysis

The dynamic analysis take into account the time varying effects due to mass, damping and fluid acceleration. Hence, drag forces and inertia forces are taken into account as presented in Figure 4.14.

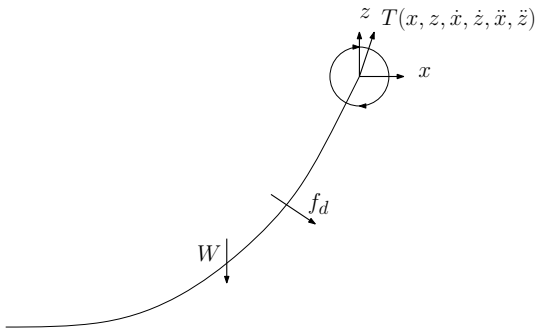

Figure 4.14: Dynamic analysis of mooring line tension.

The dynamic calculated tension due the WF and LF motions is here expressed by equation 4.21

$$T_{dyn} = T(x, z, \dot{x}, \dot{z}, \ddot{x}, \ddot{z}) \tag{4.21}$$

The time varying motions at the fairlead is calculated form the surge, sway, heave, roll, pitch and yaw motions of the structure. Dynamic models are used to predict the mooring line responses due to the motions at the fairlead (API Recommended Practice, 2005).

Dynamic analysis of time domain simulations accounts for several non-liner effects. The four primary nonlinear effects that may have an important influence on the mooring line behavior is (API Recommended Practice, 2005):

- Nonlinear stretching behavior of the line
- Changes of geometry
- Fluid loading
- Bottom effects

The nonlinear stretching behavior of the line is caused by the fact that the strain or tangential stretch of the line is a function of the tension magnitude. This nonlinear behavior typically occurs only in synthetic materials such as polyester. Generally, chain and wire rope can be regarded as linear.

A geometric non-linearity is associated with large changes in shape of the mooring line.

Generally, Morison's equation is used to describe the fluid loading effects on the mooring lines. The drag force on the line is thus proportional to the square of the relative velocity of the fluid and the line. Hence, the force is non-linear.

For many mooring designs, a considerable portion of the line may be in contact with the seafloor. Interaction between the mooring line and the seafloor is usually considered as a frictional process. Consequently, it is a non-linear effect. In addition, the length of the line in contact with the seafloor will constantly change. This causes an interaction between the non-linearities caused by bottom effects and by change of geometry (API Recommended Practice, 2005).

4.3.3 Extreme Value Statistics

The time domain method results are given in terms of time series. In order to obtain characteristic values, extreme value statistics applied. The following is based on (B. Leira, 2010).

The instantaneous surface elevation is assumed to be Gaussian distributed and narrow-banded, hence all maxima are identically Rayleigh distributed. All maxima are also assumed to be statistically independent. Satisfying these assumptions, the Gumbel distribution may be used to find the characteristic value most probable maximum (MPM). This value equals a probability level of 0.37 of the Gumbel distribution.

The Gumbel distribution is an extreme value distribution, where the samples y_1, y_2,...,y_N are given by $y = max(x_1, x_2, ..., x_n)$.

The Gumbel distribution is given by equation 4.22 and 4.23

$$F_y(y) = e^{(-e^{-\alpha(y-u)})} \qquad -\infty \leq y \leq \infty \tag{4.22}$$

$$f_y(y) = \alpha e^{(-\alpha(y-u)e^{-\alpha(y-u)})} \tag{4.23}$$

where $F_y(y)$ is the cumulative density function, $f_y(y)$ is the probability density function, and α and u are moment estimators. The moment estimators are established from equation 4.24 and 4.25

$$\hat{\alpha} = \frac{1}{\hat{s}_y}\frac{\pi}{\sqrt{6}} = \frac{1.28255}{\hat{s}_y} \tag{4.24}$$

$$\hat{u} = \hat{\mu}_y - \hat{s}_y\frac{\sqrt{6}}{\pi}0.57722 = \hat{\mu}_y - 0.45\hat{s}_y \tag{4.25}$$

where $\hat{\mu}_y$ and $\hat{s}_y$ are the mean and standard deviation, respectively, found from the sample of extreme values.

4.4 SIMA Software

SIMA is a complete tool for modeling and analysis of tasks within the field of marine technology developed as a Joint Industry Project by Marintek and Statoil. The program supports several physics engines including

- SIMO - used to model marine operations
- RIFLEX - used to model systems consisting of slender elements
- Coupled RIFLEX-SIMO - which is SIMO and RIFLEX coupled used to model slender, elastic structures within a marine operation.

The software provides a 3D graphical representation of the objects modeled, and instant validation of all changes done.

4.4.1 SIMO

SIMO, Simulation of Marine Operations, is a program for time domain simulation of motions and station keeping of multi-body systems. The program enables simultaneous simulation of total motions and analysis of station keeping behavior of complex marine operations. Flexible modeling of station keeping forces and coupling of force mechanisms, including mooring lines, ropes, thrusters, fenders, bumpers, docking guide piles, is integrated (Marintek, b).

Solving Equation of Motion in SIMO

Figure 4.15 presents a schematic of how the motion equation is solved in SIMO.

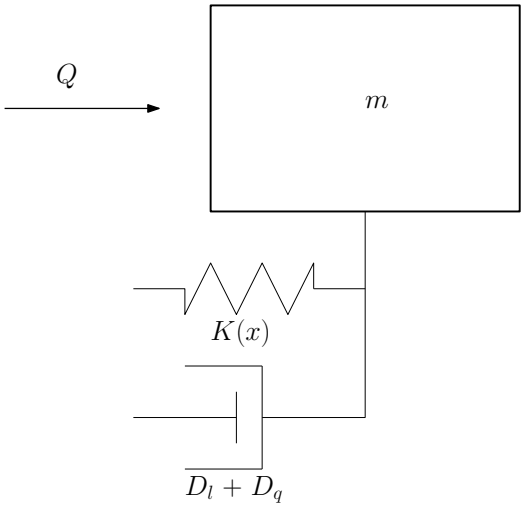

Figure 4.15: Motion equation solved in SIMO.

Assuming the equation of motion presented in equation 4.1 can be written

$$M\ddot{x} + C(\omega)\dot{x} + D_l\dot{x} + D_q f(\dot{x}) + K(x)x = Q(t, x, \dot{x}) \tag{4.26}$$

with

$$\begin{aligned} M &= m + A(\omega) \\ A(\omega) &= A_\infty + a(\omega) \\ A_\infty &= A(\omega = \infty) \\ C(\omega) &= C_\infty + c(\omega) \\ C_\infty &= C(\omega = \infty) \equiv 0 \end{aligned} \tag{4.27}$$

where m is the body mass matrix and f is a vector function where each element is given by $f_i = \dot{x}_i|\dot{x}_i|$.

Two different solution methods are available in SIMO in order to solve the equation of motion; solution by convolution integral and separation of motions. Solution by convolution integral determines the motion by solving the whole equation of motion in the time domain. Separation of motions however, solves the equation of motion by separating the LF and WF motions. A more detailed description of these two methods, based on (Marintek, 2013), is presented in the following.

Solution by convolution integral

Solution by convolution integral involves time integration of the whole motion equation in the time domain. A brief mathematical description of this method is given.

Assuming that equation 4.26 can be divided into internal and external forces, forming a dynamic equilibrium with respect to the frequency-dependent coefficients, it can be written

$$A(\omega)\ddot{x} + C(\omega)\dot{x} = f(t) = Q(t,x,\dot{x}) - D_l\dot{x} - D_q\dot{x}|\dot{x}| - M\ddot{x} - K(x)x \tag{4.28}$$

given that the right-hand side force varies sinusoidally at one single frequency ω.

Fourier transformation of equation 4.28 gives the equation in the frequency domain

$$(-\omega^2 A(\omega) + i\omega C(\omega))X(\omega) = F(\omega) \tag{4.29}$$

Assuming that $A_\infty = A(\omega = \infty)$ and $C_\infty = C(\omega = \infty) \equiv 0$, equation 4.29 can be written into

$$-\omega^2 A_\infty X(\omega) + i\omega(i\omega a(\omega) + c(\omega))X(\omega) = F(\omega) \tag{4.30}$$

In order to attain a motion equation in time domain, an inverse Fourier transformation is performed on equation 4.30

$$A_\infty\ddot{x}(t) + \int_{-\infty}^{\infty} h(t-\tau)\dot{x}(\tau)\,\mathrm{d}\tau = f(t) \tag{4.31}$$

where $h(t-\tau) = 0$ for $t < 0$ and $h(t-\tau) \equiv 0$ for $\tau > t$ due to physical limitations

$$A_\infty\ddot{x}(t) + \int_0^t h(t-\tau)\dot{x}(\tau)\,\mathrm{d}\tau = f(t) \tag{4.32}$$

The motion equation to be solved by time integration can then be written as

$$(M + A_\infty)\ddot{x} + D_l\dot{x} + D_q\dot{x}|\dot{r}| + K(x)x + \int_0^t h(t-\tau)\dot{x}\,\mathrm{d}\tau = Q(t,x,\dot{x}) \tag{4.33}$$

where $h(\tau)$ is the retardation function, which transfers the frequency dependent features into the time domain. This function is computed by transformation of frequency dependent added mass and damping, and may be written as

$$h(\tau) = \frac{2}{\pi}\int_0^\infty c(\omega)cos(\omega\tau)\mathrm{d}\omega = -\frac{2}{\pi}\int_0^\infty \omega a(\omega)sin(\omega\tau)\mathrm{d}\omega \tag{4.34}$$

The motion equation 4.33 is solved for each time step with respect to the position vector x. The choice of time step is crucial for the stability and accuracy of the time domain analysis. Generally, it depends on the periods of the responses, degree of non-linearity and the analysis formulation (API Recommended Practice, 2005).

Separation of Motions

Separation of motions is an alternative to solving the whole equation in the time domain. This method reduces the complexity and computational effort compared to solution by convolution integral. In this approach, the motions are separated into a WF part and a LF part. The wave frequency motions are solved in the FD, which requires the motions to be linear responses of the waves. Hence, the quadratic damping, D_q, is set to zero and the stiffness, K, is constant.

The exciting force, $Q(t,x,\dot{x})$, is separated into a WF part, Q^{WF}, and a LF part, Q^{LF}.

$$Q(t,x,\dot{x}) = Q^{WF} + Q^{LF} \tag{4.35}$$

where

$$\begin{aligned} Q^{WF} &= q_{wa}^{(1)} \\ Q^{LF} &= q_{wi} + q_{wa}^{(2)} + q_{cu} \end{aligned} \tag{4.36}$$

and $q_{wa}^{(1)}$ and $q_{wa}^{(2)}$ is the first and second order wave loads, respectively.

Hence, the total position vector contains contributions from both the WF and LF motions

$$x_{TOT} = x_{WF} + x_{LF} \tag{4.37}$$

where x_{WF} is the wave frequency motion and x_{LF} is the low frequency motion.

The WF motions are solved in the frequency domain by use of transfer functions, as expressed in equation 4.38

$$(m + A(\omega))\ddot{x}_{WF} + (D_l + C(\omega))\dot{x}_{WF} + Kx_{WF} = q_{wa}^{(1)} \tag{4.38}$$

The dynamic equilibrium equation for the LF motions are given by equation 4.39

$$(m + A(\omega = 0))\ddot{x}_{LF} + D_l\dot{x}_{LF} + D_q\dot{x}_{LF}|\dot{x}_{LF}| + Kx_{LF} = q_{wi} + q_{wa}^{(2)} + q_{cu} \tag{4.39}$$

this equation is solved in the time domain.

Mooring Line Tension

Mooring line tension may in SIMO be calculated by three different methods (Marintek, 2013):

- Quasi-static analysis
- Simplified dynamic analysis
- Finite element method (FEM) analysis

The simplified dynamic analysis and FEM analysis will not be covered here. However, the quasi-static analysis of mooring line tension is applied in this thesis work, and is briefly described in the following.

All the mooring lines are in SIMO treated individually, and may therefore have completely different properties. The mooring lines are modeled by the catenary equations, and the procedure for calculating the mooring line configurations is based on a shooting method. This implies iteration on the boundary conditions at one end in order to satisfy specified boundary conditions at the other.

Friction at the bottom is neglected so the line will rotate freely about the anchor. Transverse drag on the lines is also neglected. The total line tension and angle of upper end from vertical is thereby determined by the location of the upper end relative to the anchor. This is done in the vertical plane, and a two dimensional line characteristics table is calculated.

Interpolation on the characteristics table through the time simulation is performed. Hence, each time the line characteristics data are changed, the line characteristics table is updated.

4.4.2 RIFLEX

RIFLEX, Riser System Analysis Program, is an advanced program for static and dynamic analysis of slender marine structures, applying finite element. The line dynamics calculated by this program includes both drag and mass forces on the mooring lines (Marintek, b).

A schematic of a mooring system modeled in RIFLEX is presented in Figure 4.16.

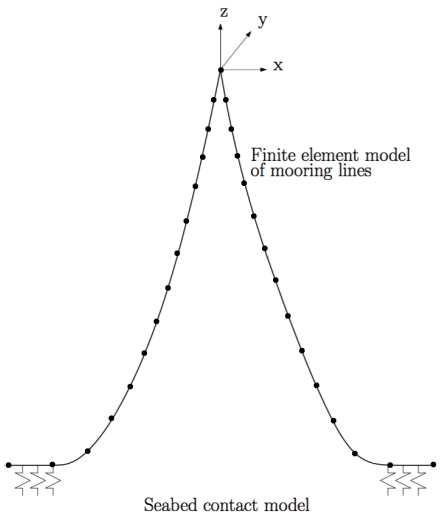

Figure 4.16: Mooring system modeled in RIFLEX.

The mooring lines are slender marine structures modeled by means of finite elements. Three-dimensional bar elements are used to represent mooring lines and other components where bending stiffness is negletable, while a three-dimensional beam elements are used for elements where bending stiffness may be of importance.

The load model for these slender structures accounts for weight, buoyancy and hydrodynamic loads. A generalized Morison load model computes the hydrodynamic loads.

Springs and friction models simulate seabed contact.

Separated Analysis in RIFLEX

The motions of the vessel, calculated in SIMO, may be imported into RIFLEX in order to analyze the system. This corresponds to the separated analysis approach described in section 4.2.1. Figure 4.17 presents a schematic of this approach.

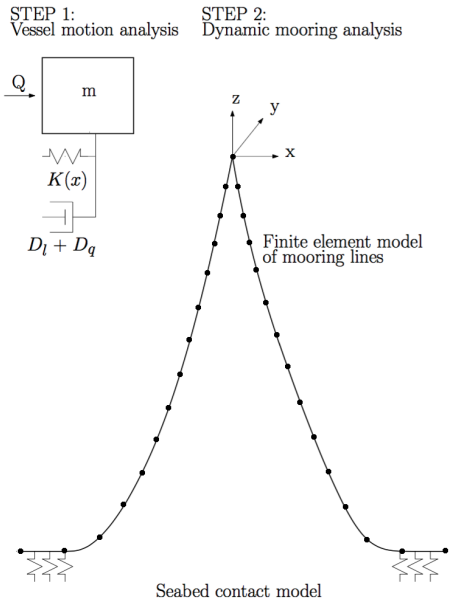

Figure 4.17: Separated analysis in RIFLEX.

The motions of the vessel due to environmental excitation are calculated in SIMO, either by used of solution by convolution integral or separation of motion as described in section 4.4.1. These motions are applied as top end motions of mooring line modeled in RIFLEX, and the response is calculated based on finite element.

There are some shortcomings of this method compared to the coupled analysis approach. These shortcomings are presented in section 4.2.3.

4.4.3 Coupled RIFLEX-SIMO

Coupled RIFLEX-SIMO enables combining SIMO and RIFLEX in order to model slender, elastic structures within a marine operation. This is the coupled analysis approach as presented in section 4.2.2.

Figure 4.18 present a schematic of a coupled analysis performed in Coupled RIFLEX-SIMO.

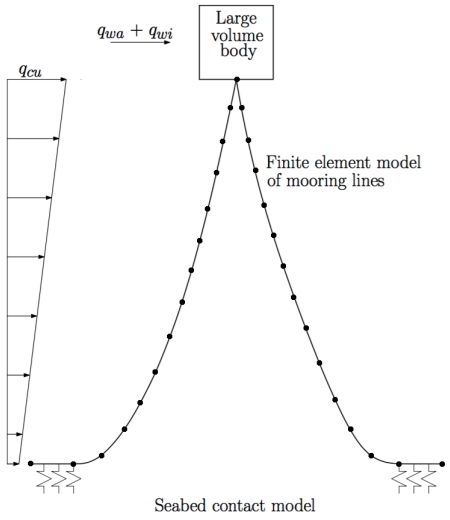

Figure 4.18: Coupled analysis in RIFLEX.

A description of the coupled analysis approach is presented in section 4.2.2. The following is based on (H. Ormberg and K. Larsen, 1998).

In the coupled analysis approach, all the system components are described in a finite element model. The applied finite element procedure is a displacement formulation that allows for unlimited displacements and rotations in the three-dimensional space, while strains are assumed to be moderate.

The mooring lines are modeled as in RIFLEX by means of finite elements, as described in section 4.4.2. However, the force models of the vessel are implemented as nodal forces at the top end of the finite element model of the mooring lines. The vessel is modeled as a large volume body represented by a six degree of freedom rigid body. The load model for this body accounts for wind, wave and current forces. Hence, full interaction is taken into account, and accurate vessel motions and dynamic loads of the mooring lines are obtained simultaneously.

Chapter 5

Automated Optimization Algorithms

5.1 Optimization Theory

Optimization is an important tool in the analysis of physical systems. In order to make use of this tool, an objective function must be identified. The objective function is a quantitative measure of the performance of the system under study. The objective depends on certain characteristics of the system, called variables or unknowns. The goal is to find values of the variables that optimize the objective. Often the variables are restricted, or constrained, in some way.

Mathematically, optimization is the minimization or maximization of a function subjected to constraints on its variables. The problem is geometrically presented in Figure 5.1.

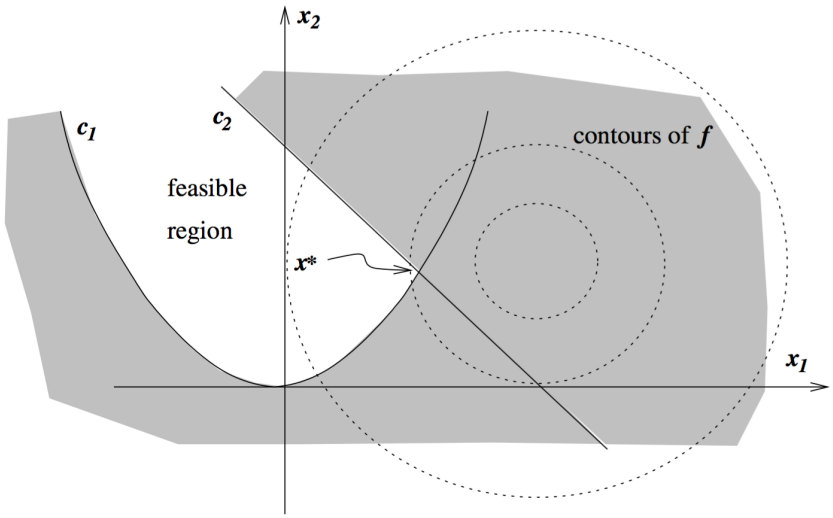

Figure 5.1: Geometrical representation of the optimization problem (J. Nocedal and S. J. Wright, 2006).

The following notation is here used:

- x is the variables

- f is the objective function, a function of x that shall be minimized or maximized
- c_j are constraint functions, which are scalar functions of x that define certain equations and inequalities that the variable x must satisfy.

Using this notation, the optimization problem can be written as follows

$$\min_{x \in \mathbb{R}} f(x) \quad \text{subjected to} \quad \begin{matrix} c_j(x) = 0, & j \in J \\ c_j(x) \geq 0, & j \in K \end{matrix} \tag{5.1}$$

The process of identifying objective, variables and constraints for a given problem is known as modeling. Construction of an appropriate model is an important part of the optimization process. If the model is too simplistic, it will not give useful insights to the practical problem. If it is too complex, it may be too difficult to solve.

Once the model has been formulated, an optimization algorithm can be used to find its solution. There is no universal optimization algorithm, but rather a collection of algorithms. Each algorithm is tailored to a particular type of optimization problem. The choice of algorithm is important as it may determine whether the problem is solved rapidly or slowly and, indeed, whether the solution is found at all (J. Nocedal and S. J. Wright, 2006).

5.1.1 Sequential Quadratic Programming

Subsequential quadratic programming (SQP) methods belong to the most powerful non-linear programming algorithms known today for solving differentiable non-linear programming problems of the form in equation 5.2. The optimization method generates a sequence of quadratic programming problems that are to be solved successively. SQP is the standard general purpose method to solve smooth non-linear optimization problems when the following assumptions apply (K. Schittkowski, 2011):

- The problem is not too large
- Functions and gradients can be evaluated with sufficiently high precision
- The problem is smooth and well-scaled

In addition, SQP methods are preferable when solving problems with significant non-linearities in the constraints (J. Nocedal and S. J. Wright, 2006).

NLPQLP

SIMA applies the mathematical optimization algorithm NLPQLP. This is a Fortran subroutine that solves smooth non-linear programming problems by a SQP algorithm. The following theory is based on (K. Schittkowski, 1986) and (K. Schittkowski, 2011).

The code is designed to solve the general optimization problem to minimize an objective function f under

non-linear equality and inequality constraints,

$$\begin{aligned} & min \quad f(x) \\ x \in \mathbb{R}^n : & \\ & c_j(x) = 0, \quad j = 1,...,m_e \\ & c_j(x) \geq 0, \quad j = m_e+1,...,m \\ & x_l \leq x \leq x_u \end{aligned} \tag{5.2}$$

where x is an n-dimensional parameter vector. All problem functions $f(x)$ and $c_j(x)$, $j = 1,...,m$, are assumed continuously differentiable on the whole $\mathbb{R}^n$.

The principle idea is to formulate and solve a quadratic programming subproblem in each iteration that is obtained by linearizing the constraints and approximating the Lagrangian function

$$L(x,u) := f(x) - \sum_{j=1}^{m} u_j c_j(x) \tag{5.3}$$

quadratically, with $x \in \mathbb{R}^n$ as the primal variable and $u = (u_1,...,u_m)^T \in \mathbb{R}^m$ as the multiplier vector.

In order to formulate the quadratic programming subproblem, one proceed from given iterates $x_k \in \mathbb{R}^n$, an approximation of the solution, $v_k \in \mathbb{R}^m$, and approximation of the multipliers, and $C_k \in \mathbb{R}^{n\times n}$, and approximation of the Hessian of the Lagrange function. The quadratic programming problem

$$\begin{aligned} & min \quad \frac{1}{2} d^T C_k d + \nabla f(x_k)^T d \\ d \in \mathbb{R}^n : & \\ & \nabla c_j(x_k)^T d + c_j(x_k) = 0, \quad j = 1,...,m_e \\ & \nabla c_j(x_k)^T d + c_j(x_k) \leq 0, \quad j = m_e+1,...,m \\ & x_l - x_k \geq d \geq x_u - x_k \end{aligned} \tag{5.4}$$

is then solved. Where d_k is the optimal solution and u_k the corresponding multiplier of this subproblem. A new iterative is obtained by

$$\begin{pmatrix} x_{k+1} \\ v_{k+1} \end{pmatrix} := \begin{pmatrix} x_k \\ v_k \end{pmatrix} + \alpha_k \begin{pmatrix} d_k \\ u_k - v_k \end{pmatrix} \tag{5.5}$$

where $\alpha_k \in (0,1]$ is a suitable steplength parameter.

The steplength parameter α_k is required in equation 5.5 to enforce global convergence of the SQP method.

α_k should satisfy at least a sufficient decrease condition of a merit function $\phi_r(\alpha)$ given by

$$\phi_r(\alpha) := \psi_r\left(\begin{pmatrix} x \\ v \end{pmatrix} + \alpha \begin{pmatrix} d \\ u - v \end{pmatrix}\right) \tag{5.6}$$

with a suitable penalty function $\psi_r(x, v)$. The augmented Lagrangian function is here implemented

$$\psi_r(x, v) := f(x) - \sum_{j \in I}(v_j c_j(x) - \frac{1}{2} r_j c_j(x)^2) - \frac{1}{2}\sum_{j \in K} v_j^2 / r_j \tag{5.7}$$

with

$$J := \{1, ..., m_e\} \cup \{j : m_e < j \leq m, \quad g_j(x) \leq v_j / r_j\}$$
$$K := \{1, ..., m\} \setminus J$$

The objective function is penalized as an iterative leaves the feasible domain. The corresponding penalty parameters r_j, $j = 1, ..., m$ which control the degree of constraint violation is carefully chosen to guarantee a descent direction of the merit function to get

$$\phi'_{r_k}(0) = \nabla \psi_{r_k}(x_k, v_k)^T \begin{pmatrix} d_k \\ u_k - v_k \end{pmatrix} < 0 \tag{5.8}$$

The Hessian matrix of the Lagrangian function, C_k, is by standard approach approximated and updated by the Broyden–Fletcher–Goldfarb–Shanno quasi-Newton formula.

Although the matrix C_k is guaranteed positive definite, it is possible that equation 5.4 is not solvable due to inconsistent constraints. In order to avoid this disadvantage, an additional variable $\delta \in \mathbb{R}$ may be introduced, leading to a modified quadratic programming problem

$$\begin{aligned} & min \quad \frac{1}{2} d^T C_k d + f(x_k)^T d + \frac{1}{2}\rho_k \delta^2 \\ & d \in \mathbb{R}^n \\ & \delta \in \mathbb{R}: \\ & \quad \nabla c_j(x_k)^T d + (1 - \delta) c_j(x_k) \leq 0, \qquad j \in J_k \\ & \quad \nabla c_j(x_{k(j)})^T d + c_j(x_k) \leq 0, \qquad j \in K_k \\ & \quad x_l - x_k \geq d \geq x_u - x_k \\ & \quad 0 \geq \delta \geq 1 \end{aligned} \tag{5.9}$$

where

$$J_k := \{1, ..., m_e\} \cup \{j : m_e < j \leq m, \quad c_j(x_k) \leq \epsilon \quad or \quad v_j^{(k)} > 0\}$$
$$K_k := \{1, ..., m\} \setminus J_k$$

$v_k = (v_1^{(k)}, ..., v_m^{(k)})^T$ and ϵ are user provided tolerance. The index $k(j)$ indicates gradients which have been calculated in previous iterations. The term ρ_k is an additional penalty parameter designed to reduce the influence of δ on a solution of equation 5.9.

5.2 Specification of Optimization Problem for Mooring Systems

The engineering process for mooring systems has become more complicated and cumbersome with advances in the design of mooring systems, more complicated rules and a tendency to increase utilization. Automated optimization algorithms refer to the application of mathematical search algorithms in the optimization process. In the optimization of a mooring system, this may contribute with considerable gains (I. J. Fylling, 2013).

The optimization theory concerning mooring systems described in this section is based on (I. J. Fylling, 2013).

The process can be describes with Figure 5.2.

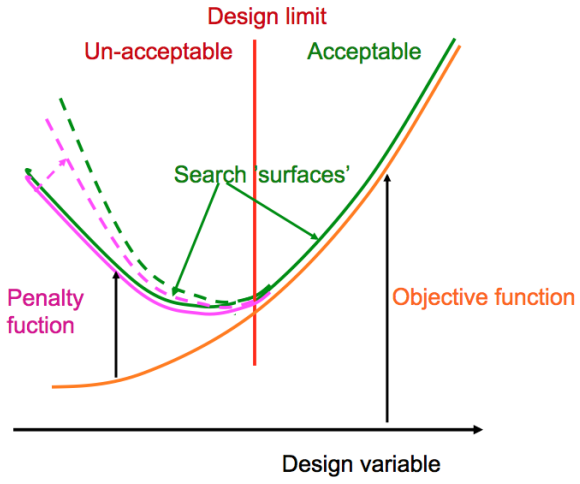

Figure 5.2: The objective function with variables and constraints (I. J. Fylling).

An iterative process is carried out in order to minimize the cost, represented by the objective function. In addition, the constraints, representing the design limit, needs to be satisfied in order for the system to stay within the acceptable range. The optimization is performed by modifying the parameters chosen as design variables.

5.2.1 Objective Function

The objective function describes the quantity to be minimized. Generally, this includes the sum of mooring and riser material cost, and can be denoted as

$$\text{Cost function} = \text{Cost function}_{\text{MOORING}} + \text{Cost function}_{\text{RISER}} \tag{5.10}$$

where the mooring cost is represented as

$$\text{Cost function}_{\text{MOORING}} = \sum_{\substack{\text{all} \\ \text{mooring} \\ \text{lines}}} \sum_{\substack{\text{all} \\ \text{segments}}} C_{M,i} m_i l_i \tag{5.11}$$

$C_{M,i}$ is the cost/ton, m_i is the mass/length and l_i is the length of segment i. The riser cost can be described by two different cost models

- Offset dependent riser cost
- Cost of riser pipe, proportional with riser line length and of riser buoyancy material

The first alternative assumes higher cost for higher extreme vessel offset. A detailed riser analysis within the optimization program is for this alternative not required. Thus, a separate riser design optimization is carried out, where optimum cost is determined as a function of vessel offset. For the second alternative, a riser modeling that reflects the relationship between design variables and critical riser responses is required.

5.2.2 Constraints

The constraints describe the design requirements that have to be satisfied. The following constraints are allowed:

- Maximum tension in mooring line segments
- Minimum tension in mooring line segments
- Maximum mooring line slope at anchor
- Minimum fatigue life of mooring lines
- Minimum clearance to obstructions
- Maximum vertical pretension force
- Maximum offset
- Maximum tension in riser line segments
- Minimum curvature radius of riser line segments

- Maximum riser slope at lower end
- Riser slope range at lower end

The specified constraints values may differ for different cases, representing operational, survival, intact, one line failure cases. The constraint level, capacity and/or safety factors must account for uncertainties in the applied analysis method.

The response parameters, including maximum tension, line angles and offset, used for checking the design requirements are converted to constraint functions. These functions are required non-negative for acceptable design.

A brief description of the maximum tension constraint function is given in the following.

Maximum Tension Constraint Function

The conventional extreme load capacity requirement is represented by a single safety factor. The maximum tension constraint is in this case

$$g_{sf} = \frac{SF - SF_{MIN}}{SF_{MIN}} \tag{5.12}$$

where SF_{MIN} is the minimum required safety factor, and SF is the lowest calculated safety factor, including all environmental conditions. A negative g_{sf} implies a unacceptable design.

The single safety factor has in recent design codes, including (DNV GL, 2013), been replaced by a set of partial safety factors. Hence, one factor for the static loads and one for the dynamic loads. The design requirement can with partial load factors be expressed by

$$F_b = F_{stat} \cdot f_s + F_{dyn} \cdot f_d \tag{5.13}$$

where F_b is the maximum allowable utilization, the breaking strength divided by the material factor. F_{stat} and F_{dyn} are the static and dynamic loads, respectively. f_s and f_d are the corresponding load factors.

The constraint function for the partial safety factor is thus given by

$$g_{plf} = \frac{F_b - (F_{stat} \cdot f_s + F_{dyn} \cdot f_d)}{F_b} \tag{5.14}$$

and g_{plf} is required non-negative.

5.2.3 Variables

The optimization variables specify the parameters allowed to modify in the process. There are three types of variables that can be specified:

- Vessel variables
- Line variables
- Segment variables

Buoyancy force can also be specified as a variable if discrete buoyancy or clump weight modules are included in the system.

Non-physical or non-practical solutions are avoided by defining a lower and upper limit of the variation range for all optimization variables.

Vessel Variables

Specified neutral heading can be optimized, which is the reference for the mooring line directions.

Line Variables

The line variables include variation in the line direction relative to the vessel and the pretension or the distance to the anchor. Analyzes in several environmental directions are necessary if the line direction is used as variable.

Segment Variables

Segment variables may be divided into mooring segment variables and riser segment variables.

For the mooring lines, segment length and one cross-section parameter can be set as variables. Specifying mooring line diameter as variable imply that other cross-section data, as submerged weight, mass and breaking strength, are scaled proportional with the diameter squared.

The segment variables, including line diameter, segment length and submerged weight, have direct influence on the objective function, thus the cost. The remaining variables, including line directions, pretension and distance to anchor, have a direct influence on the constraint functions only. They will indirectly affect the optimum objective function by affecting the range of the allowable design space.

5.3 Automated Optimization in SIMA Workbench

SIMA contains a general purpose optimization tool, where the user may formulate a optimization problem for any parameterized model using variables. Typical applications of this optimization tool are (Marintek, a):

- Mooring system optimization using SIMO, RIFLEX or Coupled.
- Riser optimization using RIFLEX or Coupled.
- Optimization of marine operations using SIMO

This master thesis performs optimization of mooring systems using SIMO. The following section presents a description of how optimization of mooring systems using SIMO is carried out using in SIMA workbench.

5.3.1 Mooring System Optimization Using SIMO

SIMA demands the optimization problem to consist of the following building blocks:

- A workflow to be optimized with optimization variables as input and cost function and constraint values as output.
- A workflow with an optimization node referring to the workflow above, and where the user specifies the optimization calculation parameters.
- A post processor with a cost function to be minimized and constraints to be satisfied.

These building blocks are presented in Figure 5.3

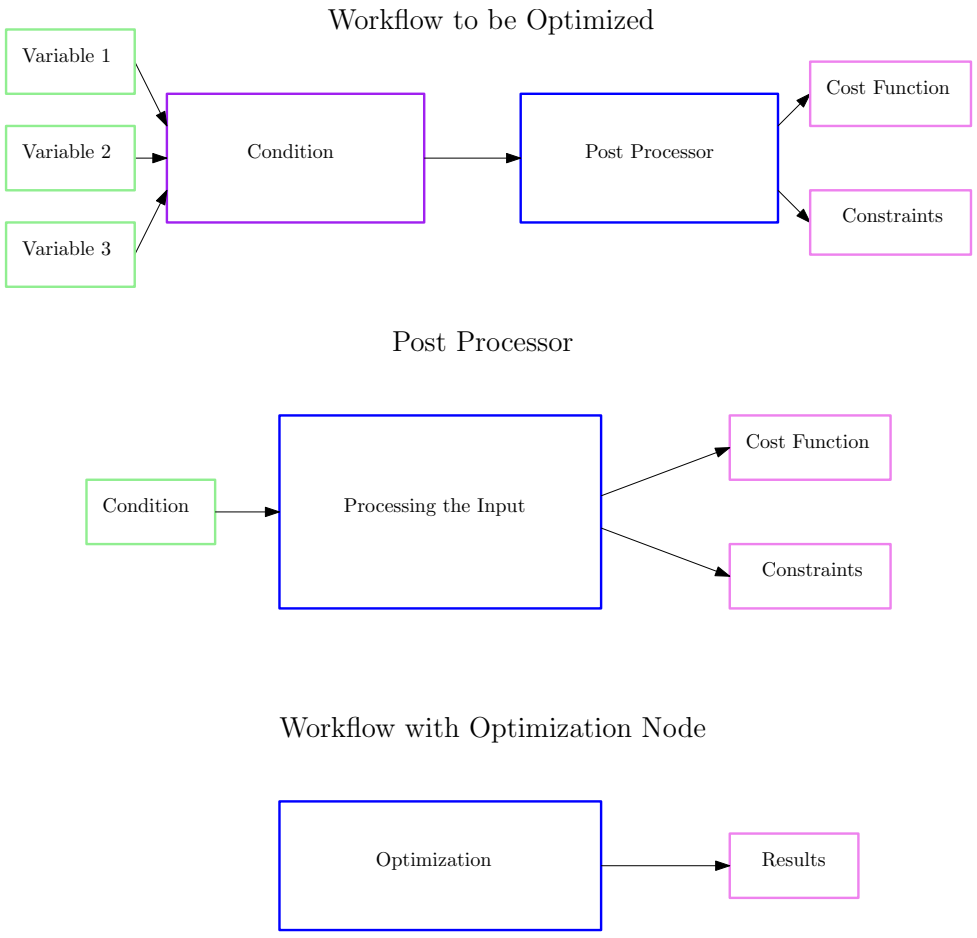

Figure 5.3: Schematic of the optimization process in SIMO.

A more detailed description of the elements included in the different building blocks is presented below.

Workflow to be Optimized

The three light green blocks, labeled *Variable 1*, *Variable 2* and *Variable 3*, in Figure 5.4 presents the optimization variables. These variables are the input to the workflow, and will be updated for each iteration of the optimization.

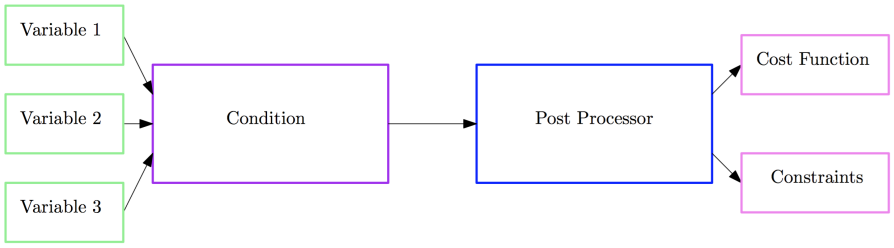

Figure 5.4: Schematic of the workflow to be optimized.

The variables are imported into the purple *Condition* block. A condition involves either a static or dynamic analysis of the model for a specified environment. Several condition blocks may be included with different environments. The results from the analysis are imported to the post processor.

The output from the post processor is the cost function and the constraints. These are used as input for the workflow with the optimization node.

Post Processor

The input to the post processor is the results from the condition or conditions, as presented in Figure 5.5.

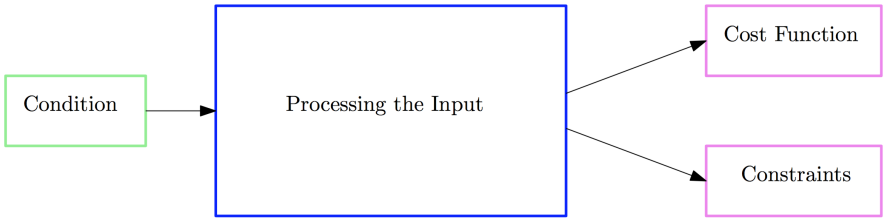

Figure 5.5: Schematic of the post processor.

These results are processed by used of different tools in order to create the cost function and desired constraints.

The tools available in the post processor are divided into several groups:

- Arithmetic
- Statistics
- Filtering
- Signal Structure
- Spectral Analysis
- Fatigue
- Code Check
- Other

Arithmetic constraints different mathematical operators, including the basic operators multiply, divide, add, subtract and square root. Calculating the magnitude of a distance, finding absolute value of each element in a signal, raise each element in a signal to an exponent, apply a function on an input, scale and square the signal is also possible.

Statistics contains different statistical tools in order to find minimum, maximum, mean, standard deviation, kurtosis and skewness of the results. Tools for merging results, compute cumulative distribution, normalize results, compute maximum amplitude and find peaks are also included.

Filtering contains band pass, high pass and low pass filters. Polynomial fit, removal of mean from signal, selecting value at given index in signal and select a window from the signal are the other tools available in this category.

Signal structure allows the user to flatten, join or split input trees.

Spectral analysis enables cross spectrum and auto spectrum to be computed. Fast Fourier transform is another tool included in this category.

Fatigue includes finding axial stress, calculate fatigue and calculate different types of pipe stress.

Code check may also be included, and involves DNV OS-F201, ISO 13628-7 and ISO 19901-7.

The category other allows the user to check towards collision, set constraints on signals, differentiate signals, calculate distance between a globally fixed line and a line, calculate distance between two lines, create a function, create a new signal based on linear interpolation, merge selected constant signals into one and transform body response into a point.

Connectors are used in order to connect the different tools together in the post processor. A connector may be modified in order to select specific signals as input to the tools.

The output from the post processor is the cost function and the constraints.

Workflow with Optimization Node

The workflow presented in Figure 5.6 contains the optimization node. Inside the optimization node the cost function, constrains and optimization variables are specified. Start, minimum and maximum values are specified for all the optimization variables. Delta values for the optimization variables to be used in the calculation of gradients are also specified.

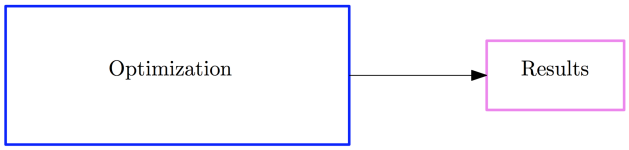

Figure 5.6: Schematic of the workflow with optimization node.

Calculation parameters include desired final accuracy of result and max iterations during the optimization. Tolerance for the quadratic programming solver, minimum step length and maximum function calls is also specified here.

The results are displayed in plots. The plots include cost function, optimization variables, and constraints. Plots of the constraint gradient and the cost function gradient are also included. All plots are given with iteration number on the x-axis.

Chapter 6

The Simulation Model

The model used in this master thesis is the deep draft semisubmersible DEMO2000, presented in Figure 6.1. This is a semisubmersible developed by Statoil, and is the same model as used for the simulation case in the project thesis.

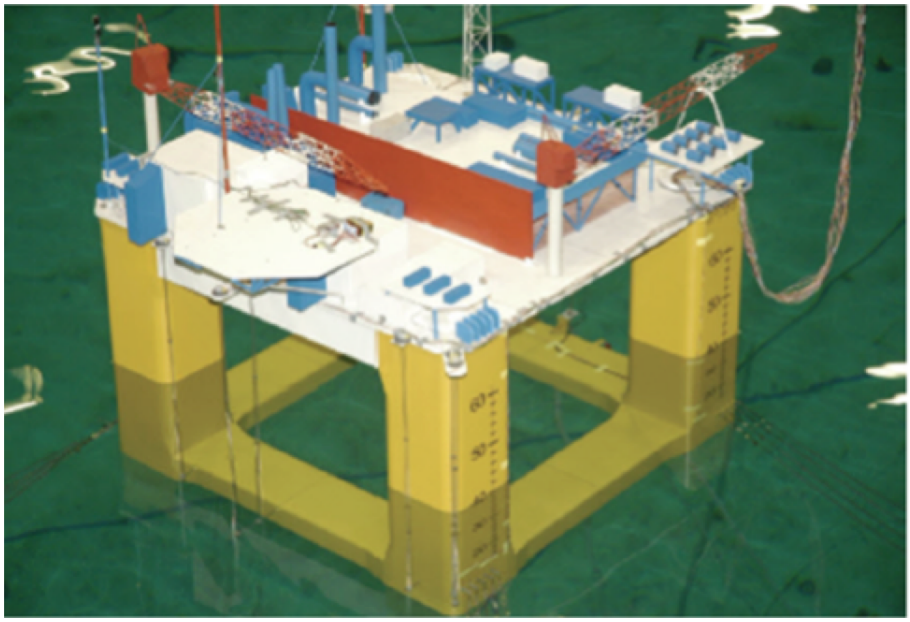

Figure 6.1: Model of deep draft semisubmersible DEMO2000.

The semisubmersible and its mooring system are designed for a water depth of 1500 m. The main parameters of the semisubmersible are presented in Table 6.1. Information provided beyond this is limited.

Displacement	75710 ton
Draught	40.0 m
Freeboard	24.0 m
Distance between cylinders	71.5 m
Cylinder cross section	15×15 m^2
Pontoon height	10.0 m

Table 6.1: Main parameters for DEMO2000.

The setup of the SIMO model in SIMA and an evaluation of the model data are in this chapter presented.

6.1 SIMO Model in SIMA

The semisubmersible with mooring system is modeled in SIMO using SIMA. In the following, a description of the coordinate systems and the setup of the SIMO model in SIMA are presented.

6.1.1 Coordinate Systems

SIMO applies four right-handed Cartesian coordinate systems, with positive rotations defined counter-clockwise.

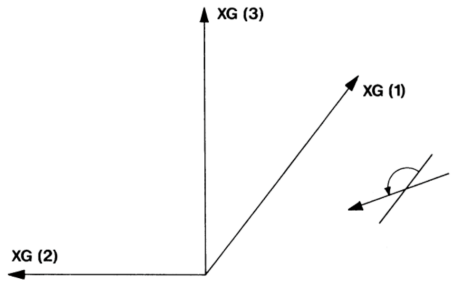

Figure 6.2: The global earth-fixed coordinate system (Marintek, 2013).

The global earth-fixed coordinate system, XG, is presented in Figure 6.2. The xy-plane coincides with the calm water plane, and the z-axis is pointing upwards. This coordinate system works as a reference for all positions of the local systems. In addition, all user specified propagation directions of the environment refers to this coordinate system.

A local body-fixed coordinate system, XB, follows the body motions, and is used to describe the coordinates of positioning elements and coupling elements.

The body horizontal motion of the floating vessel is following the body-related coordinate system, XR. The z-axis is pointing upwards, while the xy-plane is located at the calm water surface. Most force coefficients

and motion transfer functions refers to this coordinate system.

Coordinate systems XG, XB and XR are shown together in Figure 6.3.

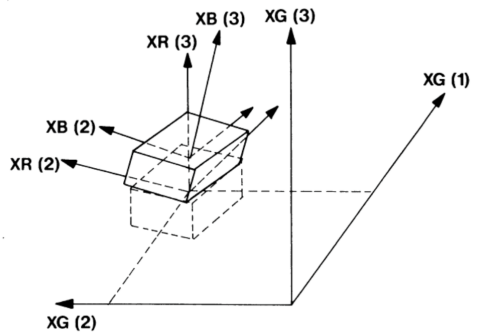

Figure 6.3: Global, local and body-related coordinate systems (Marintek, 2013).

The initial coordinate system, XI, coincides with the body-related coordinate system when the time domain simulation starts, and remains fixed throughout the simulation. First-order wave forces and wave drift may be pregenerated in this coordinate system. (Marintek, 2013).

6.1.2 Arrangement of SIMO Model

The model is created through a SIMO task. Two options are available, either the model can be modeled from scratch in SIMA, or data may be imported to the task. SIMA supports input from:

- MIMOSA
- SESAM SIF
- SIMO System Description File
- VERES
- WAMIT

The model in this master thesis is based on the input files from MIMOSA used in the project thesis. Hence, the *Vessel Description File* and the *Mooring System File* is imported into the SIMO task.

Figure 6.4 presents the setup of the SIMO model for this master thesis. The model data is divided into three main categories:

- Model
- Variables
- Conditions

A further description of these categories is presented in the following.

Model

Model contains all the data describing the simulation model, the simulation environment and the calculation parameters of the simulation.

Bodies

This subcategory contains the all the data about the model to be analyzed. This data is divided into three groups:

- Body Points
- Caternary System
- Kinetics

Body Points contains a list of the attachment points at the semisubmersible of all the mooring lines. The points are given by x-, y- and z-coordinate according to the body fixed coordinate system.

Catenary System is divided into two groups; *Catenary Lines* and *Segmented Line Types*. The data included in *Catenary Lines* may be presented in three different ways. Either by anchor position specified by horizontal distance and direction, anchor position specified by global x- and y-coordinate or by anchor position specified by line pretension. Breaking strength of each mooring line is also included here. *Segmented Line Types* includes all data concerning line characteristics.

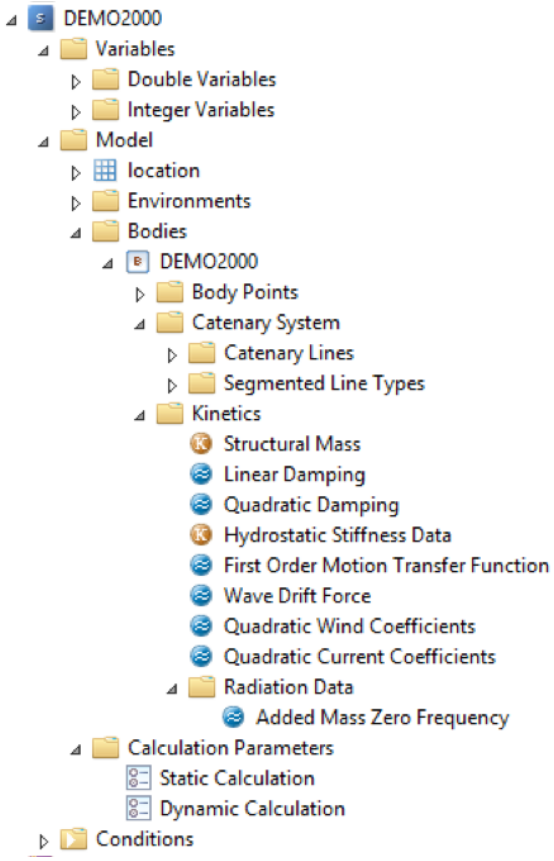

Figure 6.4: Setup of model in SIMO

Kinetics contains all necessary data concerning the semisubmersible. The data included here depends on the body type chosen for the analysis in SIMO. There are four different body types available:

1 Large volume, with total motion simulated in the TD (6 d.o.f.)
2 Large volume, with separation of motions in FD WF motions and TD LF motions (6 d.o.f.)
3 Small volume, with position dependent hydrodynamic coefficients (3 translational d.o.f.)
4 As 1 but with fixed or prescribed body position

Bode type number 2 is used for the model in this master thesis. Thus, *Kinetics* includes structural mass, linear damping, quadratic damping, hydrostatic stiffness, first order wave force transfer function, wave drift force, quadratic wind coefficients and quadratic current coefficients. Radiation data is also included here,

containing added mass zero frequency.

Environments

The different combinations of waves, wind and current can here be stored into several simulation environments. These environments are used in the analysis of the model.

Calculation Parameters

This subcategory is divided into parameters for static calculation and dynamic calculation. The parameters for the static calculation can here be specified, or set as default for either marine operations or SIMO. The default settings for SIMO are used in this thesis work, as this is suitable for positioning analysis. Whether to calculate equilibrium and eigenvalues can also be specified here. It is also possible to select bodies and degrees of freedom to omit from the analysis. The dynamic calculation parameters include simulation length, time step, time series generation parameters and parameters concerning the numerical procedure.

Variables

Variables may be created and assigned to an object value. There are three types of variables:

- Double Variable
- Integer Variable
- String Variable

Double variables and integer variables are typically used to vary numbers and integer numbers, respectively. A string variable is typically used to vary a file path.

Conditions

This is the part of the SIMO task where the analysis is run and the results are studied. There are four types of conditions:

- Initial
- Condition
- Condition Set
- Condition Space

The initial condition is a special unmodifiable condition automatically created in the SIMO task. In this condition the first environment is selected and all variables have their default value.

A condition defines a run as an initial condition does, but environment and variables may be freely chosen.

A condition set defines a list of runs, or a parameter variation, based on variables defined in the SIMO task,

while other variables may be fixed for all runs.

A condition space is used to create a matrix of runs based on variables defined in the SIMO task. All variable values are run against each other.

6.2 Evaluation of Simulation Model

In order for the results from the analysis to be reliable, the model data provided to SIMO needs to be correct. An evaluation of the data concerning the model is therefore carried out.

The evaluation is carried out in accordance with the rigid-body motions defined in Figure 6.5.

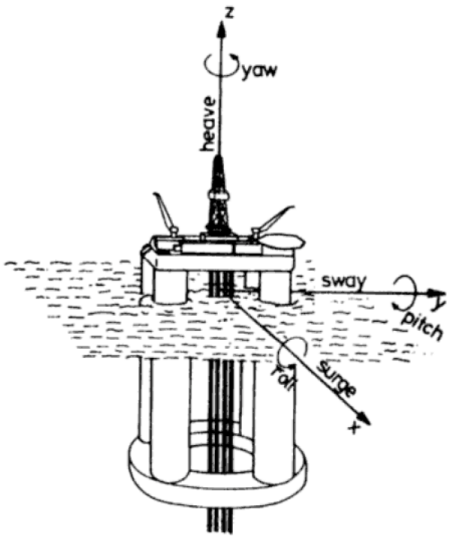

Figure 6.5: Definition of rigid-body motion modes (O. M. Faltinsen, 1990).

6.2.1 Assumptions

The following assumptions are made for the evaluation of the model:

- Added mass is not included in the model received from Statoil. An assumption of added mass equal to 50% of the structural mass is therefore assumed and included in the added mass zero frequency matrix, based on personal correspondence with the supervisor.
- The original mooring system provided by Statoil was modified in the project thesis. The modifications included reducing the number of mooring lines from 18 lines to 16 lines. The mooring line diameters were also reduced. This modification was made as the mooring system gave very high safety factors for the maximum design condition applied. All these modifications are kept for further analysis in this

master thesis.

- Due to large forces form the mooring system on the semisubmersible, the mean displacement in heave is observed to be below the waterline for the model. This could have been adjusted by applying a fixed force in the positive z-direction compensating for the large force from the mooring system. However, this was not included for the evaluation of the model presented in the following.

6.2.2 Hydrostatic Stiffness

A verification of the hydrostatic stiffness of the semisubmersible is performed for the motions in the vertical plane, including heave, roll and pitch, in accordance with (B. Pettersen, 2004).

Hydrostatic stiffness in heave, K_{33}, will be proportional to the water plane area given by

$$K_{33} = \rho g A_{\text{water plane}} \tag{6.1}$$

where ρ is water density, g is gravity and $A_{\text{water plane}}$ is water plane area. For the semisubmersible, the water plane area will equal the area of the cylinders. The cylinders are square shaped, with dimensions $15m \times 15m$.

The hydrostatic stiffness in roll and pitch are both calculated assuming a natural period of 60 s in these degrees of freedom, based on (K. Larsen, 2015). The period for rotations are given by

$$T_i = 2\pi \sqrt{\frac{I_{ii} + A_{ii}}{\rho g \nabla GM}} \tag{6.2}$$

where I_{ii} is the moment of inertia and A_{ii} is the added mass for mode i, ∇ is the displacement and GM is the metacentric height.

The hydrostatic stiffness is given by

$$K_{ii} = \rho g \nabla GM \tag{6.3}$$

Hence, the hydrostatic stiffness is estimated by

$$K_{ii} = \rho g \nabla GM = \frac{4\pi^2 (I_{ii} + A_{ii})}{T_i^2} \tag{6.4}$$

As moment of inertia and added mass are the same for this semisubmersible in roll and pitch, the hydrostatic stiffness is the same in these degrees of freedom.

The calculated hydrostatic stiffness for DEMO2000 is presented in Table 6.2.

	Translations $[N/m]$			Rotations $[Nm]$		
	Surge	Sway	Heave	Roll	Pitch	Yaw
Hydrostatic stiffness	0.00	0.00	$9.05 \cdot 10^6$	$1.83 \cdot 10^9$	$1.83 \cdot 10^9$	0.00

Table 6.2: Hydrostatic stiffness of DEMO2000.

6.2.3 Natural Periods

Further, the natural periods of DEMO2000 are estimated based on decay tests and restoring forces.

Pullout tests were performed in SIMO in all six degrees of freedom. The restoring forces established form these tests are presented in Figure 6.6.

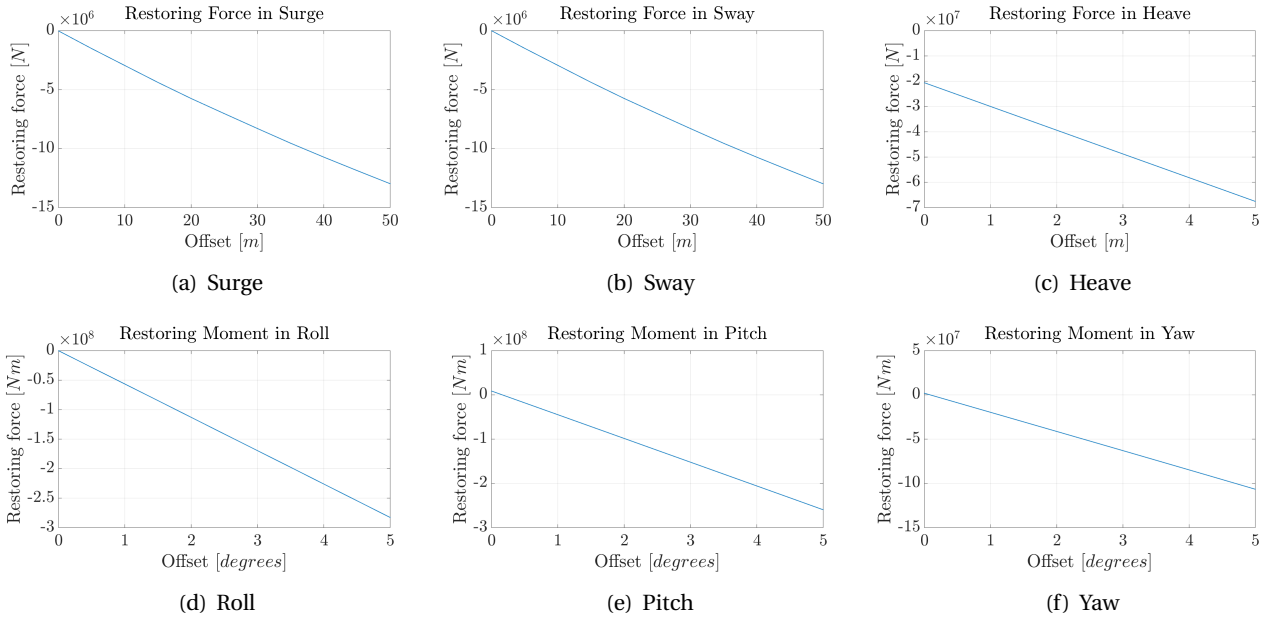

(a) Surge (b) Sway (c) Heave

(d) Roll (e) Pitch (f) Yaw

Figure 6.6: Restoring forces and moments.

The natural period, T_i, is then calculated by

$$T_i = 2\pi\sqrt{\frac{M + A_{ii}}{K_{ii,linear}}} \tag{6.5}$$

for the translations, and by

$$T_i = 2\pi\sqrt{\frac{I_{ii} + A_{ii}}{K_{ii,linear}}} \tag{6.6}$$

for the rotations. M is the structural mass, $K_{ii,linear}$ is the linearized stiffness found from the restoring curve, I_{ii} is moment of inertia and A_{ii} is added mass in mode i.

Decay tests were also performed in SIMO for all six degrees of freedom. All additional damping is removed from the system during these tests. The decay tests are presented in Figure 6.7.

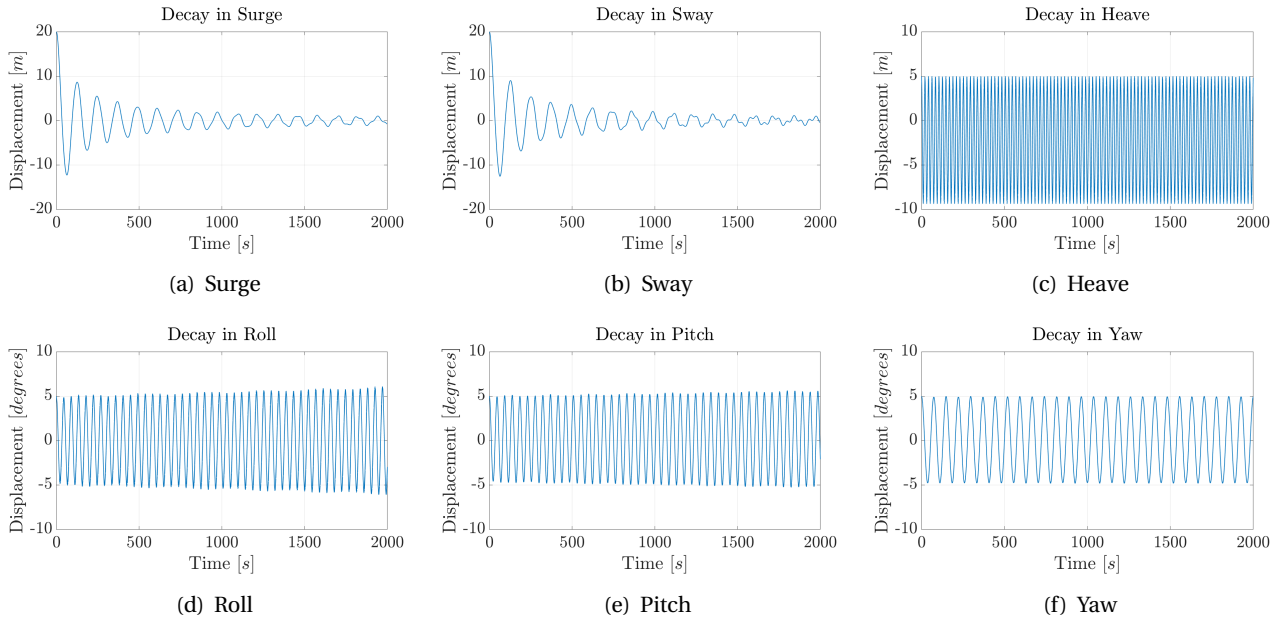

(a) Surge (b) Sway (c) Heave

(d) Roll (e) Pitch (f) Yaw

Figure 6.7: Decay tests.

The natural periods calculated from the restoring forces and estimated from the decay test shows good compliance for each degree of freedom. The natural periods of DEMO2000 are presented in Table 6.3.

	Surge	Sway	Heave	Roll	Pitch	Yaw
Natural period [s]	120.6	120.4	21.4	47.6	46.3	72.5

Table 6.3: Natural periods of DEMO2000.

6.2.4 Damping

The damping level of a semisubmersible is, according to the supervisor, empirically estimated to equal about 40% of the critical damping. In order to achieve this damping level in the model, additional linear damping is included. This additional damping accounts for viscous damping and damping from the mooring system.

Critical Damping

The critical damping of DEMO2000 is established through the calculations presented in the following.

The critical damping of the system in mode i, $C_{ii,critical}$, is calculated by

$$C_{ii,critical} = 2\sqrt{(M + A_{ii})K_{ii,linear}} = 2(M + A_{ii})\omega_{i,0} \tag{6.7}$$

for the translations and by

$$C_{ii,critical} = 2\sqrt{(I_{ii} + A_{ii})K_{ii,linear}} = 2(I_{ii} + A_{ii})\omega_{i,0} \tag{6.8}$$

for the rotations. M is the structural mass, $K_{ii,linear}$ is the linearized stiffness, A_{ii} is added mass, I_{ii} is moment of inertia and $\omega_{i,0}$ is the natural frequency for mode i.

The calculated critical damping values are presented in Table 6.4.

	Translations $[Ns/m]$			Rotations $[Nsm]$		
	Surge	Sway	Heave	Roll	Pitch	Yaw
Critical damping	$1.1 \cdot 10^7$	$1.1 \cdot 10^7$	$6.3 \cdot 10^7$	$4.4 \cdot 10^{10}$	$4.5 \cdot 10^{10}$	$2.9 \cdot 10^{10}$

Table 6.4: Critical damping of DEMO2000.

Added Linear Damping

The decay test for surge and sway presented in Figure 6.7 show some damping present in these degrees of freedom. This damping is caused by the current model, as force from current in SIMO is expressed by

$$q_{cu}^{(i)} = C_1^{(i)}|v_1 - \dot{x}_1|^2 + C_2^{(i)}|v_2 - \dot{x}_2|^2 \tag{6.9}$$

where i is the degree of freedom, C_1 and C_2 is linear and quadratic current force coefficient respectively, v_1 and v_2 is the current velocity components and x_1 and x_2 are the vessel velocity components.

According to this current model, force from current will be present as there is a relative velocity between the vessel and the fluid. As only quadratic current coefficients are defined in this model, the damping observed for both surge and sway will be on the form

$$q_{cu}^{(i)} = -C_2^{(i)}|\dot{x}_2|\dot{x}_2 \tag{6.10}$$

The fact that this is a quadratic damping can be observed by the way the damping is large for large velocities, and relatively small damping for small velocities.

In order for the total damping level to equal about 40 % of the critical damping, the magnitude of this damp-

ing is estimated. The calculation is performed accordance with (C. M. Larsen, 2014).

As observed from the decay test, the damping in surge and sway is subcritical. The oscillations, $u(t)$, are hence assumed to follow the expression

$$u(t) = e^{-\xi\omega_0 t} R cos(\omega_d t - \theta) \tag{6.11}$$

where ξ is the damping ratio, ω_0 is the natural frequency, t is time, $R = (u_0^2 + \frac{\dot{u}_0}{\omega_0^2})^{\frac{1}{2}}$ is the amplitude, θ is the phase angle and ω_d is the damped natural frequency defined by

$$\omega_d = \omega_0\sqrt{1-\xi^2} \tag{6.12}$$

The damping is estimated by the relation of the amplitudes at the time t_i and $t_i + nT_d$, where T_d is the damped natural period. This relation is given by

$$\frac{u_i}{u_{i+n}} = \frac{u(t_i)}{u(t_i + nT_d)} = \frac{e^{-\xi\omega_0 t_i} R cos(\omega_d t_i - \theta)}{e^{-\xi\omega_0 (t_i + nT_d)} R cos(\omega_d (t_i + nT_d) - \theta}) = e^{\xi\omega_0 nT_d} \tag{6.13}$$

The logarithmic decrement of damping, Λ, is given by

$$\Lambda = ln(\frac{u_i}{u_{i+1}}) \tag{6.14}$$

where u_i and u_{i+1} is two amplitudes with a interval of T_d.

The relation between Λ and the damping ratio ζ is then found by

$$\Lambda = \xi\omega_0 T_d = 2\pi\frac{\xi}{\sqrt{1-\xi^2}} \tag{6.15}$$

assuming small ξ, this relation may be written

$$\Lambda = 2\pi\xi \tag{6.16}$$

The damping in translation mode i, C_{ii}, is then estimated by

$$C_{ii} = 2\xi\omega_{i,0}(M + A_{ii}) \tag{6.17}$$

where M is structural mass, $\omega_{i,0}$ is the natural frequency and A_{ii} is added mass in mode i.

The additional damping included in the linear damping matrix is presented in Table 6.5.

	Translations $[Ns/m]$			Rotations $[Nsm]$		
	Surge	Sway	Heave	Roll	Pitch	Yaw
Linear damping	$3.8 \cdot 10^6$	$3.8 \cdot 10^6$	$2.5 \cdot 10^7$	$1.8 \cdot 10^{10}$	$1.8 \cdot 10^{10}$	$1.1 \cdot 10^{10}$

Table 6.5: Added linear damping.

6.2.5 Excitation Forces

The excitation forces from waves, wind and current are included in the model as force coefficients and transfer functions. All plots of the excitation forces are included in Appendix A.

The excitation forces from waves, wind and current are all defined as going towards in SIMO, in accordance with Figure 6.8.

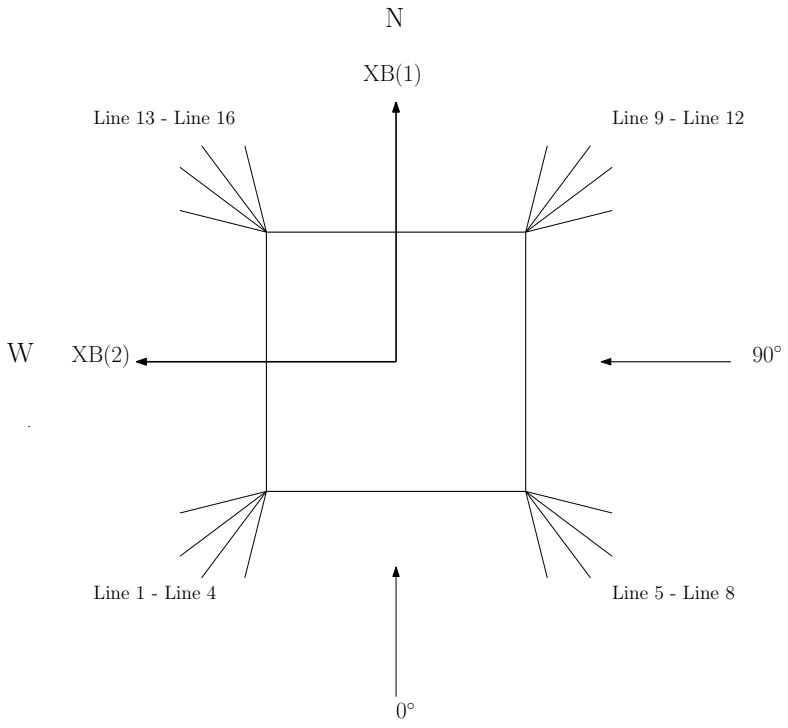

Figure 6.8: Environmental loading directions for DEMO2000 in SIMO.

Considering the given coordinate system for the semisubmersible, for 0° the direction of the environmental loads will be in the positive x-direction. At 90° the environmental loads will act in the positive y-direction, while for 180° the environmental loads will be in the negative x-direction.

A verification of the excitation forces is presented in the following.

Quadratic Current Coefficients

The quadratic current coefficients are given in the range 0° to 180°. Plots of the current coefficients are given in Appendix A.1.

In surge, the current coefficient is positive at 0°, zero at 90° and negative at 180°. While for sway the coefficient is zero at 0° and 180°, and with a positive maximum at 90°. Considering the given coordinate system, this is reasonable.

The forces in y-direction, creating sway motions, are dominating in order to obtain roll. Hence, a coincidence between the current coefficient for roll and sway is expected. As roll motion are defined positive for counter-clockwise rotations about the x-axis, the current coefficient will be zero at 0° and 180°, while a positive maximum will be present at 90°.

The forces in x-direction, creating the surge motions, are dominating in order to obtain pitch. Similarities in the current coefficient for surge and pitch are thus expected. As pitch motion are defined positive for counter-clockwise rotations about the y-axis, the current coefficient will be negative for 0°, zero at 90° and positive 180°.

Both current coefficients in heave and yaw are here neglected. For yaw this can be justified by the symmetry of the submerged part of the structure.

Quadratic Wind Coefficients

The quadratic wind coefficients are given in the range 0° to 180°. Plots of the wind coefficients are given in Appendix A.2.

For surge, the wind coefficient is positive at 0° and negative at 180°. At 90° the wind coefficient is zero, due to no force acting in the x-direction. The wind coefficient in sway at 0° and 180° are both zero, as there are no force contribution in y-direction. In the range 50° to 125°, the wind coefficient has its maximum positive values, with two local extreme points at 60° and 110°. Hence, the wind coefficient is not at maximum value for sway when the wind is acting directly in the y-direction, but at some degrees higher and lower than this. This may be explained by the exposed area at the top side. The shadowing effects will here obviously be larger when the wind is coming from 60° and 110°.

The same will be valid for the roll and pitch motions as for the current coefficients. Hence, roll will mainly depend on sway motion and pitch will mainly depend on surge motion, resulting in similarities in the plots. However, the wind force will attack the top side of the semisubmersible.

Both wind coefficients in heave and yaw is here neglected.

Wave Drift Force Coefficients

The wave drift force coefficients are plotted against period for the directions 0°, 45° and 90° in Appendix A.3.

In general, large forces will be present when the period is small, and then decrease with increasing period. This can be justified by the explanation that for small periods the floater appears as a solid wall, while for large periods the floater will follow the wave motion.

The coefficient in surge has its largest positive values for the direction of 0°, some smaller positive values for 45° and zero 90°. While the coefficients in sway have its largest positive values for 90°, some smaller positive values for 45° and zero for 0°. Given the coordinate system this is reasonable.

The wave drift force in heave is neglected.

The wave drift coefficients in roll and pitch are also here similar to the coefficients in sway and surge, respectively. The wave drift force will act on the deep draft semisubmersible in the water surface. The coefficient in roll will therefore have maximum negative values for direction of 90°, some smaller negative values for 45° and no contribution for 0°. Similarly, the coefficient in pitch will have maximum positive values for 0°, smaller positive values for 45° and no contribution for 90°.

Generally, no clear pattern can be justified for the coefficient in yaw.

Several local maxima/minima points are observed in the wave drift force coefficient plots. The points occurring in the period range 5 *s* - 10 *s* are probably caused by cancellation effects. In addition, all plots present a peak at a period of about 23 *s*. This is the heave resonance, as observed in the transfer function in heave.

First Order Motion Transfer Functions

The first order motion transfer functions for the semisubmersible are plotted against period for the directions 0°, 45° and 90° in Appendix A.4.

The first order wave forces are in SIMO described in the frequency domain as a transfer function between wave elevation and force, given by equation 4.19 in section 4.1.3 (Marintek, 2013).

The resonance response in surge and sway for a semisubmersible is located at a period larger than 100 *s* (K. Larsen, 2015). Since the plots are given in the range 5 $s \leq T \leq 30$ *s*, the resonance peaks for surge and sway are therefore not present in these plots. The transfer function in surge has its largest value for 0°, some smaller values for 45° and is zero for 90°. While for the transfer function in sway, the largest values are given for 90°, smaller values for 45° and zero for 0°. Both transfer functions approaches an amplitude equal one for large

periods. This is reasonable, as the semisubmersible will follow the wave motion at large periods. Hence, this corresponds well with the expected.

The response in heave for a semisubmersible will have a resonance period in the range 20 *s* - 25 *s* (K. Larsen, 2015). The plot shows a resonance peak at about 23 *s*. This is thus reasonable. Some cancellations, or counteracting, effects can be observed in the plot. In addition, it can be observed that the amplitude at about 15 *s* is below 0.4. It is desirable to keep this value low for a deep draft semisubmersible as a large amount of wave energy is found in the range 10 *s* - 20 *s*. A value below 0.4 is acceptable.

Roll and pitch will for a semisubmersible have a period located in the range of 45 *s* - 60 *s* (K. Larsen, 2015). Thus the resonance peak is not present is not present in the plot. The plots are reasonable in the sense that the amplitudes are for roll and pitch present for 90° and 0°, respectively. Both plots have smaller amplitudes at 45°, and an amplitude of zero is found for pitch at 90° and for roll at 0°.

The response in yaw will have resonance at a period equal or larger than 100 *s* (K. Larsen, 2015). As seen from the plot, the amplitudes for the transfer functions in yaw are very small. This can be justified by the symmetry of the hull.

6.2.6 Mooring System

The mooring system consists of 16 mooring lines divided into four groups. Each group contains four mooring lines, and is located at a corner of the semisubmersible as shown in Figure 6.9.

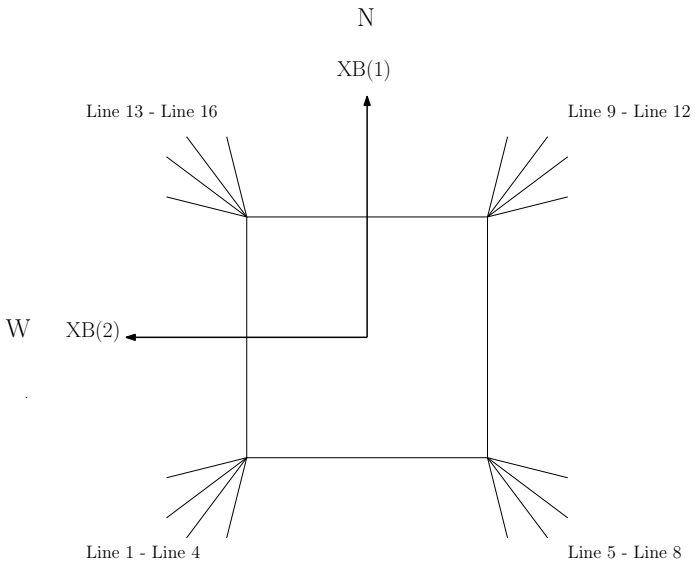

Figure 6.9: Semisubmersible with mooring lines in body related coordinate system.

Two different line characteristics are present in the model. Mooring line 1 - 8 have line characteristic 1, while mooring line 9 - 16 have line characteristic 2. The composition of the mooring lines are presented in Figure 6.10 and the mooring segment properties of line characteristic 1 and line characteristic 2 are listed in Table 6.6 and Table 6.7, respectively.

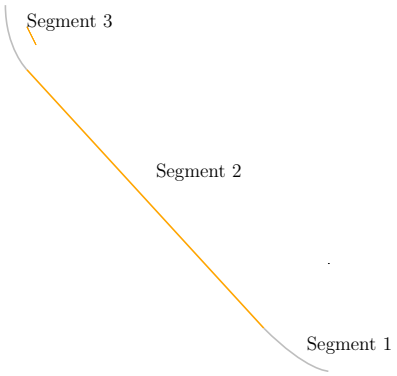

Figure 6.10: Composition of mooring line.

	Type	Length $[m]$	Diameter $[m]$	Modulus of Elasticity $[N/m^2]$	Weight in air $[N/m]$	Transverse drag $[-]$	Longitudinal drag $[-]$
Segment 1	Chain	150	0.1064	$3.5 \cdot 10^{10}$	2220.8	2.6	1.4
Segment 2	Polyester	2100	0.1792	$6.003 \cdot 10^{9}$	205.7	1.6	0.1
Segment 3	Chain	142	0.1064	$3.5 \cdot 10^{10}$	2220.8	2.6	1.4

Table 6.6: Mooring line segment properties for line characteristic 1.

	Type	Length $[m]$	Diameter $[m]$	Modulus of Elasticity $[N/m^2]$	Weight in air $[N/m]$	Transverse drag $[-]$	Longitudinal drag $[-]$
Segment 1	Chain	150	0.1064	$3.5 \cdot 10^{10}$	2220.8	2.6	1.4
Segment 2	Polyester	2100	0.1792	$6.003 \cdot 10^{9}$	205.7	1.6	0.1
Segment 3	Chain	159	0.1064	$3.5 \cdot 10^{10}$	2220.8	2.6	1.4

Table 6.7: Mooring line segment properties for line characteristic 2.

6.3 Analyzes Performed in Project Thesis

Analysis of the mooring system based on the system provided by Statoil, presented in section 6.2.6, was in the project thesis performed in the frequency domain using the software MIMOSA. The analyzes were

performed in accordance with the design regulations presented in Chapter 3 for both intact mooring system and for mooring system with one line failure.

6.3.1 Maximum Design Condition

The maximum design condition used in these analyzes were based on the metocean data from the Heidrun field (K. J. Eik and E. Nygaard, 2004), which is located in the Haltenbanken region of the Norwegian Sea.

The extreme wind speed with a return period of 100 years over a one hour average period 10 m above sea level for the Heidrun field was given as $U_{1hour,10m} = 36\ m/s$. The wind gust was defined by an ISO spectrum.

Figure 6.11 presents the extreme contour lines for 1, 100 and 10000-year condition. As required, 100-year combinations of H_s and T_p were applied in the analyzes. A double peak spectrum, also called the Torsethaugen spectral model, was here applied as the wave frequency spectrum. This spectrum is a superposition of two JONSWAP like spectra, where the first presents the wind sea and the second presents the swell system (K. J. Eik and E. Nygaard, 2004).

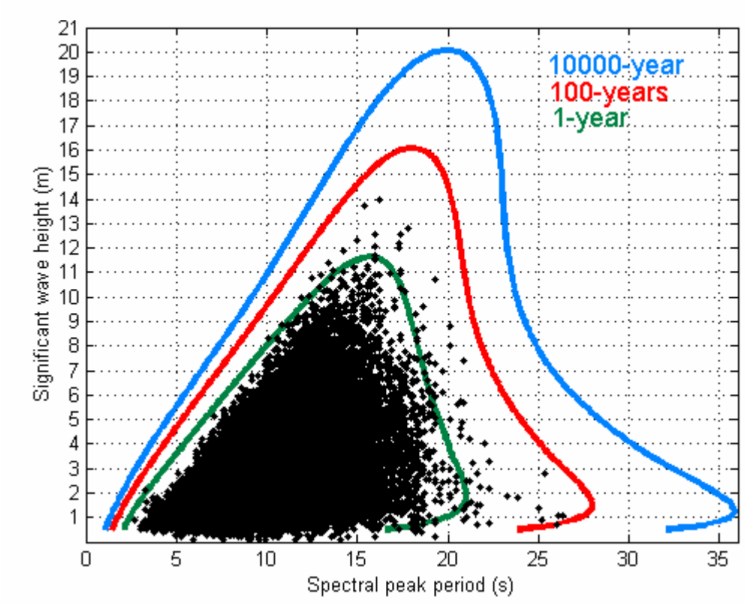

Figure 6.11: 1, 100 and 10000-year extreme contour lines in the H_s - T_p plane. Sea state duration: 3 hours (K. J. Eik and E. Nygaard, 2004).

Current speed was for the Heidrun field given for different depths. A simplification was here made by only considering the current surface speed, $V_c = 0.94\ m/s$ (K. J. Eik and E. Nygaard, 2004).

The three environmental conditions chosen for the analyzes carried out in the project thesis are presented

in Table 6.8. The conditions contained maximum wind speed, maximum current speed in the surface, and combinations of wave specific heights and wave peak periods on the 100-year contour line.

	$H_s\ [m]$	$T_p\ [s]$	$U_{1hour,10m}\ [m/s]$	$V_c\ [m/s]$
Condition 1	15.00	15.50	36.00	0.94
Condition 2	16.00	18.20	36.00	0.94
Condition 3	15.00	19.80	36.00	0.94

Table 6.8: Environmental conditions defined in project thesis.

In accordance with (DNV GL, 2013), in-line and in-between directions were analyzed. The waves, wind and current were assumed to all have the same direction.

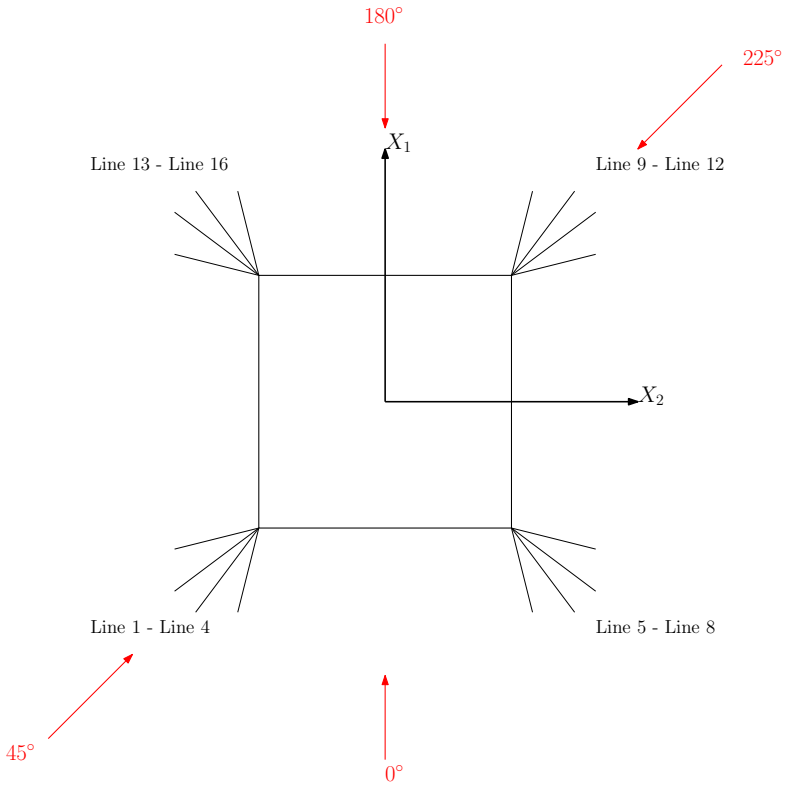

Figure 6.12: Environmental loading directions at DEMO2000 in MIMOSA coordinate system.

The directions analyzed in MIMOSA for these conditions included environmental loads propagating from South, Southwest, North and Northeast, as presented in Figure 6.12. In MIMOSA this corresponded to environmental loads applied from 0°, 45°, 180° and 225°, respectively.

The analyzes performed in MIMOSA stated that environmental load applied from the direction 225° was most critical for the semisubmersible. Out of the three environmental conditions analyzed, Condition 3 gave slightly larger motions and higher line tensions then the other two conditions.

6.4 Comparison of Results from SIMO and MIMOSA

In order to further control the model established in SIMO, a comparison of the result from MIMOSA and SIMO is presented in the following. However, the theory concerning frequency domain analysis and MIMOSA was covered in detail in the project thesis, and is therefor not covered in this master thesis.

The comparison is carried out for the most critical loading condition and direction established in the project thesis work, corresponding to Condition 3 applied from Northeast. Figure 6.13 present a comparison of the coordinate systems utilized in MIMOSA and SIMO. As seen from the figure, an environmental loading direction of 225° in MIMOSA corresponds to a direction of 135° in SIMO.

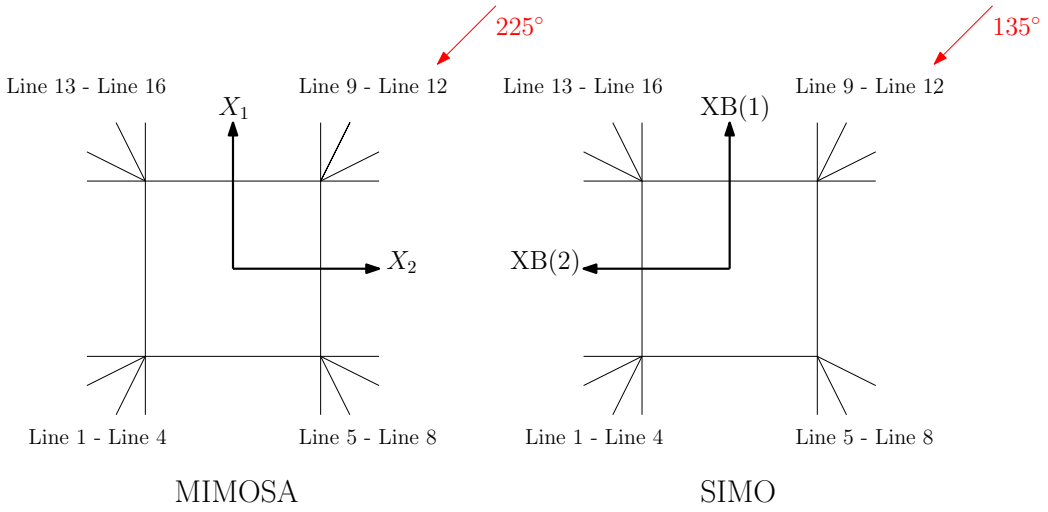

Figure 6.13: Composition of coordinate systems in MIMOSA and SIMO.

The simulation length in SIMO is here set to three hours.

6.4.1 Natural Periods

Natural periods are for MIMOSA calculated based on the mass and stiffness matrix using equation 6.5 and equation 6.6. A comparison of the natural periods calculated in MIMOSA and SIMO is presented in Table 6.9.

	Natural period [s]					
	Surge	Sway	Heave	Roll	Pitch	Yaw
MIMOSA	125.9	126.4	21.5	45.8	46.3	68.4
SIMO	120.6	120.4	21.4	47.6	46.3	72.5

Table 6.9: Natural periods of DEMO2000 estimated in MIMOSA and SIMO.

A good correspondence between the natural periods calculated in MIMOSA and SIMO is observed in the table. The largest deviations for the natural periods are present for surge and sway. However, these deviations are within a reasonable range.

6.4.2 Restoring Curves

The restoring curves calculated in MIMOSA and SIMO are presented in Figure 6.14.

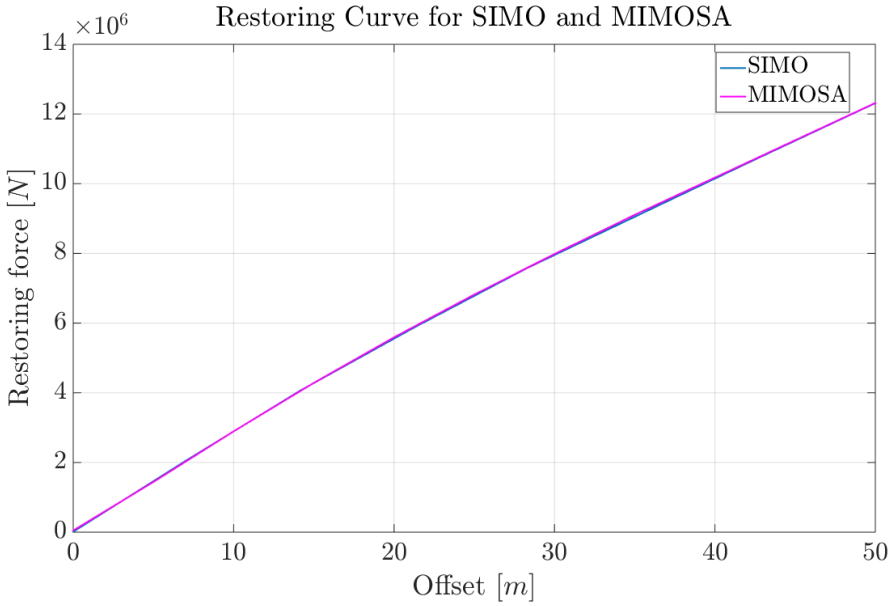

Figure 6.14: Restoring curve in direction 225° (MIMOSA) and 135° (SIMO).

As seen from the figure, there is a good correspondence of the restoring curve estimated in MIMOSA and SIMO.

6.4.3 Static Forces and Moments

Static forces and moments on DEMO2000 calculated in MIMOSA and SIMO is presented in Table 6.10 and 6.11, respectively. The static forces from SIMO is an average of 20 realizations.

	Static forces $[N]$			Static moments $[Nm]$		
	Surge	Sway	Heave	Roll	Pitch	Yaw
Wind	$-3.7815 \cdot 10^6$	$-4.0625 \cdot 10^6$	0.0000	$-8.1251 \cdot 10^7$	$7.5630 \cdot 10^7$	0.0000
Wave drift	$-5.3650 \cdot 10^5$	$-5.3650 \cdot 10^5$	0.0000	$-2.1887 \cdot 10^6$	$2.1462 \cdot 10^6$	$-3.1500 \cdot 10^4$
Current	$-1.7170 \cdot 10^6$	$-1.7078 \cdot 10^6$	0.0000	$4.6111 \cdot 10^7$	$-4.1212 \cdot 10^7$	0.0000

Table 6.10: Static forces and moments on DEMO2000 in MIMOSA.

	Static forces $[N]$			Static moments $[Nm]$		
	Surge	Sway	Heave	Roll	Pitch	Yaw
Wind	$-3.8147 \cdot 10^6$	$4.0332 \cdot 10^6$	0.0000	$-8.0663 \cdot 10^8$	$-7.6296 \cdot 10^7$	0.0000
Wave drift	$-4.8886 \cdot 10^5$	$4.8886 \cdot 10^5$	0.0000	$-1.9555 \cdot 10^6$	$-1.9555 \cdot 10^6$	$5.0630 \cdot 10^3$
Current	$-1.7398 \cdot 10^6$	$1.7027 \cdot 10^6$	0.0000	$4.5974 \cdot 10^7$	$4.1759 \cdot 10^7$	0.0000

Table 6.11: Static forces and moments on DEMO2000 in SIMO.

As observed in the tables, small differences in the static forces are present. These deviations are due to the different calculation method used in MIMOSA and SIMO. However, the differences are neglectable.

6.4.4 Motions

The motions of the semisubmersible calculated in MIMOSA an SIMO are presented in Table 6.12. All motions in the table are given in the direction of loading. The $\overline{x}$, x_{sign}^{WF} and x_{sign}^{LF} are the mean motion, significant wave frequency motion and significant low frequency motion, which in SIMO are calculated as the mean value of 20 realizations. x_{max}^{WF}, x_{max}^{LF} and X_{max}^{TOT} is the maximum wave frequency motion, maximum low frequency motion and total maximum motion. These motions are the most probable maximum value determined by a Gumbel distribution of the maximum values of the 20 realizations, as described in section 4.3.3, carried out in SIMO.

	Motion $[m]$					
	$\overline{x}$	x_{max}^{WF}	x_{sign}^{WF}	x_{max}^{LF}	x_{sign}^{LF}	X_{max}^{TOT}
MIMOSA	34.65	7.24	4.10	12.39	7.45	51.00
SIMO	35.17	7.24	4.07	11.15	6.84	49.51

Table 6.12: Motion of DEMO2000 in MIMOSA and SIMO. Motion x is given in direction of loading.

As seen from the table, the values calculated in MIMOSA and SIMO are almost equal. A small difference is observed in the mean offset, $\overline{x}$, which may be explained by a small difference in the restoring curve shown in Figure 6.15

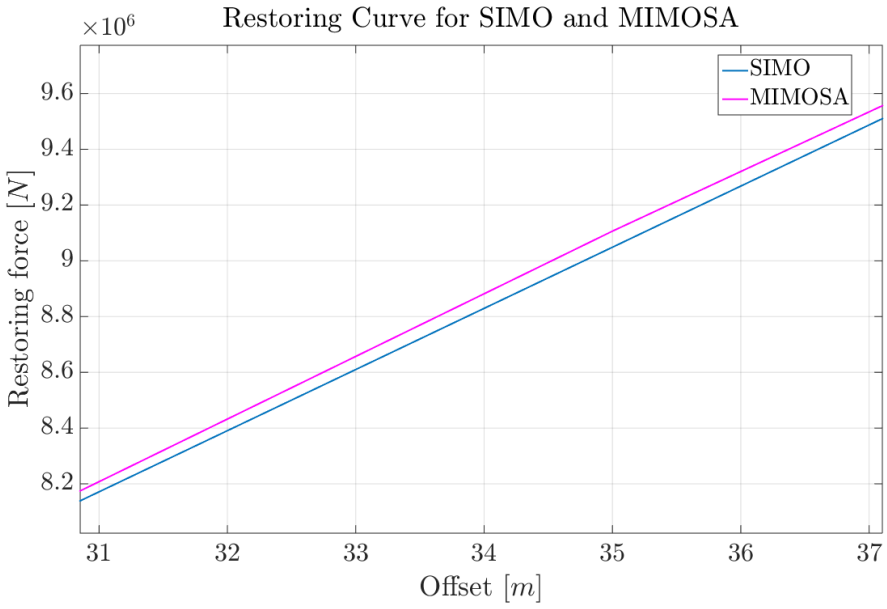

Figure 6.15: Cut out of restoring curve in direction 225° (MIMOSA) and 135° (SIMO).

as $\overline{x}$ is related to $K(x)$ by

$$K(x)\overline{x} = Q \tag{6.18}$$

However, this difference is neglectable.

6.4.5 Mooring Line Tensions

The tension of the most loaded line calculated in MIMOSA and SIMO is presented in Table 6.13. For SIMO, the maximum total top tension is the most probable maximum value determined by a Gumbel distribution of the maximum values of 20 realizations, described in section 4.3.3. The static value for SIMO is the mean value of 20 realizations. Quasi-static analysis of the mooring line tension is performed in both software.

		Top tension [kN]	
	Line	Static	Maximum total
MIMOSA	10	3472.2	4426.1
SIMO	10	3432.4	4323.0

Table 6.13: Comparison of top tension for MIMOSA and SIMO.

As seen from the table, minor differences are observed in the calculations performed in MIMOSA and SIMO. These differences are due to the difference in calculation method in MIMOSA and SIMO.

Chapter 7

Optimization of Mooring System for Deep Draft Semisubmersible

In this chapter, the automated optimization of the deep draft semisubmersible DEMO2000 is carried out. The optimization is carried out in SIMO, and includes only the mooring system. Optimization of cost for riser system and mooring system combined, as described in section 5.2, is not studied here.

The optimization includes two mooring systems with different composition of the mooring lines. Both systems consist of 16 mooring lines of the same length, with four mooring lines attached at each corner of the semisubmersible as presented in Figure 7.1.

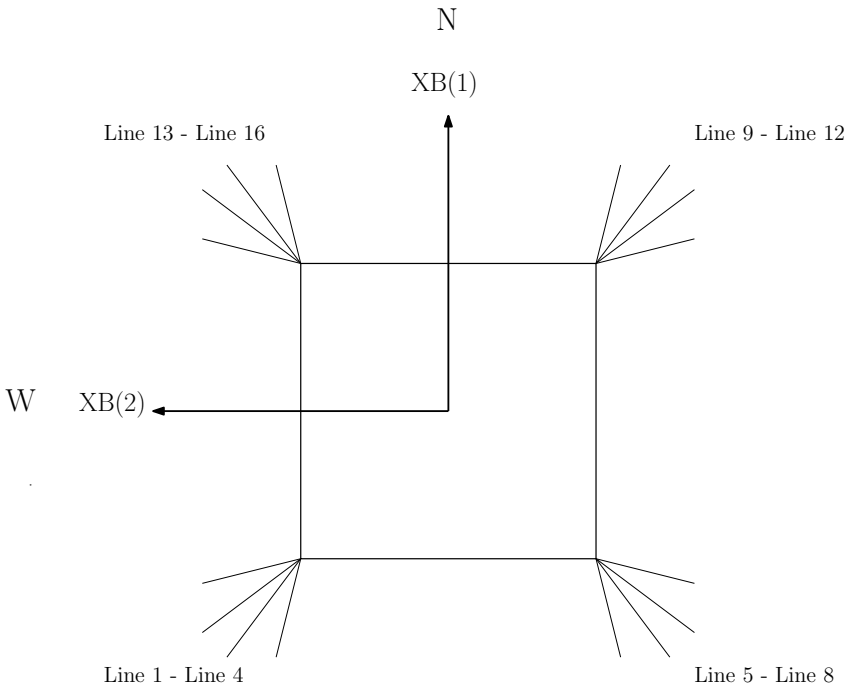

Figure 7.1: Semisubmersible with mooring lines in body related coordinate system.

One of the mooring systems is a combination of studless chain and steel wire rope, while the other is composed of studless chain and polyester rope.

7.1 Optimization Problem

The optimization problem for this master thesis concerns minimizing the cost of each of the two mooring systems.

Both mooring systems are optimized with respect to the maximum design condition found in the project thesis, presented in section 6.3. This corresponds the combination of waves, wind and current presented in Table 7.1.

$H_s\ [m]$	$T_p\ [s]$	$U_{1hour,10m}\ [m/s]$	$V_c\ [m/s]$
15.00	19.80	36.00	0.94

Table 7.1: Maximum design condition.

The environmental loads are applied propagating from Northeast, corresponding to 135° in SIMO.

7.1.1 Formulation of Optimization Problem

The optimization model including variables, objective function and constraints are presented in the following.

Variables

The optimization variables in this thesis include line and segment variables, as described in section 5.2.3.

The segment variables are the length and diameter of each of the three segments presented in Figure 6.10 in section 6.2.6. While the line variable is the pretension of the mooring lines. The pretension is included as an optimization variable in terms of the factor between pretension and breaking strength of the mooring lines. The factor is presented in equation 7.1

$$\text{Pretension factor} = \frac{\text{Pretension}}{\text{Minimum breaking load}} \tag{7.1}$$

with pretension defined as

$$\text{Pretension} = \text{Pretension factor} \cdot \text{Minimum breaking load} \tag{7.2}$$

Objective Function

The objective function, or cost function, is here defined as

$$\begin{aligned}\text{Cost of segments} = \frac{\pi}{4} \cdot (&\text{Length}_{\text{segment1}} \cdot \text{Weight in air}_{\text{segment1}} \cdot \text{Price}_{\text{segment1}} \\ &+\text{Length}_{\text{segment2}} \cdot \text{Weight in air}_{\text{segment2}} \cdot \text{Price}_{\text{segment2}} \\ &+\text{Length}_{\text{segment3}} \cdot \text{Weight in air}_{\text{segment3}} \cdot \text{Price}_{\text{segment3}})\end{aligned} \tag{7.3}$$

where length is given in m, weight in air is given in N/m and the price of the segment is given in NOK/N. The function provides the total cost of the segments for one mooring line.

Prices for chain, polyester and steel wire is presented in Table 7.2. These prices are estimates provided by Statoil.

	Chain	Steel Wire Rope	Polyester Rope
Price $[NOK/N]$	2.50	5.00	7.00

Table 7.2: Estimate of price of chain, steel wire rope and polyester rope given in NOK/N.

Constraints

Two constraints are applied in the optimization:

1. Constraint to the safety factor of the most loaded line, where

$$\text{SF} = \frac{\text{Minimum breaking load of mooring line}}{\text{Maximum tension in most loaded mooring line}} \tag{7.4}$$

2. Constraint to the total motion in direction of the environmental loading of the semisubmersible.

7.1.2 Optimization Cases

Three optimization cases are studied in this thesis. The cases are presented in Table 7.3.

	Case 1	Case 2	Case 3
Minimum SF	2.2	1.8	2.2
Maximum offset	150 m	150 m	75 m
Pretension	10 % - 25 % MBL	10 % - 25 % MBL	10 % - 25 % MBL

Table 7.3: Optimization cases.

The cases are based on correspondence with the supervisor. All cases are preformed for both the polyester rope and chain mooring system and the steel wire rope and chain mooring system.

Case 1 is the base case in this thesis. The case examines the optimization of a mooring system satisfying the regulations for the NCS with a safety factor of 2.2, as described in section 3.1.1. The maximum allowed offset is set to 10 % of the water depth, corresponding to 150 m. Pretension shall be in the range of 10 % to 25 % of the breaking strength of the mooring lines.

Case 2 investigates the impact of reducing the safety factor on the cost. An optimization with a SF of 1.8, and unchanged requirement to offset and pretension, is here performed.

Case 3 optimizes a mooring system with an allowable offset of 5 % of the water depth, corresponding to 75 m. This optimization considers a less flexible riser system, with stricter requirement to horizontal offset.

7.2 Mooring Systems

The initial mooring systems are described in detail in the following. The breaking strength, pretension and cost of the mooring line, in addition to safety factor and maximum offset of the initial mooring systems presented are all based on one realization. The optimization variables for the specific mooring system with minimum and maximum values are also presented.

7.2.1 Polyester Rope and Chain Mooring System

The mooring system consisting of polyester rope and chain is based on the mooring system presented in section 6.2.6. However, in order for changes in the variables to be accounted for correctly throughout the optimization, it is here necessary to base the data for the mooring line segments on (Bridon, 2013) and (Ramnäs Bruk, 2015). Small differences in the line characteristics are therefore present for the polyester rope and chain mooring system presented in this chapter compared to the mooring system introduced in Chapter 6. For simplicity, one line characteristic is applied for all mooring lines.

Initial Mooring System

The mooring lines consist of a combination of studless chain and superline polyester rope. The line characteristic for the mooring line is presented in Table 7.4, with the mooring line segments as given in Figure 6.10 in section 6.2.6.

	Type	Length [m]	Diameter [m]	Weight in air [N/m]	Modulus of Elasticity [N/m^2]	Transverse drag [$-$]	Longitudinal drag [$-$]
Segment 1	Chain	150	0.107	2246.5	$3.500 \cdot 10^{10}$	2.6	1.4
Segment 2	Polyester	2100	0.185	214.8	$6.003 \cdot 10^{9}$	1.6	0.1
Segment 3	Chain	159	0.107	2246.5	$3.500 \cdot 10^{10}$	2.6	1.4

Table 7.4: Initial mooring line segment properties for polyester rope and chain mooring system.

The breaking strength, pretension and cost of the mooring line, in addition to safety factor and maximum offset of the initial mooring system is presented in Table 7.5.

Constrains				
Safety factor [-]	Offset [m]	MBL [N]	Pretension [N]	Cost [NOK]
2.2075	48.5210	$9.8100 \cdot 10^{6}$	$1.7650 \cdot 10^{6}$	$4.7109 \cdot 10^{6}$

Table 7.5: Parameters for initial polyester rope and chain mooring system.

Figure 7.2 shows the mooring system as presented in SIMO.

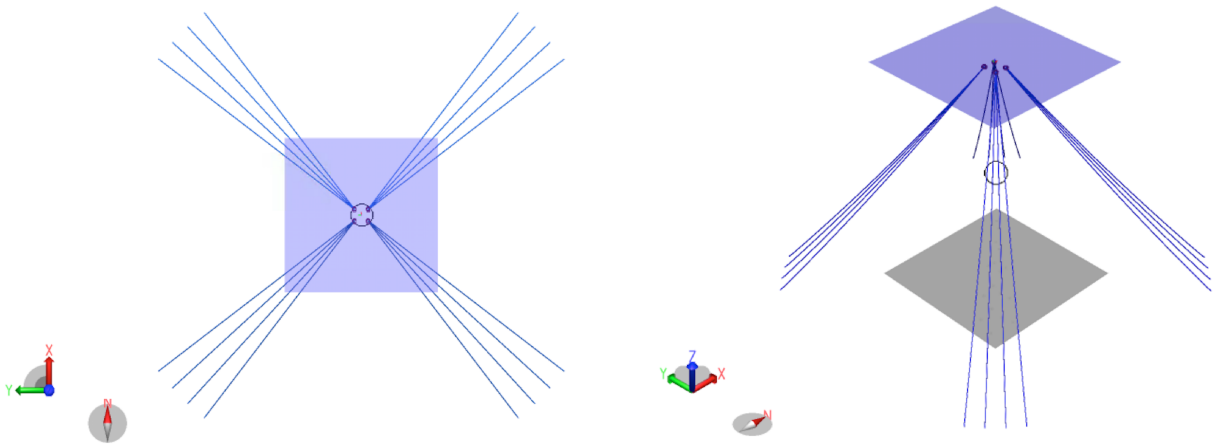

(a) Mooring system viewed diagonally

(b) Mooring system view from above

Figure 7.2: Polyester rope and chain mooring system in SIMO.

Optimization Variables

The optimization variables with maximum, minimum and delta value are presented in Table 7.6.

		Diameter			Length		
		Segment 1	Segment 2	Segment 3	Segment 1	Segment 2	Segment 3
Type		Chain	Polyester	Chain	Chain	Polyester	Chain
Initial Value	[m]	0.107	0.185	0.107	150	2100	159
Min Value	[m]	0.076	0.126	0.076	50	150	50
Max Value	[m]	0.177	0.296	0.177	500	3500	500
Delta	[-]	0.001	0.001	0.001	0.1	0.1	0.1

Table 7.6: Optimization variables for polyester rope and chain mooring system.

The choice of the minimum and maximum values of the segment diameters are based on (Ramnäs Bruk, 2015) and (Bridon, 2013). The minimum value of segment 1 and segment 3 is chosen in order to allow for winching and to avoid seabed contact for the polyester rope, respectively. The maximum and minimum value of segment 2 is based on an iteration process in MIMOSA. Delta values are chosen based on correspondence with co-supervisor.

7.2.2 Steel Wire Rope and Chain Mooring System

A mooring system consisting of steel wire rope and chain is constructed based on the polyester rope and chain mooring system.

Initial Mooring System

The mooring lines consist of a combination of studless chain and spiral stand wire rope with plastic sheathing. There are 16 mooring lines. The line characteristics are presented in Table 7.7, with mooring line segments as given in Figure 6.10 in section 6.2.6.

	Type	Length [m]	Diameter [m]	Weight in air [N/m]	Modulus of Elasticity [N/m^2]	Transverse drag [$-$]	Longitudinal drag [$-$]
Segment 1	Chain	800	0.107	2246.5	$3.500 \cdot 10^{10}$	2.6	1.4
Segment 2	Steel Wire	1800	0.110	571.9	$1.140 \cdot 10^{11}$	1.2	0.1
Segment 3	Chain	159	0.107	2246.5	$3.500 \cdot 10^{10}$	2.6	1.4

Table 7.7: Initial mooring line segment properties for steel wire rope and chain mooring system.

The diameters of segment 1 and segment 3 are the same as for the mooring system consisting of polyester rope and chain. The diameter of segment 2 is chosen based on a typical diameter for this type of segment presented in (K. Larsen, 2015), and in accordance with (Bridon).

The length of the segments are based on an iterative process carried out in MIMOSA in order to assure the steel wire rope segment has an appropriate distance to the seabed when subjected to environmental loads.

The breaking strength, pretension and cost of the mooring line, in addition to safety factor and maximum offset is presented in Table 7.8.

Constrains				
Safety factor [-]	Offset $[m]$	MBL $[N]$	Pretension $[N]$	Cost $[NOK]$
2.4086	110.95	$1.1118 \cdot 10^7$	$2.5000 \cdot 10^6$	$9.5493 \cdot 10^6$

Table 7.8: Parameters for initial steel wire rope and chain mooring system.

The mooring system as shown in SIMO is presented in Figure 7.3.

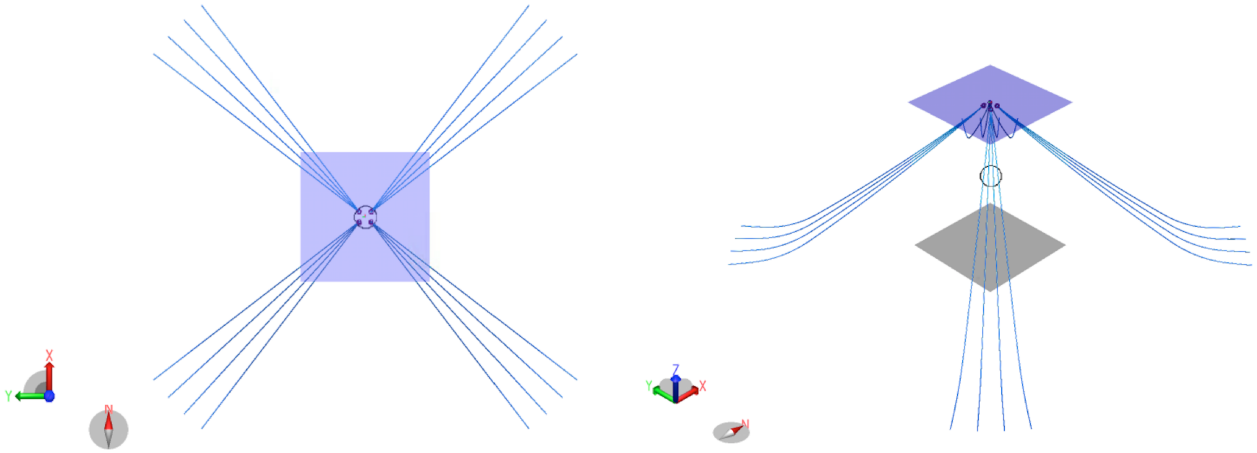

(a) Mooring system viewed diagonally

(b) Mooring system view from above

Figure 7.3: Steel wire rope and chain mooring system in SIMO.

Optimization Variables

Table 7.9 presents the segment optimization variables. The minimum and maximum values of the segment diameters are based on the product catalogues (Ramnäs Bruk, 2015) and (Bridon). The minimum and maximum values of the segment lengths are based on iterations in MIMOSA in order to avoid contact between steel wire rope and seabed.

The delta values are the same as for the polyester rope and chain mooring system. Hence, the values are chosen based on correspondence with co-supervisor.

		Diameter			Length		
		Segment 1	Segment 2	Segment 3	Segment 1	Segment 2	Segment 3
Type		Chain	Steel Wire	Chain	Chain	Steel Wire	Chain
Initial Value	[m]	0.107	0.110	0.107	1800	800	159
Min Value	[m]	0.076	0.09	0.076	1500	500	50
Max Value	[m]	0.177	0.165	0.177	2000	1000	500
Delta	[-]	0.001	0.001	0.001	0.1	0.1	0.1

Table 7.9: Optimization variables for steel wire rope and chain mooring system.

7.3 Arrangement of Optimization in SIMO Workbench

According to section 6.1.2, the catenary lines may be implemented in three different ways in SIMO. For this optimization, the mooring lines are included by anchor position specified by line pretension. In this way, the anchors are allowed to move during the optimization in accordance with the pretension.

7.3.1 Double Variables

As described in Chapter 5, using an automated optimization algorithm involves an iterative process where the optimization variables are updated for each iteration. However, adjusting the optimization variables affects several other parameters. In order for the optimization to be carried out in an easy and correct way, the parameters depending on the optimization variables are implemented as scripts in SIMA.

The breaking strength of the mooring line depends on the segment diameters. A script based on the breaking strengths provided by (Bridon, 2013), (Bridon) and (Ramnäs Bruk, 2015) is created in order to account for the change in diameters. However, only one breaking strength is applied for the whole mooring line. The script therefore calculates the breaking strength of all three segments and uses the minimum of these values as the breaking strength of the whole mooring line.

The weight in air for the mooring line, used in the calculation of the cost, will also depend on the segment diameter. A script is therefore also introduced here. This script is, as for the breaking strength, based on (Bridon, 2013), (Bridon) and (Ramnäs Bruk, 2015).

The pretension of the mooring line is in the optimization included as a variable in terms of a pretension factor. However, the pretension is defined as a script providing the product of the pretension factor and the breaking strength, as presented in equation 7.1.

7.3.2 Optimization Workflows

Figure 7.4 presents a picture of the workflow to be optimized in SIMA workbench. As seen from the figure, and described in section 5.3, the maximum design condition from Table 7.1 is applied to DEMO2000 in a

condition. The optimization variables are connected to this environmental condition, and updated for each iteration of the optimization.

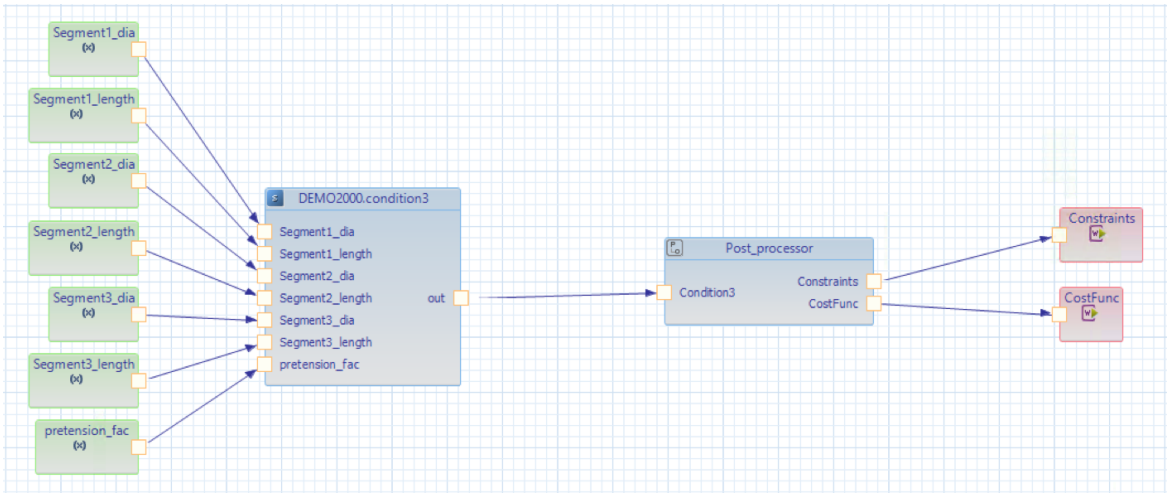

Figure 7.4: Workflow to be optimized.

The results from this environmental condition with the current variables values are sent to the post processor, which again has the cost function and the constraints as output. The output from this workflow is given as input to the workflow with the optimization node.

The setup of the post processor in this optimization is presented in Figure 7.5.

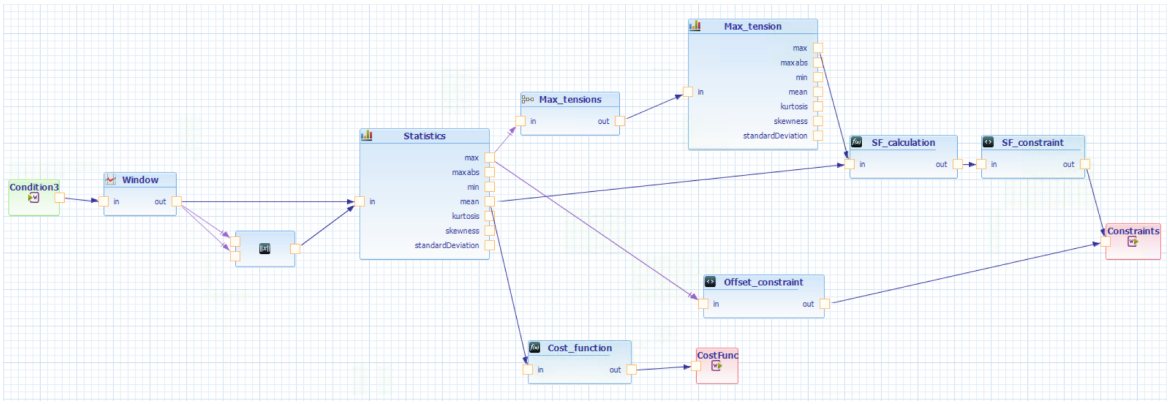

Figure 7.5: Post processor.

The results from the environmental condition calculation are provided as input to post processor. The simulation length for the environmental condition is set to 12000 *s*. However, *Window* removes a transient phase

corresponding to the first 1200 *s*. This results in a time series with a duration of three hours.

The offset is calculated by using a built in arithmetic function estimating the magnitude of the distance in direction 135°, provided the total motion in x-direction and y-direction as input. The maximum calculated distance is then selected by the *Statistics*, and fed to *Offset constraint* where the constraint to the maximum offset is set. The calculated maximum offset is then sent to *Constraints*.

The safety factor is calculated selecting the maximum tension present in each mooring line by *Statistics*, merge all these maximum tensions into one signal with *Max tensions* and then select the maximum tension form this signal with *Max tension*. This maximum tension is used in *SF calculation* to calculated the safety factor with equation 7.4. The breaking strength is updated for each iteration as it is defined as a double variable. The constraint to the safety factor is introduced in *SF constraint*, and then sent to *Constraints*.

The cost function is defined in *Cost function*. The lengths, weights in air and prices are here forming equation 7.3. The calculated cost is then sent to *CostFunc*.

The cost function and the constraints are then sent to the workflow to be optimized, and then as input to the workflow with the optimization node presented in Figure 7.6.

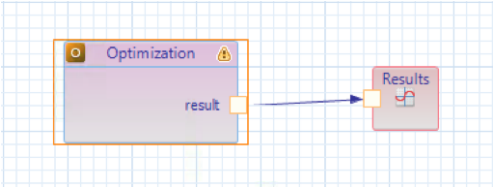

Figure 7.6: Workflow with optimization node.

Optimization also defines the optimization variables. The initial, minimum, maximum and delta values for variables are defined here as presented in Figure 7.7.

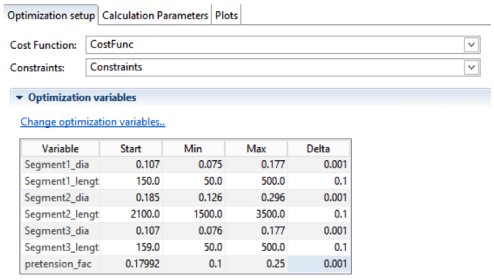

Figure 7.7: Optimization settings for polyester rope and chain mooring system.

The results may be studied in *Results* in form of plots. These plots include the values of cost, optimization variables and constraints plotted versus iteration. The constraint gradients and cost function gradients are also included in the results.

7.4 Optimization Results

The optimization results are in this section first presented and discussed for the polyester rope and chain mooring system, then for the steel wire rope and chain mooring system.

7.4.1 Assumptions

The following is assumed for the optimization:

- Only the intact mooring systems are considered.
- The results presented are all based on the same realization, the same realization as used in the presentation of the initial mooring systems in section 7.2.1 and 7.2.2. As the optimization is based on one singe realization there are no extreme values statistics carried out on the results. This is a simplification and will provide some uncertainty in the safety factors and maximum offsets. However, this approach is chosen in order to reduce the computation time. High accuracy in the results are nor needed as this is the initial step in the optimization and quasi-static analysis of the mooring line tension is performed.
- The desired final accuracy defined in SIMO is for these simulations set to 0.01. This is a convergence parameter affecting both the cost function and the constraints. Reducing this parameter would give more accurate results, but the computational cost would be larger. However, this value is chosen as this is the default value in SIMO.

7.4.2 Polyester Rope and Chain Mooring System

The following section presents the results of the three cases in Table 7.3 for the polyester rope and chain mooring system. In addition, appropriate sensitivity studies are performed in order to validate the optimization workflow and results. All sensitivity studies are carried out based on Case 1.

Case 1

Optimization of the cost for Case 1 is presented in Figure 7.8.

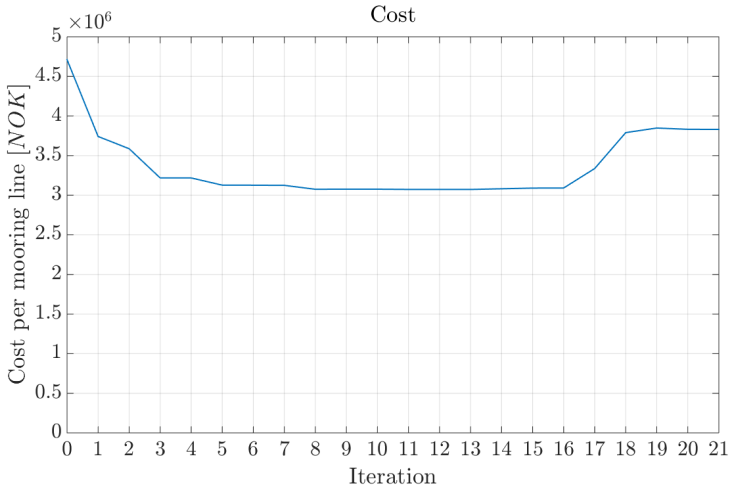

Figure 7.8: Cost for polyester rope and chain mooring system for Case 1.

As seen from the figure, the cost is strongly reduced during the first iterations followed by an increase before stabilizing at a cost level lower than the initial value. Observing the segment variables in Figure 7.9(a), the same trend can be seen for the diameters. However, the length of segment 2 slightly increases, while a slight decrease in the length of segment 1 and segment 3 is observed. Thus, the reduction in cost is mainly obtained by the reduction in diameter of the segments.

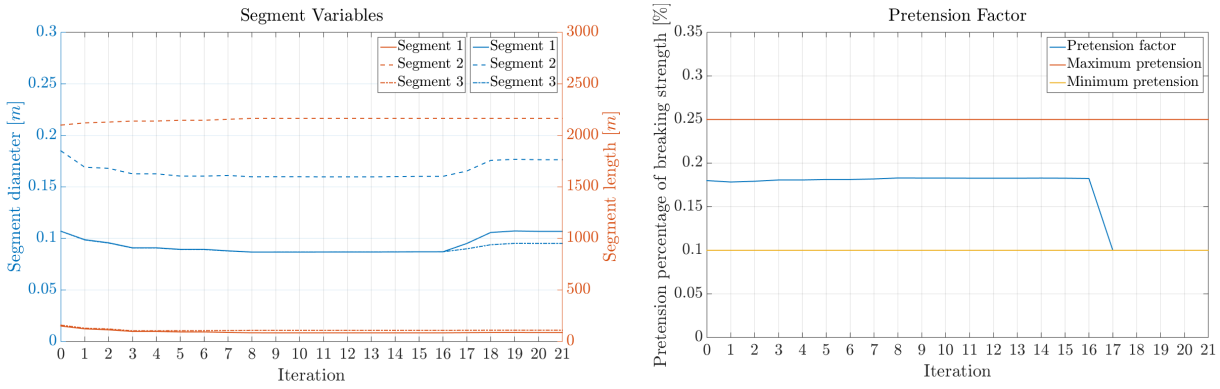

(a) Segment variables

(b) Pretension factor

Figure 7.9: Optimization variables.

The pretension factor is presented in Figure 7.9(b). As seen from the figure, the factor decreases to minimum value at iteration 17.

The optimization constraints are presented in Figure 7.10.

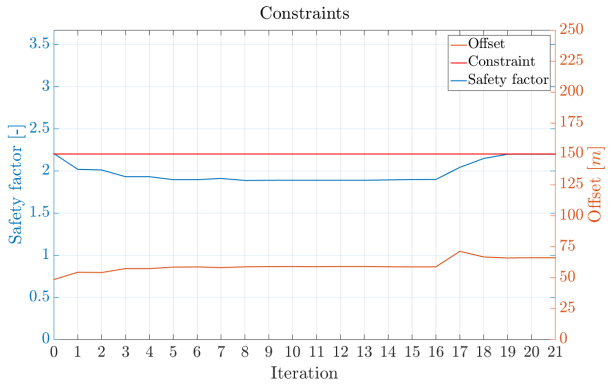

Figure 7.10: Optimization constraints.

The safety factor is calculated based on the breaking strength of the mooring line, which is proportional to the square of the segment diameter. The optimization workflow uses the lowest breaking strength of all three segments at the current iteration as breaking strength for the whole mooring line, as described in section 7.3.1. The lowest breaking strength will be present for segment 2 during the first 18 iterations, before the diameter of this segment increases to such extent that the breaking strength of the polyester rope segment no longer is the lowest. The breaking strength is dominated by the diameter of segment 3 during the last iterations.

The offset of the vessel is observed to somewhat increase during the optimization process in Figure 7.10.

The final values of all the optimization variables are presented in Table 7.10.

Diameter [mm]			Length [m]			Pretension
Segment 1	Segment 2	Segment 3	Segment 1	Segment 2	Segment 3	Factor [-]
106.840	176.380	95.199	87.402	2165.500	109.62	0.10000

Table 7.10: Optimized variables for polyester rope and chain mooring system for Case 1.

The resulting breaking strength, pretension and cost of the mooring line, in addition to safety factor and maximum offset is presented in Table 7.11.

Constrains				
Safety factor [-]	Offset [m]	MBL [N]	Pretension [N]	Cost [NOK]
2.2002	66.092	$8.8008 \cdot 10^6$	$8.8008 \cdot 10^5$	$3.8305 \cdot 10^6$

Table 7.11: Parameters for polyester rope and chain mooring system for Case 1.

Comparing the values from Table 7.11 to the values in Table 7.5 in section 7.2.1, the safety factor is observed to decrease from 2.2075 to 2.2002. This is due to the approximately 12 mm decrease in diameter of segment 3, observed in Table 7.10.

The offset of the vessel has increased approximately 18 m during the iteration. The maximum offset of the vessel, x_{max}, may be studied by use of equation 7.5

$$x_{max} = \overline{x} + x_{LF} + x_{WF} \tag{7.5}$$

where $\overline{x}$ is the mean offset, x_{LF} is offset due to the LF forces and x_{WF} is the offset due to the WF forces.

The mean offset may be written

$$\overline{x} = \frac{\overline{Q}}{K} \tag{7.6}$$

where $\overline{Q}$ is the mean excitation forces and K is the stiffness of the mooring system. For small damping, x_{LF} can be approximated by (O. M. Faltinsen, 1990)

$$x_{LF} = S_F(\mu_n)\frac{\pi}{C \cdot K} \tag{7.7}$$

where $S_F(\mu_n)$ is slow-drift load spectrum, μ_n is the LF resonance frequency and C is the damping.

$\overline{x}$ and x_{LF} will dominate the maximum offset of the vessel. Hence, x_{WF} will not be taken into account here. Comparing the pretension of the mooring line from Table 7.11 to the pretension in Table 7.5 in section 7.2.1, a noticeable decrease is observed. This decrease of the pretension occurs due to both decrease in the pretension factor and reduction of the breaking strength. Decreasing the pretension of the mooring lines reduces the stiffness of the mooring system. A reduced stiffness will, as seen from equation 7.6 and 7.7, increase the both the mean offset and the offset due to LF forces. Hence, larger maximum offset of the vessel is present compared to the initial mooring system presented in section 7.2.1.

The optimization reduces the cost of the mooring system by approximately 19 %.

Case 2

The optimization of the cost for Case 2 is presented in Figure 7.11.

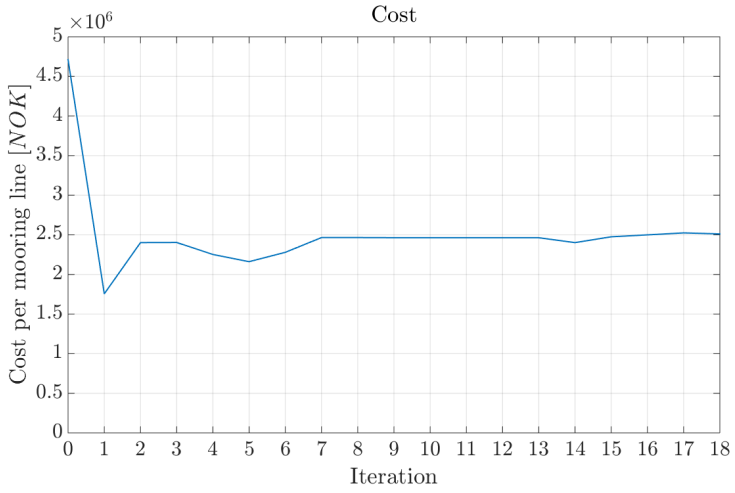

Figure 7.11: Cost for polyester rope and chain mooring system for Case 2.

For this case the cost also decreases strictly during the first iterations. However, the cost stabilizes at a lower value than for Case 1. Observing 7.12(a) it is seen that the segment diameters also here follow the same trend as the cost, while the length of segment 2 increases and the length of segment 1 and segment 3 decreases. This results in an overall shorter mooring line with decreased diameter of each segment.

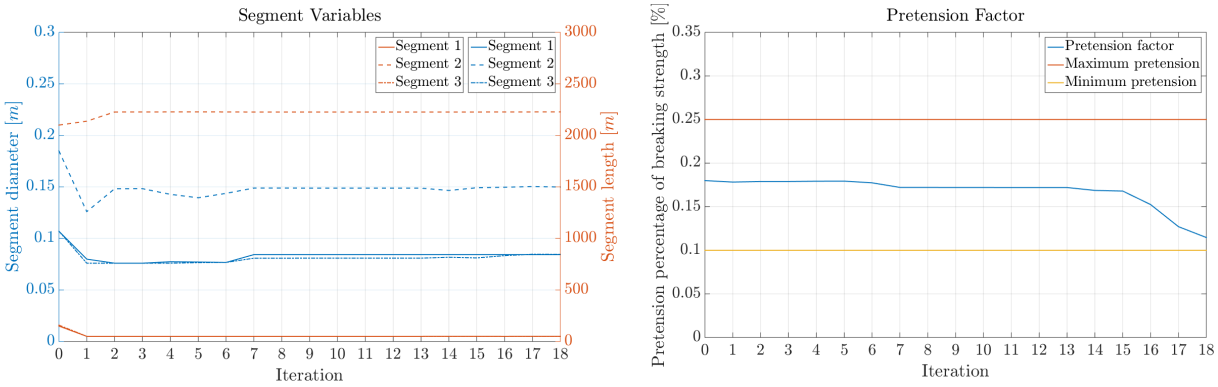

(a) Segment variables

(b) Pretension factor

Figure 7.12: Optimization variables.

The pretension factor, presented in Figure 7.12(b), is also here reduced during the optimization.

The optimization constraints are presented in Figure 7.13.

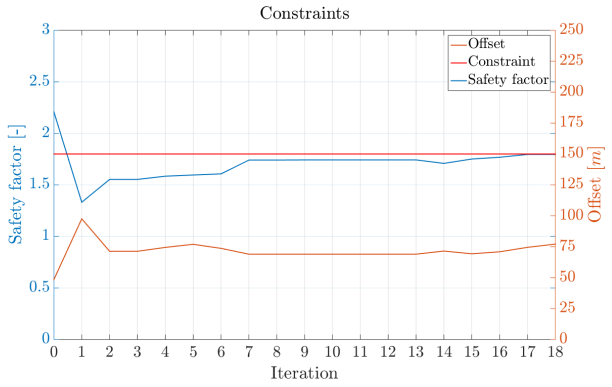

Figure 7.13: Optimization constraints.

As seen from the figure, the constraint to the safety factor is lower for this case compared to Case 1. The safety factor is observed to reduce rapidly during the first iteration. For this case, the dependence of the breaking strength alternates between the diameter of segment 3 and segment 2. Both of the diameters decreases strongly during the first iterations followed by a slight increase before stabilizing, as observed in Figure 7.12(a). The same trend is observed for the safety factor, it increases before it stabilizes at the constraint. Segment 2 is the segment with the lowest breaking strength at the end of the optimization.

The offset increases strongly during the first iteration, before it reduces and stabilizes at a value larger than the initial value.

The final values of all the optimization variables are presented in Table 7.12.

Diameter [mm]			Length [m]			Pretension
Segment 1	Segment 2	Segment 3	Segment 1	Segment 2	Segment 3	Factor [-]
84.328	149.920	84.563	50.172	2227.600	50.000	0.11464

Table 7.12: Optimized variables for polyester rope and chain mooring system for Case 2.

The resulting breaking strength, pretension and cost of the mooring line, in addition to safety factor and maximum offset is presented in Table 7.13.

Constrains				
Safety factor [-]	Offset [m]	MBL [N]	Pretension [N]	Cost [NOK]
1.7956	77.137	$6.4423 \cdot 10^6$	$7.3855 \cdot 10^5$	$2.5115 \cdot 10^6$

Table 7.13: Parameters for polyester rope and chain mooring system for Case 2.

Comparing the optimization variables of Case 2 presented in Table 7.12 to the variables in Case 1, presented

in Table 7.10, it is observed that the all diameters are smaller for Case 2 than for Case 1. The length of segment 1 and segment 3 is also smaller, while the length of segment 2 is somewhat larger for Case 2 compared to Case 1.

The reduction in diameter for segment 2 results in lower breaking strength of the mooring lines. This reduced breaking strength combined with the reduced pretension factor results in lower pretension for Case 2 than for Case 1. This is as expected as the reduced constraint to the safety factor allows for lower breaking strength for the mooring lines.

The offset is larger for Case 2 than for Case 1. This is as expected considering equation 7.5. Reducing the pretension results in reduced stiffness, which by equation 7.6 and 7.7, results in larger maximum offset.

The reduction in the cost for Case 2 compared to Case 1 is 34 %, while the reduction of cost of Case 2 compared to the initial mooring system is approximately 47 %.

Case 3

The optimized cost for Case 3 is presented in Figure 7.14.

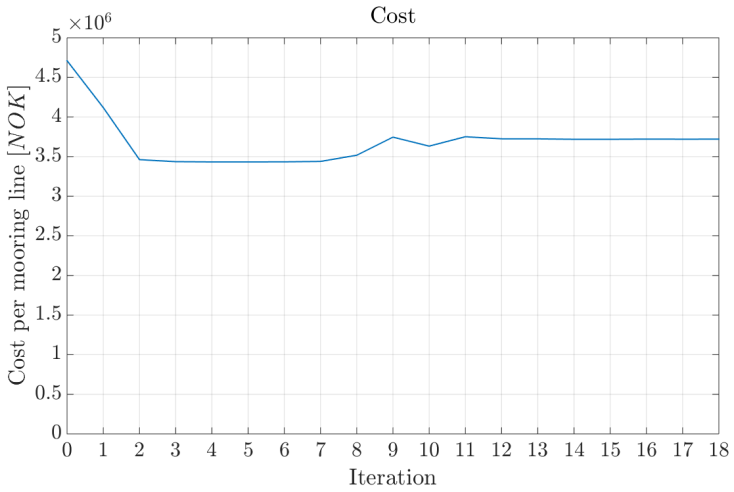

Figure 7.14: Cost for polyester rope and chain mooring system for Case 3.

A decrease in the cost during the first iterations is present also for Case 3. However, this decrease is not as strict as for Case 1 and Case 2. During the rest of the optimization a slight increase of the cost occurs before stabilization.

All segment diameters decreases during the first iterations, as seen from Figure 7.15(a). Also the length of segment 1 and segment 3 decreases during the process, while the length of segment 2 stays approximately

constant.

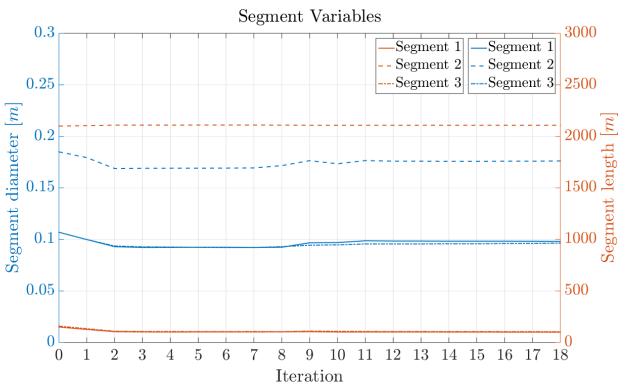

(a) Segment variables

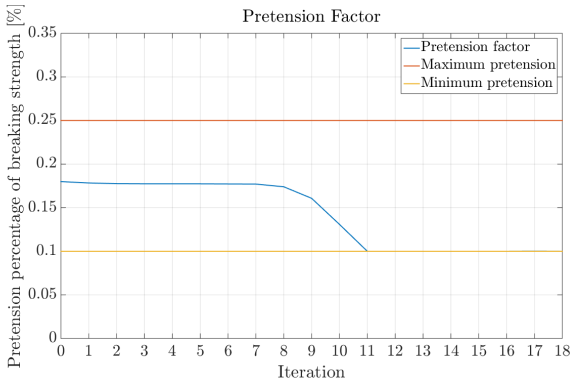

(b) Pretension factor

Figure 7.15: Optimization variables.

The pretension factor, presented in Figure 7.15(b), decreases during iteration 8 to iteration 11 to the minimum value.

The optimization constraints are presented in Figure 7.16.

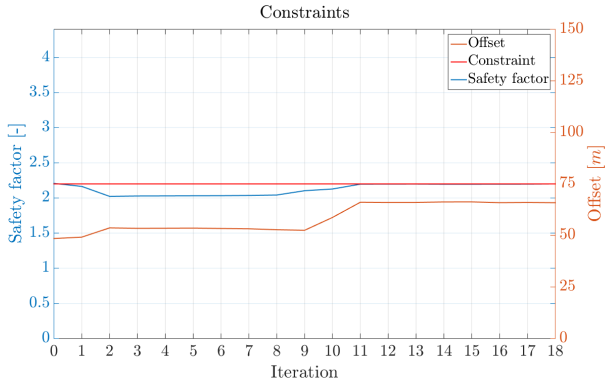

Figure 7.16: Optimization constraints.

Also for Case 3 the diameter of segment 2 dominated the breaking strength of the mooring line. A correspondence between this diameter and the safety factor is therefore present. As the diameter decreases during the first iterations, as shown in Figure 7.15(a), the breaking strength reduces, which results in a reduction of the safety factor. A slight increase of the diameter occurs during the rest of the optimization, resulting in the safety factor reaching the constraint level.

The offset of the vessel increases in two steps. The first increase of the offset occurs during the first iterations while the diameter decreases. The reduction in diameter reduces the breaking strength, while the pretension factor is approximately constant, as seen in Figure 7.15(b). This results in a reduced pretension, and stiffness, of the mooring lines. The second step observed for the offset occurs as the pretension factor reduces to minimum value. Hence, the pretension is here further reduced and consequently the stiffness of the mooring system is reduced. The reduction of the stiffness results in larger maximum offset, as seen from equation 7.5, 7.6 and 7.6.

The final values of all the optimization variables are presented in Table 7.14.

Diameter [mm]			Length [m]			Pretension
Segment 1	Segment 2	Segment 3	Segment 1	Segment 2	Segment 3	Factor [-]
98.086	176.140	96.456	99.962	2108.2	104.2	0.10000

Table 7.14: Optimized variables for polyester rope and chain mooring system for Case 3.

The resulting breaking strength, pretension and cost of the mooring line, in addition to safety factor and maximum offset is presented in Table 7.15.

Constrains				
Safety factor [-]	Offset [m]	MBL [N]	Pretension [N]	Cost [NOK]
2.2003	65.876	$8.8928 \cdot 10^6$	$8.8928 \cdot 10^5$	$3.7208 \cdot 10^6$

Table 7.15: Parameters for polyester rope and chain mooring system for Case 3.

Comparing the optimization variables of Case 3 presented in Table 7.14 to the variables in Case 1 presented in Table 7.10, small differences are observed in the segment variables. Diameter of segment 1 and segment 3 is smaller for Case 3 compared to Case 1, while the diameter of segment 2 is approximately the same for both cases. The length of segment 1 is larger for Case 3 than for Case 1, while the length of segment 2 and segment 3 is slightly larger for Case 1 than for Case 3.

The safety factor and offset is approximately the same for both mooring systems, while there is some difference in the breaking strength and pretension of the mooring lines. The breaking strength and pretension is somewhat higher for Case 3 than for Case 1. This is due to the difference in the diameter of segment 3.

The cost of the system is slightly lower for Case 3 compared to Case 1. This indicates that the composition of the segment diameters and lengths for Case 3 provides a less expensive solution than for Case 1. As the constraint level for the offset is the only difference between Case 1 and Case 3, and the offset is observed to end up at approximately the same value, it is most likely the same minimum for the cost function. The difference in cost may be explained by the fact that changing the offset constraint changes the optimization problem as stated in equation 5.1 in section 5.1. This changes in the mathematical formulation, which affects the search pattern of the optimization. Most likely both cases would have given the same minimized

cost if the tolerance parameter was decreased.

The reduction of cost for the mooring system in Case 3 compared to the initial mooring system is approximately 21 %.

Sensitivity Study: Environment

In order to verify the reliability of the optimization workflow constructed for this master thesis, comparison of results with slightly different significant height values is carried out. An optimization of the system with an H_s reduced by 5 cm is performed. Figure 7.17 presents the cost of the Case 1 with the initial and the reduced H_s.

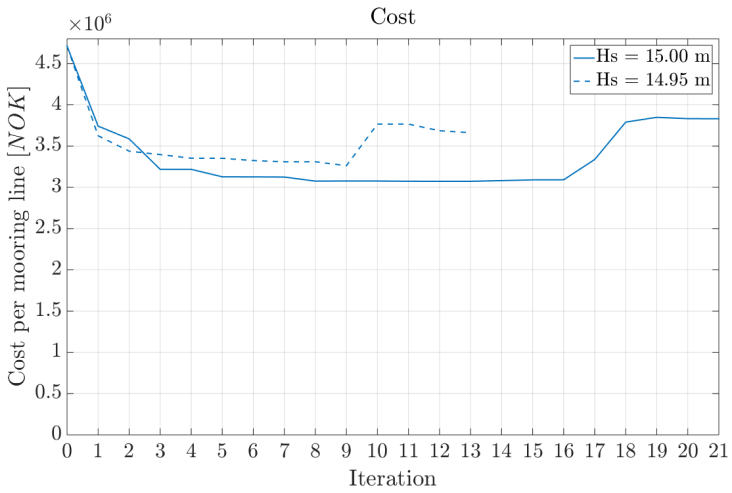

Figure 7.17: Cost for polyester rope and chain mooring system with variation in H_s for Case 1.

As seen from the figure, the optimization of the cost is different for the two values of H_s. It is observed that the number of iterations is less for the lower H_s than for the initial H_s. However, similarities in optimizations are present, and the cost ends up at similar values for both H_s.

The segment variables are presented in Figure 7.18.

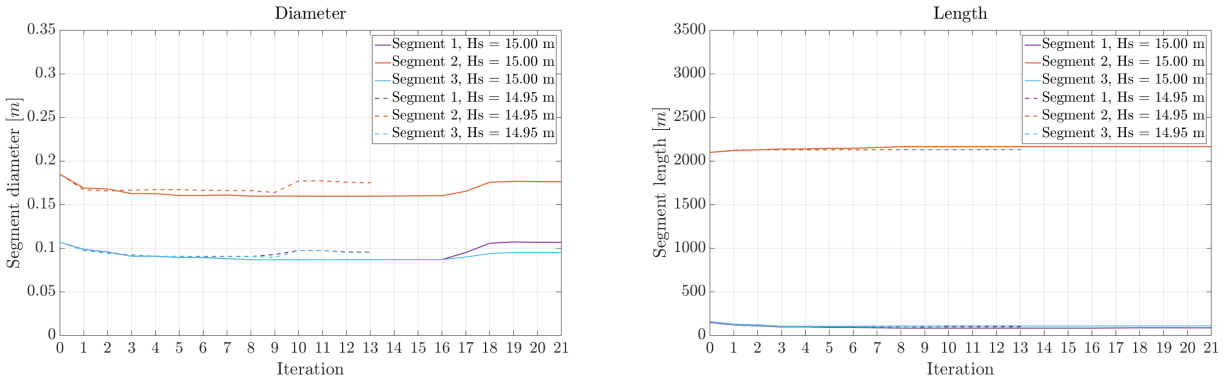

(a) Segment diameter

(b) Segment length

Figure 7.18: Segment variables.

As seen from Figure 7.18, the optimization of all the segment lengths are approximately the same. However, there are small differences in the optimization of the segment diameters.

The pretension factor is presented in Figure 7.19.

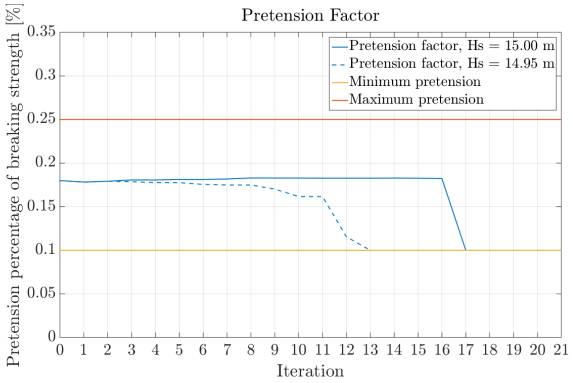

Figure 7.19: Pretension factor.

Similarities are also observed for the optimization pattern of the pretension factor, with both optimizations seeking the minimum value.

The constraints to the optimization is presented in Figure 7.20.

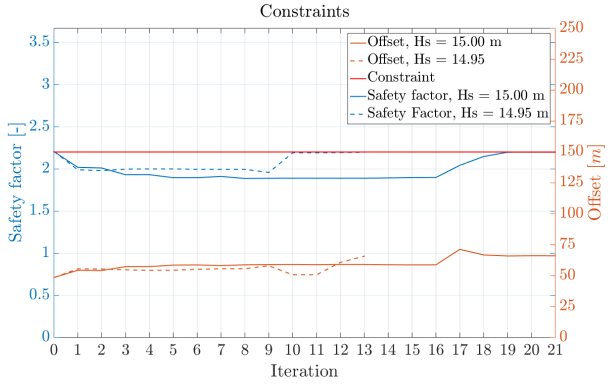

Figure 7.20: Optimization constraints.

The safety factor is during the optimization slightly higher for the case with reduced H_s compared to the case with initial H_s. This is reasonable by observing the diameters, which are slightly larger for the case with reduced H_s compared to the case with initial H_s.

Some similarities are also present for the optimization pattern of the offset for both values of H_s. The offset ends up at approximately the same value in both cases.

The final values of all the optimization variables for both values of H_s are presented in Table 7.16.

	Diameter $[mm]$			Length $[m]$			Pretension
H_s $[m]$	Segment 1	Segment 2	Segment 3	Segment 1	Segment 2	Segment 3	Factor [-]
14.95	95.382	175.150	95.732	105.460	2130.600	93.885	0.10000
15.00	106.840	176.380	95.199	87.402	2165.500	109.620	0.10000

Table 7.16: Optimized variables for polyester rope and chain mooring system for Case 1 with H_s = 14.95 m and H_s = 15.00 m.

The resulting breaking strength, pretension and cost of the mooring line, in addition to safety factor and maximum offset for both values of H_s are presented in Table 7.17.

	Constrains				
H_s $[m]$	Safety factor [-]	Offset $[m]$	MBL $[N]$	Pretension $[N]$	Cost $[NOK]$
14.95	2.1998	65.771	$8.7931 \cdot 10^6$	$8.7931 \cdot 10^5$	$3.6620 \cdot 10^6$
15.00	2.2002	66.092	$8.8008 \cdot 10^6$	$8.8008 \cdot 10^5$	$3.8305 \cdot 10^6$

Table 7.17: Parameters for polyester rope and chain mooring system for Case 1 with H_s = 14.95 m and H_s = 15.00 m.

As seen from Table 7.16, some most noticeable difference for the segment variables are present for the diameter and length of segment 1, in addition to the length of segment 2 and segment 3.

The differences in safety factor and offset are neglectable. The difference in pretension and breaking strength is also small. As the pretension factor is the same for both cases of H_s, these differences are due to the difference in the breaking strength. The breaking strength for the case with reduced H_s is dominated by the diameter of segment 1, while the breaking strength for the case with initial H_s is dominated by the diameter of segment 3.

The cost of the mooring system with H_s = 14.95 s is observed to be about 4 % less than for the mooring system with H_s = 15 s. This is reasonable as the environmental loads are slightly lower for the mooring system with a reduced H_s.

Although the reduction is H_s is small in this sensitivity, the change in environmental loading is observed to affect the mathematical problem of the optimization. The reduction in H_s will mainly change the mathematical formulation through the influence on the safety factor constraint. This indicates that the breaking strength and pretension can be reduced, which results in a reduction of the diameters. Hence, the search pattern of the two cases will be slightly different, as seen from the above.

Sensitivity Study: Offset Constraint

Comparing Case 1 and Case 3 showed that a stricter constraint on the maximum allowed offset gave a slightly lower cost for the mooring system. In order to investigate how the offset constraint affects the optimization of the cost function, a sensitivity study is performed by reducing the maximum allowed offset stepwise.

Optimization for several different maximum allowed offsets in the range 150 m - 70 m is here performed. This range is chosen as the offset for both Case 1 and Case 3 ended up at approximately 65 m. The optimization of the cost for the different maximum allowed offsets is presented in Figure 7.21.

As seen from the figure, the deviation in cost for the different optimizations are for some of the maximum allowed offsets quite large. However, there are no clear connection between the cost and the maximum allowed offset. Both maximum allowed offsets of 150 m and 70 m seem to end up at the same cost, while a maximum allowed offset of 125 m gives the lowest cost.

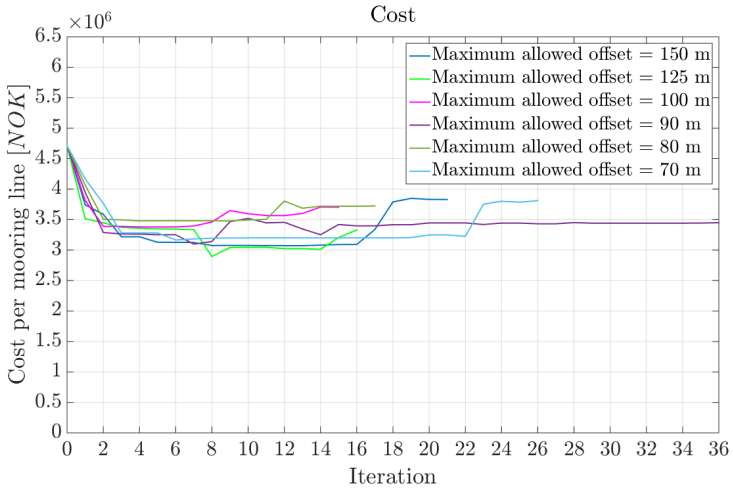

Figure 7.21: Cost for polyester rope and chain mooring system with varying maximum offset constraints for Case 1.

Plots of the segment variables are presented in Appendix B.1.1. As seen from these plots, the largest differences are present for the segment lengths. There are also some differences in the diameters. However, the differences in diameters is mostly present for segment 1 and segment 3 for the cases with maximum allowed offset of 150 m and 70 m. The optimization of the pretension factor follows the same trend for most of the maximum allowed offsets, all seeking the minimum value. However, for the case with maximum allowed offset of 70 m this factor ends up at much larger value.

The optimization constraints are presented in Figure 7.22.

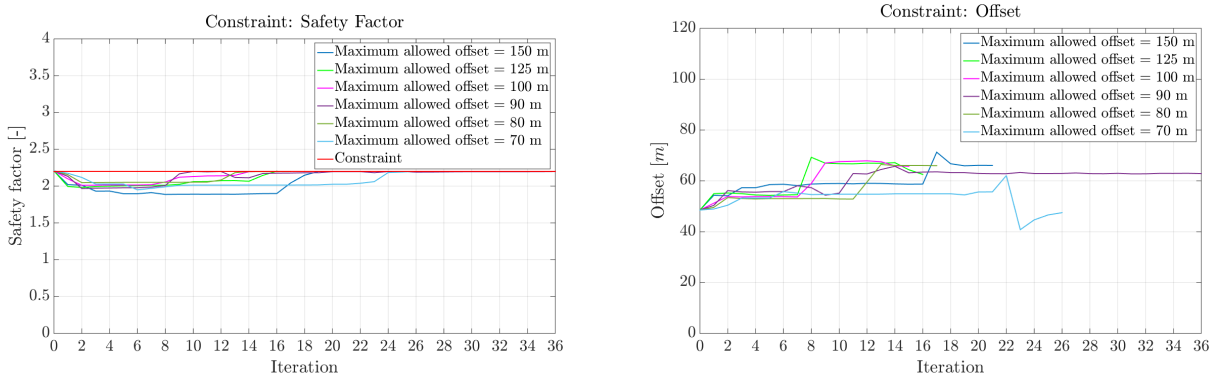

(a) Safety factor

(b) Offset

Figure 7.22: Optimization constraints.

From Figure 7.22(b) it is observed that the all the maximum allowed offsets, except 70 m, ends up at offsets in the range 60 m - 70 m. However, for an maximum allowed offset of 70 m the offset is reduced to below 50 m. Observing Figure 7.22(a) it is seen that the safety factor, and thus the breaking strength, for maximum allowed offset of 70 m is at the same level as the other maximum allowed offsets. The reason for the reduced offset is therefore due to the pretension factor. As this factor is much higher for the maximum allowed offset of 70 m, the pretension and the stiffness is larger. This results in reduced offset as seen from equation 7.5, 7.6 and 7.7.

The final values of all the optimization variables for all the different maximum allowed offsets are presented in Table 7.18.

Allowed	Diameter [mm]			Length [m]			Pretension
offset [m]	Segment 1	Segment 2	Segment 3	Segment 1	Segment 2	Segment 3	Factor [-]
150	106.840	176.380	95.199	87.402	2165.500	109.62	0.10000
125	95.881	176.350	96.305	57.012	2123.500	50.000	0.10000
100	96.840	176.220	97.326	106.240	2101.500	97.904	0.10000
90	96.598	177.360	96.798	50.116	2090.400	82.865	0.10000
80	96.392	175.910	95.681	98.252	2115.300	110.58	0.10000
70	102.220	180.510	112.480	77.150	2108.700	77.990	0.17732

Table 7.18: Optimized variables for polyester rope and chain mooring system for Case 1 with maximum allowed offset of 150 m, 125 m, 100 m, 90 m, 80 m and 70 m.

The resulting breaking strength, pretension and cost of the mooring line, in addition to safety factor and maximum offset for all the values of maximum allowed offset are presented in Table 7.19.

Allowed	Constrains				
offset [m]	Safety factor [-]	Offset [m]	MBL [N]	Pretension [N]	Cost [NOK]
150	2.2002	66.092	$8.8008 \cdot 10^6$	$8.8008 \cdot 10^5$	$3.8305 \cdot 10^6$
125	2.2042	62.550	$8.9140 \cdot 10^6$	$8.9140 \cdot 10^5$	$3.3296 \cdot 10^6$
100	2.1996	65.742	$8.9009 \cdot 10^6$	$8.9009 \cdot 10^5$	$3.7045 \cdot 10^6$
90	2.1984	62.866	$9.0164 \cdot 10^6$	$9.0164 \cdot 10^5$	$3.4488 \cdot 10^6$
80	2.1990	65.986	$8.8696 \cdot 10^6$	$8.8696 \cdot 10^5$	$3.7229 \cdot 10^6$
70	2.2010	47.500	$9.3395 \cdot 10^6$	$1.6561 \cdot 10^6$	$3.8122 \cdot 10^6$

Table 7.19: Parameters for polyester rope and chain mooring system for Case 1 with maximum allowed offset of 150 m, 125 m, 100 m, 90 m, 80 m and 70 m.

Comparing the values of the segment variables presented in Table 7.18, all the maximum allowed offsets provides slightly different compositions of the segment variables. For the case with maximum allowed offset of 125 m, which gives the lowest cost, the resulting mooring line is overall one of the shortest with relatively

small diameters. However, the composition of this mooring line is very similar to the one in the case with maximum allowed offset 90 m.

The most expensive mooring lines are those for maximum allowed offset 150 m and 70 m. As seen from Table 7.18, the mooring lines in these two cases are composed of large segment diameters, and the overall length is relatively large.

The number of variables and constraints applied in the mathematical formulation of the optimization makes it complex and hard to imagine physically. However, from the results of this sensitivity it is conceivable that the minimum of the cost function is relatively flat. If the minimum is relatively flat, a large convergence parameter may provide cost minima with some deviation. The cost found for all the cases in this sensitivity is therefore most probably the same minimum of the cost function. Hence, performing the same sensitivity with a lower convergence parameter would probably provide more similar costs.

However, the optimization with maximum allowed offset of 70 m differ from the other optimizations as the pretension is very high resulting in a much smaller offset, as seen in Table 7.19. This is not as expected, as this maximum allowed offset is above the offset of the vessel for the other optimizations performed in this sensitivity. Thus, for this case the offset constraint is obviously governing, along with the safety factor, in the optimization. Compared to the other optimizations where the safety factor alone is the dominating constraint. However, this does not fully explain the strict reduction of the offset. It would here be interesting also to apply a lower value for the convergence parameter, in order to investigate how this affects the offset constraint.

Sensitivity Study: Global Minimum

The intention of the optimization is to find the minimum of the cost function, as described in Chapter 5. However, the cost function may consist of several local minima. These local minima are not of great interest, as the global minimum will give the largest reduction of the cost.

In order to investigate if the minimum for Case 1 found in section 7.4.2 is the global minimum, the optimization is carried out from three different start points. Figure 7.23 presents the optimization of the form the three different start points.

The initial start point presented in section 7.2.1 is represented by the solid line, a start point with all maximum values are represented with the dashed line and a start point with all minimum values are represented with dash-dotted line.

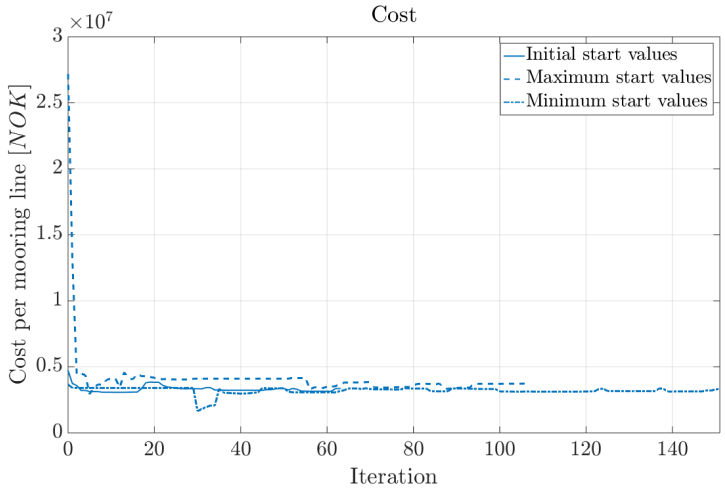

Figure 7.23: Cost of polyester rope and chain mooring system for three different start points for Case 1.

In order to investigate if the optimization from these three different start points converges towards the same minimum, which most likely is the global minimum, several optimizations is carried out for each of the start points. As one optimization ends, the optimized variables are used as initial values for the next optimization. This results in a convergence towards the global minimum for all three start points.

The optimization variables and constraints are presented in Appendix B.1.2. As seen from the plots, some differences are present in segment diameters and lengths for the three different start points, especially for segment 2. The pretension factor ends up at the minimum value for all start points, the same is observed for the safety factor. However, there are some differences in the offset. The optimization starting with all the maximum values have a somewhat larger offset than the two other optimizations. This is reasonable as the diameter of segment 2 is much smaller for this case, which indicates lower breaking strength and lower pretension. Hence, the stiffness is lower for this case and the offset is larger.

The final values of all the optimization variables for the three different start points are presented in Table 7.20.

	Diameter [mm]			Length [m]			Pretension
Start point	Segment 1	Segment 2	Segment 3	Segment 1	Segment 2	Segment 3	Factor [-]
Initial	94.965	174.63	97.278	55.972	2190.700	50.026	0.1
Maximum	88.120	161.430	88.926	50.486	2958.700	52.096	0.1
Minimum	102.350	187.830	104.190	50.879	1841.700	50.000	0.1

Table 7.20: Optimized variables for polyester rope and chain mooring system for three different start points for Case 1.

The resulting breaking strength, pretension and cost of the mooring line, in addition to safety factor and maximum offset is presented in Table 7.21.

	Constrains				
Start point	Safety factor [-]	Offset [m]	MBL [N]	Pretension [N]	Cost [NOK]
Initial	2.2064	63.136	$8.7410 \cdot 10^6$	$8.7410 \cdot 10^5$	$3.3606 \cdot 10^6$
Maximum	2.1993	77.697	$7.4695 \cdot 10^6$	$7.4695 \cdot 10^5$	$3.7391 \cdot 10^6$
Minimum	2.2004	62.664	$1.0112 \cdot 10^7$	$1.0112 \cdot 10^6$	$3.3252 \cdot 10^6$

Table 7.21: Parameters for polyester rope and chain mooring system for three different start points for Case 1.

Observing Table 7.20, some differences are found for the optimization variables. The cost, presented in Table 7.21, are also slightly different for the three starting points. This indicates, as for the sensitivity with the offset constraint, that the minimum of the cost function is relatively flat. As the mathematical formulations are different due to different initial values of the variables, the search pattern will be very different for the optimizations.

The search for the global minimum is here performed by keeping the convergence parameter constant, and using the resulting values for optimization variables for one optimizations as input for the next optimization. As the convergence parameter apparently consider the result compared to the initial value, convergence is more time demanding as the optimization approaches the minimum. The optimization for the three different start points were here stopped due to the computational time of each optimization. However, there is still some difference in minimum cost for the three start points. In order to get the solutions even closer to each other, adjusting the convergence parameter to an even smaller value could have brought the solutions even closer.

Nevertheless, this sensitivity indicates that the minimum found for Case 1 is the global, and not a local, minimum of the cost function.

7.4.3 Steel Wire Rope and Chain Mooring System

The following section presents the results of the three cases presented in Table 7.3 for the chain and steel wire rope mooring system. In addition, appropriate sensitivity studies are carried out. All sensitivity studies are also here carried out based on Case 1.

Case 1

The optimized cost for Case 1 is presented in Figure 7.24.

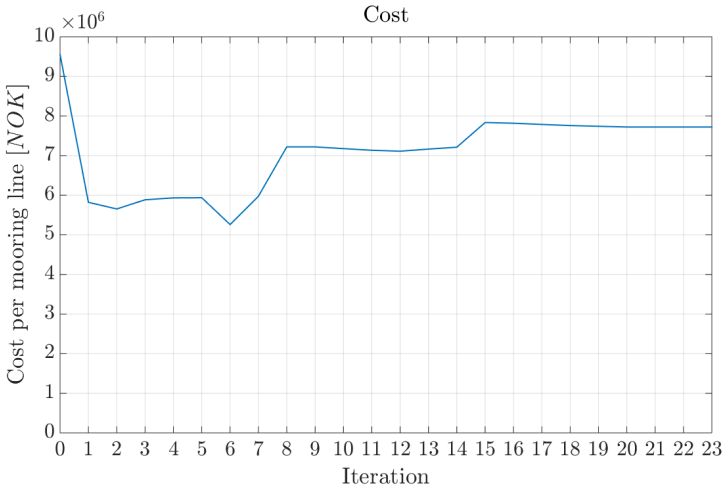

Figure 7.24: Cost for steel wire rope and chain mooring system for Case 1.

As seen from the figure, a rapid decrease in the cost is observed during the first iterations. However, the cost increases stepwise throughout the rest of the optimization before it converges a final value.

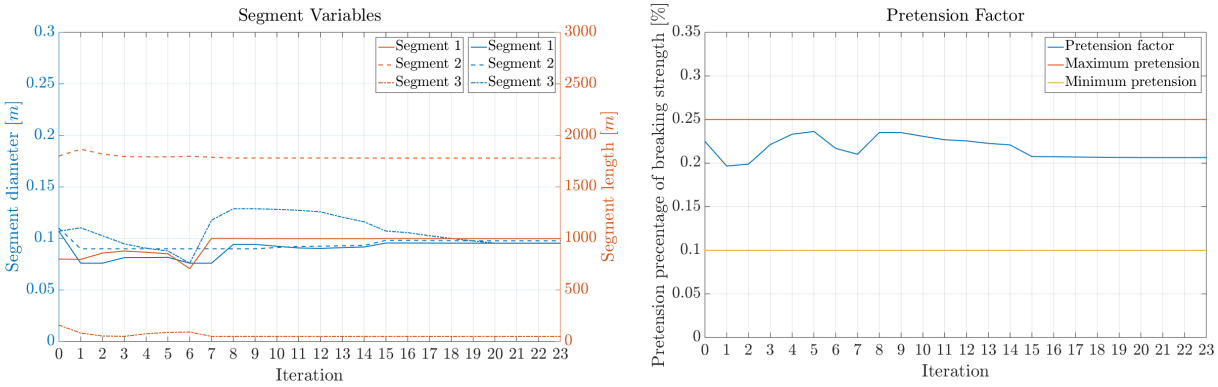

(a) Segment variables

(b) Pretension factor

Figure 7.25: Optimization variables.

Observing the optimization variables in Figure 7.25, this same pattern is present for some of the segment variables in Figure 7.25(a). The diameter of segment 1 and segment 2 and the length of segment 3 decreases during the first iterations, followed by a stepwise increase of these values until the final value is reached. The diameter of segment 3 increases during the first iterations, followed by a decrease and increase before it converges towards a somewhat smaller value than the initial value. The length of segment 1 and segment 2 both increases during the first iterations, before converging. However, the total length of the mooring line does not change significantly.

The pretension factor is presented in Figure 7.25(b). As seen from the figure, the factor varies a lot before it converges to a value somewhat lower than the initial value.

The constraint for the optimization is presented in Figure 7.26.

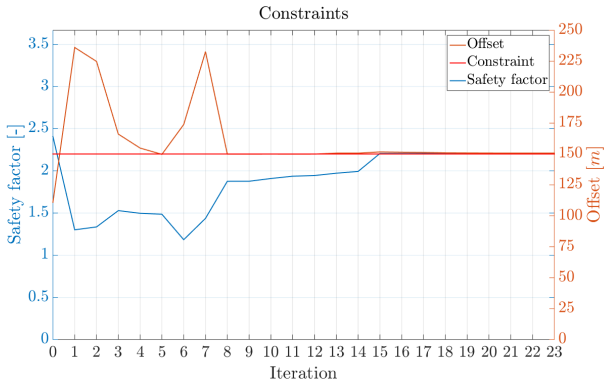

Figure 7.26: Optimization constraints.

Observing the safety factor, two significant minima can be seen. These minima can also be observed for the cost, and are present due to reduction in the diameters. The first minimum is due to a strong reduction in the diameter of segment 1. As the breaking strength is proportional to the square of the segment diameters, and the safety factor is calculated based on the breaking strength, this result is reasonable. The second minimum observed for the safety factor occurs as the length of segment 1 and the diameter of segment 3 decreases. It is conceivable that the changes in these segment variables results in an increased maximum tension of the most loaded line. As seen from equation 7.4, this will reduce the safety factor.

The maximum offset increases rapidly during the first iteration, as the pretension factor decreases. The pretension is then increased resulting in a reduced offset during iteration 5, before the offset again increases as the pretension is lowered during iteration 7. In order to meet the constraint of maximum 150 m offset, the pretension factor is again increased, while the diameter of segment 1 is increased. Increasing the diameter of segment 1, which dominates the breaking strength, increases the breaking strength of the mooring line and allows the pretension factor to be reduced. The pretension, and thus stiffness of the system, is then at an allowable value in order to meet the constraint. The relation between stiffness and offset is shown in equation 7.5, 7.6 and 7.7.

The final values of all the optimization variables are presented in Table 7.22.

Diameter [mm]			Length [m]			Pretension
Segment 1	Segment 2	Segment 3	Segment 1	Segment 2	Segment 3	Factor [-]
95.388	97.694	95.426	998.320	1780.100	50.000	0.20636

Table 7.22: Optimized variables for steel wire rope and chain mooring system for Case 1.

The resulting breaking strength, pretension and cost of the mooring line, in addition to safety factor and maximum offset is presented in Table 7.23.

Constrains				
Safety factor [-]	Offset [m]	MBL [N]	Pretension [N]	Cost [NOK]
2.2041	150.71	$8.8342 \cdot 10^6$	$1.8234 \cdot 10^6$	$7.7226 \cdot 10^6$

Table 7.23: Parameters for steel wire rope and chain mooring system for Case 1.

The segment variables presented in Table 7.22 have to some extent decreased during the optimization compared to the initial values in Table 7.9, except for the chain segment attached to the anchor which has increased. Resulting in a mooring line that has a reduced diameter, but is slightly longer than the initial mooring line.

The reduction of the diameter results in a lower breaking strength. This reduced breaking strength combined with a reduction in the pretension factor results in a decrease in the pretension has decreased and a larger offset, as explained above. These changes in the mooring system results in a cost that is approximately 19 % less expensive compared to the initial steel wire rope and chain mooring system.

Case 2

The optimization of the cost for Case 2 is presented in Figure 7.27. The optimization of the cost function for this case shows the same trend as for Case 1. The cost function strictly reduces during the first iterations before it gradually increases and converges to a value lower than the initial value.

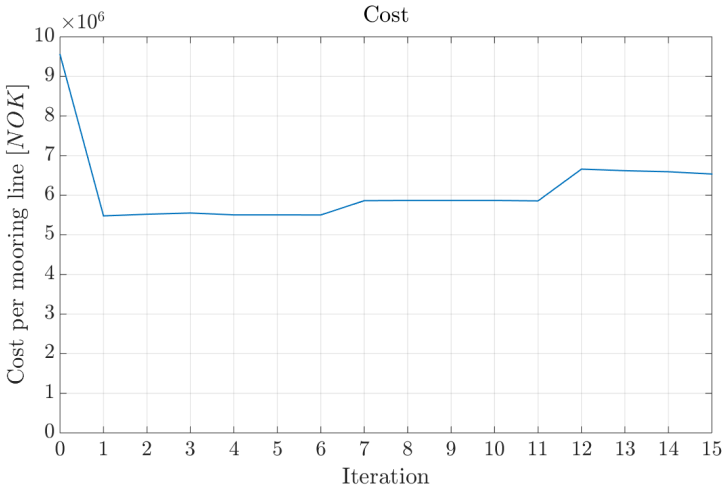

Figure 7.27: Cost for steel wire rope and chain mooring system for Case 2.

The development of the cost can be explained by observing the optimization variables in Figure 7.28. The segment optimization variables, excluding length of segment 2, are all reduced during the first iterations giving the reduced cost. However, in order to meet the constraints of the optimization, the dimensions of the variables are gradually increased. This results in the increase in cost. As seen from the figure, the overall length of the mooring line is somewhat reduced in the optimization.

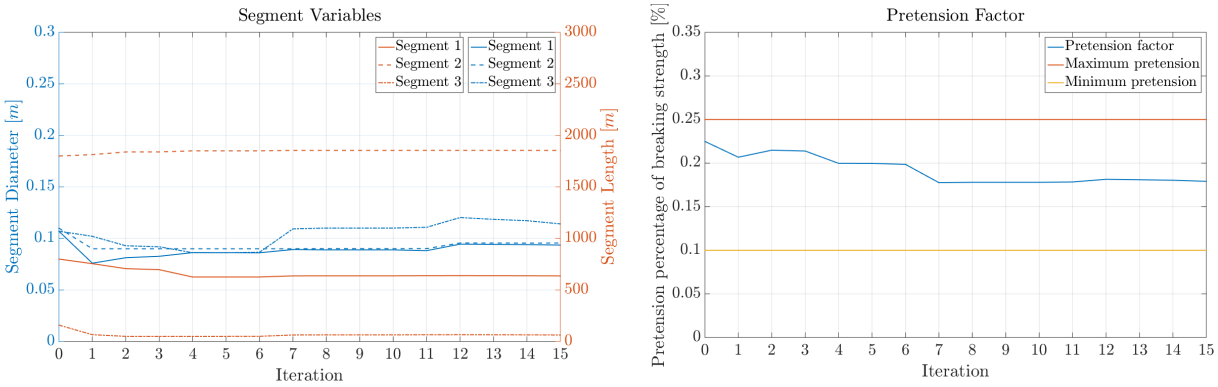

(a) Segment variables

(b) Pretension factor

Figure 7.28: Optimization variables.

The pretension factor is during this optimization decreased through several steps.

The optimization constraints are presented in Figure 7.29.

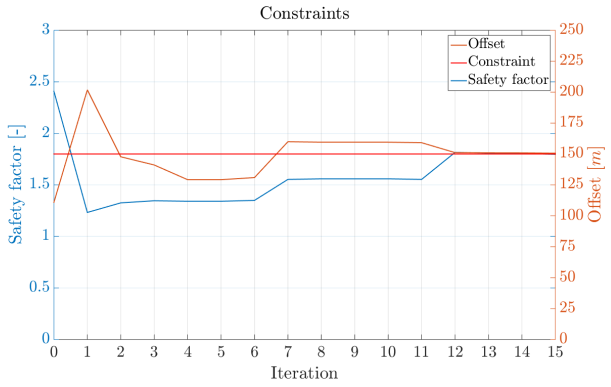

Figure 7.29: Optimization constraints.

As seen from the figure, the safety factor strictly decreases during the first iteration. This reduction of the safety factor is due to the reduction in the diameter of segment 1, and thus the breaking strength of the mooring line. The safety factor is then gradually increased as the diameter of segment 1 is increased until the constraint is reached.

The offset increases during the first iteration. This is also due the reduction in diameter of segment 1, as the breaking strength decreases and the pretension factor is almost constant. Thus, a decrease in the pretension is present and the mooring system stiffness decreases. In accordance with equation 7.5, 7.6 and 7.7 this results in increased offset. The offset is then reduced to the constraint level due to increase in diameter of segment 1, while the pretension factor is somewhat reduced.

The final values of all the optimization variables are presented in Table 7.24.

Diameter [mm]			Length [m]			Pretension
Segment 1	Segment 2	Segment 3	Segment 1	Segment 2	Segment 3	Factor [-]
93.574	95.533	114.120	636.550	1854.100	63.168	0.17908

Table 7.24: Optimized variables for steel wire rope and chain mooring system for Case 2.

The resulting breaking strength, pretension and cost of the mooring line, in addition to safety factor and maximum offset is presented in Table 7.25.

Constrains				
Safety factor [-]	Offset [m]	MBL [N]	Pretension [N]	Cost [NOK]
1.7970	150.65	$8.4477 \cdot 10^6$	$1.5128 \cdot 10^6$	$6.5347 \cdot 10^6$

Table 7.25: Parameters for steel wire rope and chain mooring system for Case 2.

Comparing the optimization variables of Case 2, presented in Table 7.24, to the variables in Case 1, presented

in Table 7.24, small differences are found in both the diameters and the lengths. The most drastic difference is the length of segment 1, which is reduced by approximately 350 m from Case 1 to Case 2. The over all length of the mooring line is also reduced.

Comparing Table 7.25 and Table 7.23, it is observed that the breaking strength is reduced for Case 2 compared to Case 1. This is due to the reduction of the diameter of segment 1. Along with a smaller pretension factor for Case 2 than for Case 1, the pretension is lower for Case 2 than for Case 1. The similarity in the offset, despite the lower pretension for Case 2, may be explained by the reduction in both length and weight of the mooring line. The reduced weight will decrease the geometric stiffness. The restoring force for these two cases will thus be different, as the play between the geometric and elastic stiffness is different.

The cost of the mooring system found in Case 2 has a cost reduced by 15.4 % compared to the mooring system found in Case 1. The reason for this large reduction in cost is the reduced constraint to the safety factor.

Case 3

The optimization of the cost for Case 3 is presented in Figure 7.30.

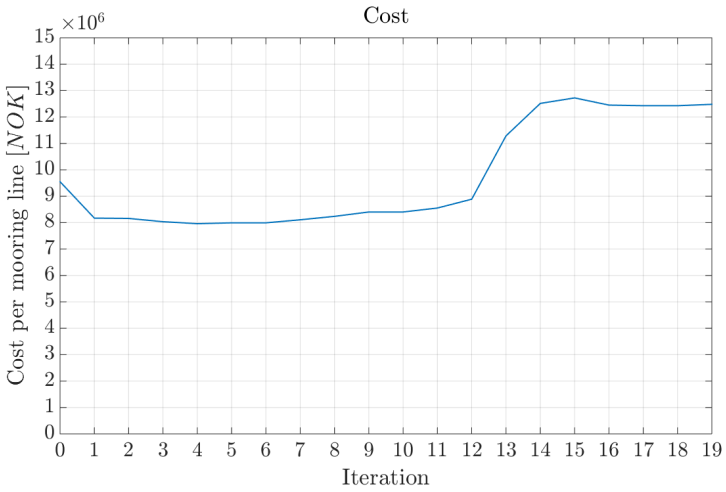

Figure 7.30: Cost for steel wire rope and chain mooring system for Case 3.

Also for this case the cost is reduced during the first iteration. A slight increase is observed until iteration 12 where the cost increases rapidly and converges at a value larger than the initial value.

The optimization variables are presented in Figure 7.31. As seen from Figure 7.31(a) the reduction in cost during the first iteration is dominated by the reduction in the diameter of the chain segments, in addition to reduction in the length of segment 3. At iteration 12 all three segment diameters are increased, while the

length of the segments stays approximately constant. Hence, it is the increase in segment diameters that increases the cost before it converges.

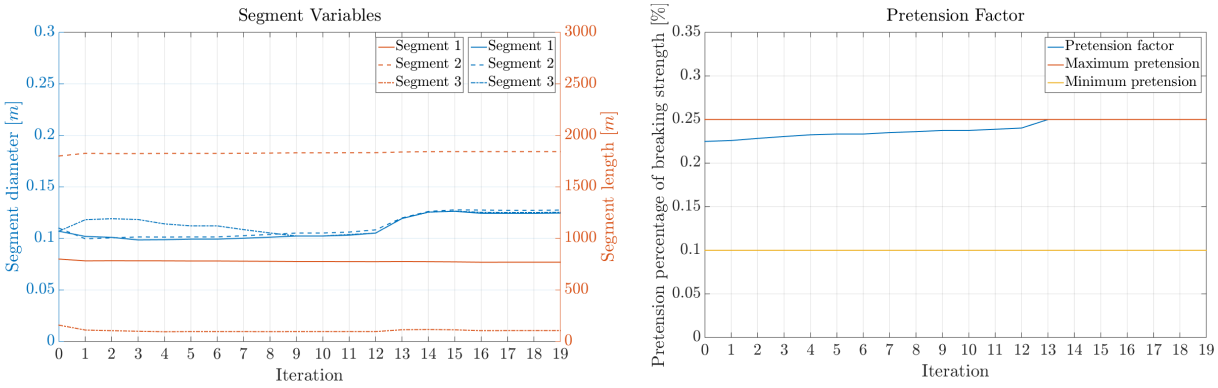

(a) Segment variables

(b) Pretension factor

Figure 7.31: Optimization variables.

The pretension factor, presented in Figure 7.31(b), is here observed to increase to the highest value during the optimization.

The optimization constraints are presented in Figure 7.32.

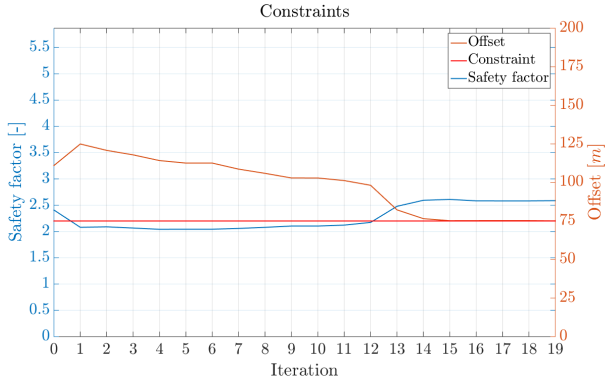

Figure 7.32: Optimization constraints.

The safety factor is reduced to a level slightly below the constraint during the first iteration as the diameter of the chain segments are decreased. However, as the segment diameters increase during iteration 12, the safety factor increases and stabilizes at a value above the constraint.

The constraint to the offset is for this case lower than for Case 1 and Case 2. The offset starts off at a value higher than the constraint. As the diameter of segment 1 and segment 3 decreases during the first iteration, the breaking strength decreases. And as the pretension factor is approximately constant during the first iterations, the pretension reduces. This gives reduced stiffness and increases the offset during the first iteration. As the breaking strength increases due to increased chain segment diameters and the pretension factor increases, the offset of the vessel decreases during the optimization until the constraint is fulfilled. This corresponds well with equation 7.5, 7.6 and 7.7.

The final values of all the optimization variables are presented in Table 7.26.

Diameter [mm]			Length [m]			Pretension
Segment 1	Segment 2	Segment 3	Segment 1	Segment 2	Segment 3	Factor [-]
124.63	127.540	125.370	769.600	1842.500	106.26	0.25000

Table 7.26: Optimized variables for steel wire rope and chain mooring system for Case 3.

The resulting breaking strength, pretension and cost of the mooring line, in addition to safety factor and maximum offset is presented in Table 7.27.

Constrains				
Safety factor [-]	Offset [m]	MBL [N]	Pretension [N]	Cost [NOK]
2.5868	75.068	$1.5057 \cdot 10^7$	$3.7641 \cdot 10^6$	$1.2480 \cdot 10^7$

Table 7.27: Parameters for steel wire rope and chain mooring system for Case 3.

Comparing the optimization variables for Case 3 presented Table 7.26 with the optimization variables for Case 1 in Table 7.22, it is observed that the segment diameters are much higher for Case 3 than for Case 1. It can also be observed that the overall length of the mooring line is larger for Case 1 than for Case 3.

The large diameters result in a much larger safety factor for Case 3 compared to Case 1, as seen from Table 7.27 and Table 7.23. The large breaking strength along with the maximum pretension factor provides large a large pretension, which results in the reduced offset.

The cost of this mooring system is 61.5 % higher than the cost of the mooring system found in Case 1. Hence, reducing the allowable offset of the vessel influences the cost greatly for the steel wire rope and chain mooring system.

Sensitivity Study: Environment

A verification of the optimization workflow for the steel wire rope and chain mooring system is also carried out, comparing the results with a minor difference in the environmental input. An optimization of the system with a significant wave height reduced by 5 cm is here performed. Figure 7.33 presents the cost of Case

1 with the initial and the reduced H_s.

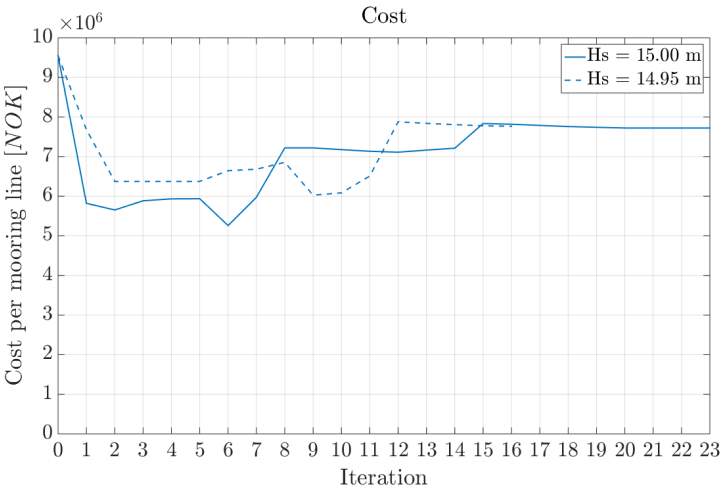

Figure 7.33: Cost for steel wire rope and chain system with variation in H_s for Case 1.

As seen from the figure, the small difference in significant height affects the search pattern of the optimization. There are similarities in these patterns, but the difference in cost is at some iterations large. However, both cost functions converges to approximately the same value, which is as expected.

The segment optimization variables are presented in Figure 7.34.

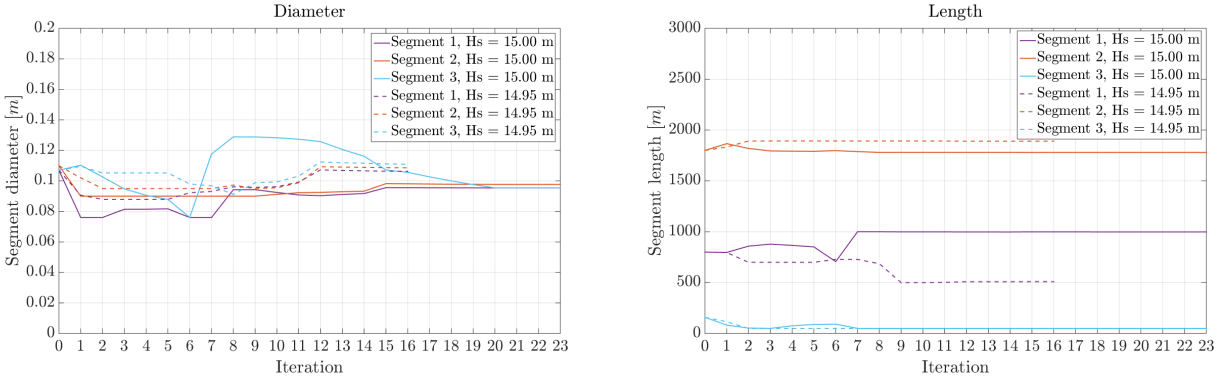

(a) Segment diameter

(b) Segment length

Figure 7.34: Segment variables.

The optimization of the segment diameters is presented in Figure 7.34(a). Some similarities in the optimization pattern for segment 1 and segment 3 are present. However, no clear similarity in the patterns is present

for segment 2. All segment diameters for the case with reduced H_s ends up at higher values than for the case with initial H_s.

The optimization of the segment lengths is presented in Figure 7.34(b). Some similarities for the search pattern of segment 3 and segment 2 are present, while for segment 2 the search patterns are quite different. Segment 2 for the case with reduced H_s ends up at a larger value than the case with initial H_s, while the opposite for is present for Segment 1. The length of segment 3 seems to end up at the same value for both values of H_s.

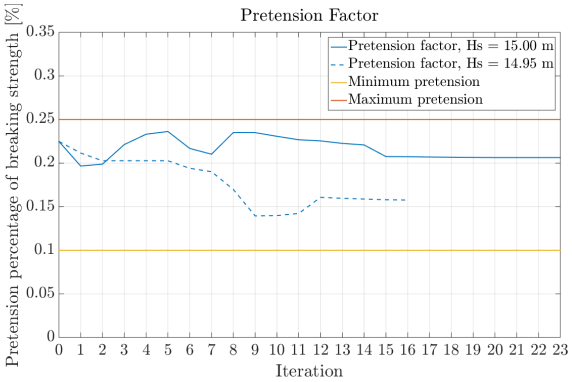

Figure 7.35: Pretension factor.

For the pretension factor, presented in Figure 7.35, the search patterns are not similar. The pretension factor ends up with a lower value for the case with reduced H_s compared to the case with the initial H_s.

The optimization constraints are presented in Figure 7.36.

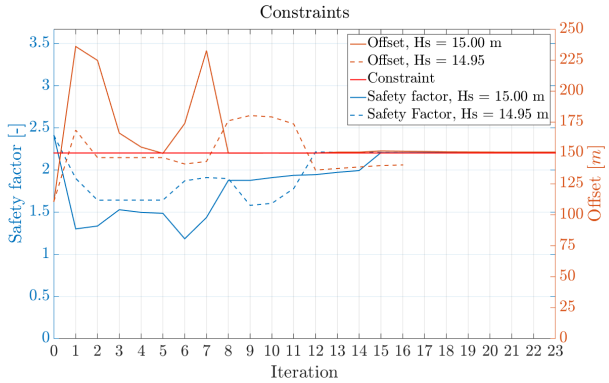

Figure 7.36: Optimization constraints.

Some similarities are present in the optimization patterns for the safety factor. This is as expected as the

breaking strength for both values of H_s mainly is depending on the diameter of segment 1.

The offset for both values of H_s is seen to peak during the first iteration. This peak is due to the reduction in breaking strength as the diameter of the chain segments decreases. However, the peak is larger for the case with the initial H_s as the pretension factor also reduces strictly for this case. The second peak for the case with reduced H_s occurs as the pretension factor reaches a minimum. The offset for the case with reduced H_s is further decreased by increasing both the breaking strength, by increasing the diameters, and increasing the pretension factor. The pretension is then increased, resulting in higher stiffness and thus by equation 7.5, 7.6 and 7.7 the offset decreases. The offset for the case with reduced H_s ends up at an offset below the offset for the case with initial H_s.

The final values of all the optimization variables for both values of H_s are presented in Table 7.28.

	Diameter [mm]			Length [m]			Pretension
H_s [m]	Segment 1	Segment 2	Segment 3	Segment 1	Segment 2	Segment 3	Factor [-]
14.95	106.280	108.590	110.89	509.070	1890.700	50.000	0.15760
15.00	95.388	97.694	95.426	998.320	1780.100	50.000	0.20636

Table 7.28: Optimized variables for steel wire rope and chain mooring system for Case 1 with H_s = 14.95 m and H_s = 15.00 m.

The resulting breaking strength, pretension and cost of the mooring line, in addition to safety factor and maximum offset for both values of H_s are presented in Table 7.29.

	Constrains				
H_s [m]	Safety factor [-]	Offset [m]	MBL [N]	Pretension [N]	Cost [NOK]
14.95	2.2066	140.35	$1.0915 \cdot 10^7$	$2.2524 \cdot 10^6$	$7.7660 \cdot 10^6$
15.00	2.2041	150.71	$8.8342 \cdot 10^6$	$1.8234 \cdot 10^6$	$7.7226 \cdot 10^6$

Table 7.29: Parameters for steel wire rope and chain mooring system for Case 1 with H_s = 14.95 m and H_s = 15.00 m.

The most noticeable difference observed in Table 7.28 is the difference in the diameters, and the length of segment 1.

The large diameters for the case with reduced H_s results in larger breaking strength of the line for this case, and thus higher pretension. The high pretension results in smaller offset compared to the case with initial H_s.

Although the composition of these two mooring systems is quite different with respect to segment diameters and lengths, the cost ends up at similar values. The mooring system with the reduced H_s is here about 0.4 %

more expensive than the mooring system with the initial H_s. This is an even smaller difference than for the polyester rope and chain mooring system.

Sensitivity Study: Global Minimum

A sensitivity study is also for the steel wire rope and chain mooring system performed in order to investigate if the minimum found for Case 1 is the global minimum of the cost function. Figure 7.37 presents the optimization of the cost from two different start points.

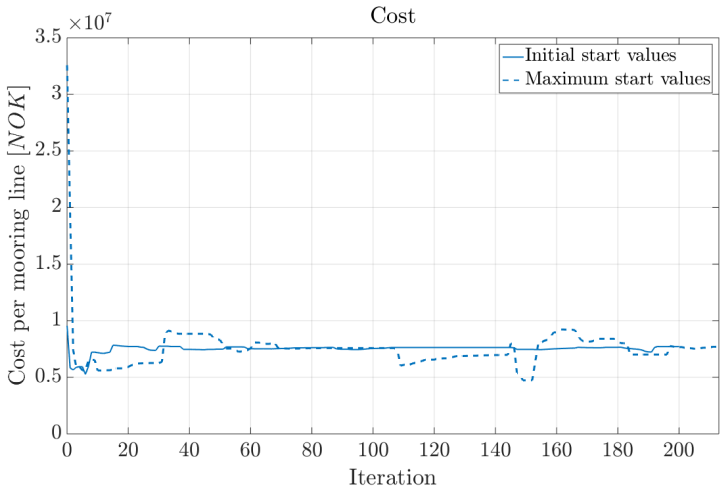

Figure 7.37: Cost for steel wire rope and chain mooring system for two different start points for Case 1.

The initial start point, presented in Chapter 7.2.2, is represented by the solid line and a start point with all maximum values are represented with the dashed line. As the optimization workflow was not able to statically configure a mooring system with all minimum values, only these to start points were considered in order to verify the global minimum of the cost function.

The description of the process is the same as presented in Chapter 7.4.2. Each time an optimization process ended, the final optimization values from this optimization were inserted as the new start values of a new optimization. This was repeated until a clear convergence for the two different start points towards the same minimum for the cost function were observed.

The optimization variables and constraints are presented in Appendix B.2.1. As seen from the plots, some differences are present for the segment diameters and lengths, especially for segment 1, for the two different start points. The pretension factor ends up lower for the optimization with the minimum values than for the initial start point. The safety factor and offset are both observed to end up at the constraint level.

The final values of all the optimization variables for the two different start points are presented in Table 7.20.

	Diameter [mm]			Length [m]			Pretension
Start point	Segment 1	Segment 2	Segment 3	Segment 1	Segment 2	Segment 3	Factor [-]
Initial	96.760	98.823	103.69	926.93	1763.20	59.417	0.20491
Minimum	108.91	110.42	107.90	500.20	1777.10	53.09	0.15126

Table 7.30: Optimized variables for steel wire rope and chain mooring system for two different start points for Case 1.

The resulting breaking strength, pretension and cost of the mooring line, in addition to safety factor and maximum offset is presented in Table 7.31.

	Constrains				
Start point	Safety factor [-]	Offset [m]	MBL [N]	Pretension [N]	Cost [NOK]
Initial	2.2004	149.98	$9.0396 \cdot 10^6$	$1.8523 \cdot 10^6$	$7.7107 \cdot 10^6$
Minimum	2.1993	150.04	$1.1286 \cdot 10^7$	$1.7071 \cdot 10^6$	$7.6898 \cdot 10^6$

Table 7.31: Parameters for steel wire rope and chain mooring system for two different start points for Case 1.

From Table 7.31 is can be seen that the cost function converges towards the same minimum. Compared to the same sensitivity performed for the polyester rope and chain mooring system, the difference in cost is even less for the steel wire rope and chain mooring system. This might be related to the larger number of iterations performed for this system compared to the polyester rope and chain system. As the convergence parameter apparently consider the result compared to the initial value, an increased number of optimizations will result in stricter convergence for the optimizations form the different start points.

7.4.4 Summary of Optimization Results

A summery of the optimization results introduced and discussed in section 7.4.2 and section 7.4.3 is in the following presented.

For the two mooring systems studied in this chapter, Case 1-3 investigated the optimization of the mooring system with different combinations of the constraints, as presented in Table 7.3. Case 1 is the base case for the optimization and requires a safety factor above 2.2 and a maximum offset in the direction of the loading of 150 m. Case 2 requires a safety factor of 1.8, while Case 3 requires a maximum offset of 75 m.

For the polyester rope and chain mooring system, the cost for each of these cases are presented in Figure 7.38.

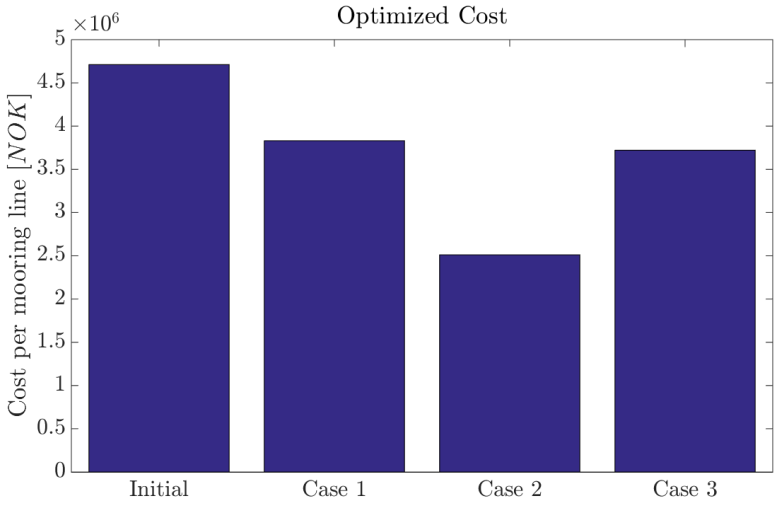

Figure 7.38: Optimized cost for polyester rope and chain mooring system.

There is as expected some differences in the cost for these three cases. Especially Case 2, with a reduced requirement to the safety factor, distinguishes from the two other cases. This is due to the fact that the optimization is observed to be governed by the safety factor constraint. The constraint to maximum offset is here set too large to influence the optimization result as the maximum offset ends up at about 65 m for Case 1. Hence, this offset is also below the offset constraint applied in Case 3. Thus, the cost of both Case 1 and Case 3 ends up very similar values.

As safety factor is dominating the optimization for the polyester rope and chain mooring system, the most remarkable differences are found for the segment diameters. This is expected as the segment diameters influence the breaking strength, which is used in the calculation of the safety factor. Some difference in the segment lengths is also observed for the three cases. However, the total length of the mooring lines does not differ remarkably for the cases.

The same three cases are carried out for the steel wire rope and chain system. The cost for each of these cases are presented in Figure 7.39.

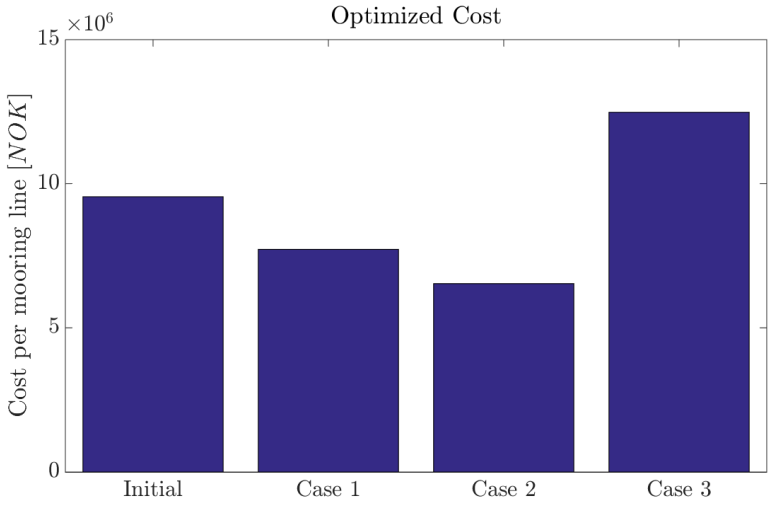

Figure 7.39: Optimized cost for steel wire rope and chain mooring system.

The cost is here very different for all three cases. This indicates that the constraints on both the safety factor and the maximum offset are of importance for the optimization of this system. The lowest cost is observed for Case 2. This is natural as this case has the lowest restrictions to both safety factor and maximum offset. The strict requirement of 75 m maximum offset is seen to raise the cost remarkably. In order to meet the offset constraint, the pretension in the lines needs to increase. The pretension is for this optimization given as a percentage of the breaking strength. Hence, increasing the diameters increases the breaking strength, which results in a higher pretension. The raise in cost is therefore here mainly due large segment diameters.

Some sensitivity studies are also carried out in order to verify the reliability of the optimization. All the sensitivities are performed based on Case 1 for each mooring system.

A small change in H_s is introduced to for both mooring systems in order to investigate how this influence the optimization results. For the polyester rope and chain system similarity in the search patterns is observed for the two cases with different H_s value, and the cost ends up at similar values. However, the composition of the mooring systems is somewhat different, with small differences for the chain segments. For the steel wire rope and chain system, the similarities in the search pattern are less distinct compared to the polyester rope and chain system. However, the cost ends up very similar also here despite some differences in the composition of the mooring lines.

A sensitivity study of the offset constraint is performed for the polyester rope and chain mooring system. This sensitivity is carried out as the maximum offset of the semisubmersible is far below the maximum offset allowed by the constraint. It is therefore desirable to investigate the influence of the chosen maximum offset constraint on the optimization. Optimizations with six different maximum offsets constraints in the

range 150 m - 70 m are carried out. Comparing these optimizations shows that this to some extent do influence the optimization result. As changing the constraints changes the mathematical formulation of the problem, the search patterns will be different for these optimizations. However, relatively large deviations are observed in the optimized costs. This is not as expected.

The last sensitivity investigates if the minimum found in Case 1 for both mooring systems is the global minimum of the cost function, and not a local minimum. The sensitivity verifies that the optimization ends up at the same minimum of the cost function regardless of starting point. Thus, the minimum is assumed to be the global minimum of the cost function. Even though the optimized cost for these different starting points indicate that the it is the global minimum that is found, the cost do not fully coincide. An attempt to converge the optimization towards the absolute lowest cost is therefore carried out. This is performed by using the optimized variables from one optimization as start values for the next optimization. For both mooring systems, all the optimizations converge towards the same cost by use of this method. However, the exact same cost is not found.

The sensitivities carried out for the two mooring systems may indicate that the global minimum of the cost functions is relatively flat. The optimization algorithm will thus have a problem with locating the exact global minimum of the function.

7.5 Evaluation of the Optimized Mooring Systems

Two mooring system are optimized in this chapter. An evaluation of the resulting mooring systems established through the optimization is presented in the following.

7.5.1 Polyester Rope and Chain Mooring System

The least expensive mooring system consisting of polyester rope and chain found from the optimization is the mooring system found in section 7.4.2 during the sensitivity study of the global minimum. The combination of the segment diameter, segment lengths and pretension is presented in Table 7.32.

Diameter [mm]			Length [m]			Pretension
Segment 1	Segment 2	Segment 3	Segment 1	Segment 2	Segment 3	[N]
102.350	187.830	104.190	50.879	1841.700	50.000	$1.0112 \cdot 10^6$

Table 7.32: Segment diameters, segment lengths and pretension providing lowest cost for polyester rope and chain mooring system.

The safety factor constraint of 2.2 is satisfied for this mooring system. The mooring lines have a breaking strength of $1.0112 \cdot 10^4$ kN, and the mooring system provides a maximum offset of 62.7 m in direction of the environmental loads applied from 135°.

This combination of segment lengths and diameters results in a cost of $3.3252 \cdot 10^6$ NOK for each mooring line. Thus the whole mooring system costs approximately $53.2 \cdot 10^6$ NOK. However, this calculation only consider the cost of the mooring line itself, and not other necessary hardware components. Compared to the initial polyester rope and chain mooring system presented in section 7.2.1 the cost for the mooring system is reduced by 29.4 %.

The mooring system as shown in SIMO is presented in Figure 7.40.

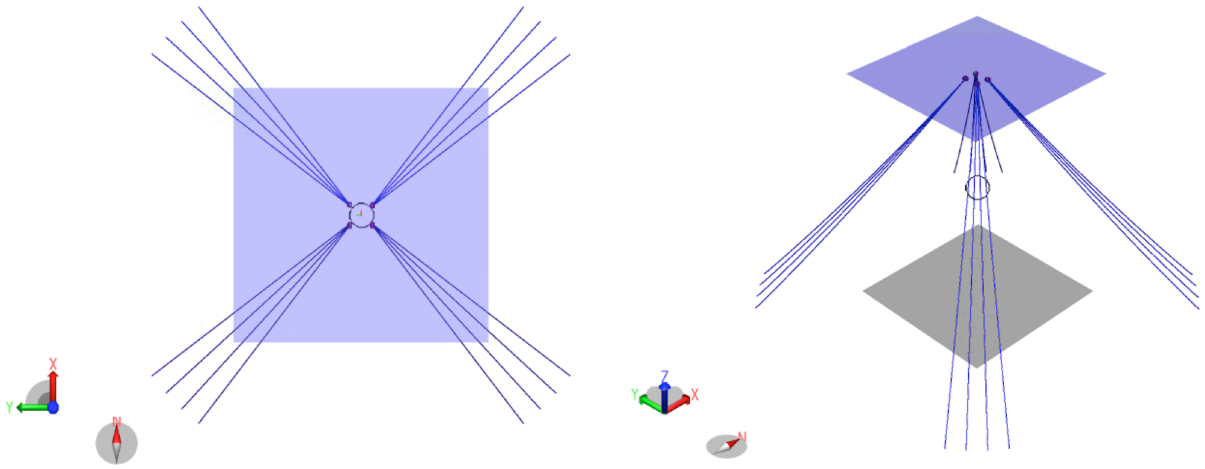

(a) Mooring system viewed diagonally

(b) Mooring system view from above

Figure 7.40: Optimized polyester rope and chain mooring system.

Comparing this mooring system to the polyester rope and chain mooring system presented in Table 7.4 and Table 7.5 in section 7.2.1, a quite large difference in the pretension of the mooring lines is observed. A relatively low pretension of about 1000 kN is observed for the optimized system.

Applying the maximum offset of the vessel to the mooring system in MIMOSA gives a suspended length of about 1900 m of the least loaded line. The length of segment 2 and segment 3 combined is 1891.7 m. Hence, contact between seabed and the polyester rope is close. Due to the abrasion characteristics of the polyester rope, contact with seabed shall not occur. An increase in the pretension, or increasing the length of the chain segment at the anchor, would therefore be important for this system in order to avoid contact.

Calculation of Vertical Load on Semisubmersible from Mooring System

Another important factor to consider during the design is the vertical load of the mooring system compared to the buoyancy of the semisubmersible. The load of the mooring system limits the amount of loads on the semisubmersible associated with production of oil and gas. A simple calculation is therefore carried out

in order to determine this load. For simplicity this calculation is carried out for the mooring system when no environmental loads are applied. The pretension of the mooring lines will therefore be the only tension present. This mooring line tension, T, will for the semisubmersible act as a force in the opposite direction. The angle α between the mooring line and the vertical line, as presented in Figure 7.41, will be the same for all mooring lines.

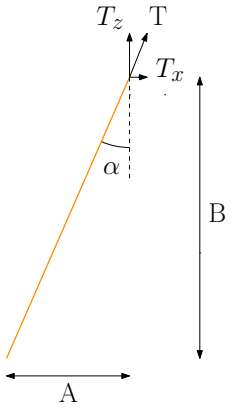

Figure 7.41: Mooring line tension.

where A is the distance to the anchor and B is the water depth. The polyester rope and chain mooring system is a taut-leg system, hence the determination of the α may here be calculated quite accurately by equation 7.8

$$\alpha = \tan^{-1}\left(\frac{\mathrm{A}}{\mathrm{B}}\right) \tag{7.8}$$

α is for this mooring system estimated to 39.4°. The vertical load of the mooring lines is then calculated by equation 7.9

$$T_z = T \cdot \cos(\alpha) \tag{7.9}$$

This calculation gives a vertical load of approximately $7.81 \cdot 10^2$ kN per mooring line. This corresponds to a total vertical load of $1.25 \cdot 10^4$ kN for the whole mooring system on the semisubmersible.

The displacement of the DEMO2000 is given in Table 6.1 in Chapter 6 as 75710 ton, which corresponds to a buoyancy force of about $7.43 \cdot 10^5$ kN. Subtracting the vertical force of the mooring system gives that $7.31 \cdot 10^5$ kN of buoyancy is left for the semisubmersible. Hence, the vertical force from the mooring system corresponds to about 1.7 % of the buoyancy of the semisubmersible. After personal correspondence with the supervisor this is acceptable.

Performing the same calculation for the initial system presented in Chapter 7.2.1, it is found that the total vertical load from the mooring system is about 29 % less for the optimized system compared to the initial

system. The angle α is larger for the initial system, giving a lower vertical load component. However, the pretension in the lines is significantly larger for the initial system compared to the optimized system. Increasing the pretension in the optimized system to a more realistic value, as discussed above, would however increase the vertical loading.

This calculation is carried out for the mooring system with no environmental forces applied. Presumably, the vertical forces will be higher when environmental forces are applied as the tension, at least in the windward lines, will increase. However, the angle α will also increase in these lines. Nevertheless, the total vertical force is assumed to increase.

7.5.2 Steel Wire Rope and Chain Mooring System

The least expensive steel wire rope and chain mooring system is found in section 7.4.3 during the sensitivity study of the global minimum. The combination of the segment diameter, segment lengths and pretension is presented in Table 7.33.

Diameter $[mm]$			Length $[m]$			Pretension
Segment 1	Segment 2	Segment 3	Segment 1	Segment 2	Segment 3	$[N]$
108.91	110.42	107.90	500.20	1777.10	53.09	$1.7071 \cdot 10^6$

Table 7.33: Segment diameter, segment lengths and pretension providing lowest cost for steel wire rope and chain mooring system.

The mooring system satisfies a safety factor of 2.2. The breaking strength of the mooring lines is $1.1286 \cdot 10^4$ kN, and the mooring system provides a maximum offset of 150 m in direction of the environmental loads applied at 135°.

The cost for this combination of segment diameters and lengths is $7.6898 \cdot 10^6$ NOK for each mooring line. The mooring system with 16 mooring lines thus has a cost of approximately $1.23 \cdot 10^7$ NOK. This cost only includes the cost of the mooring lines, and does not include other necessary mooring line hardware components. Compared to the initial steel wire rope and chain mooring system presented in section 7.2.2 the cost for the mooring system is reduced by 19.3 %.

Figure 7.42 shows the mooring system as presented SIMO.

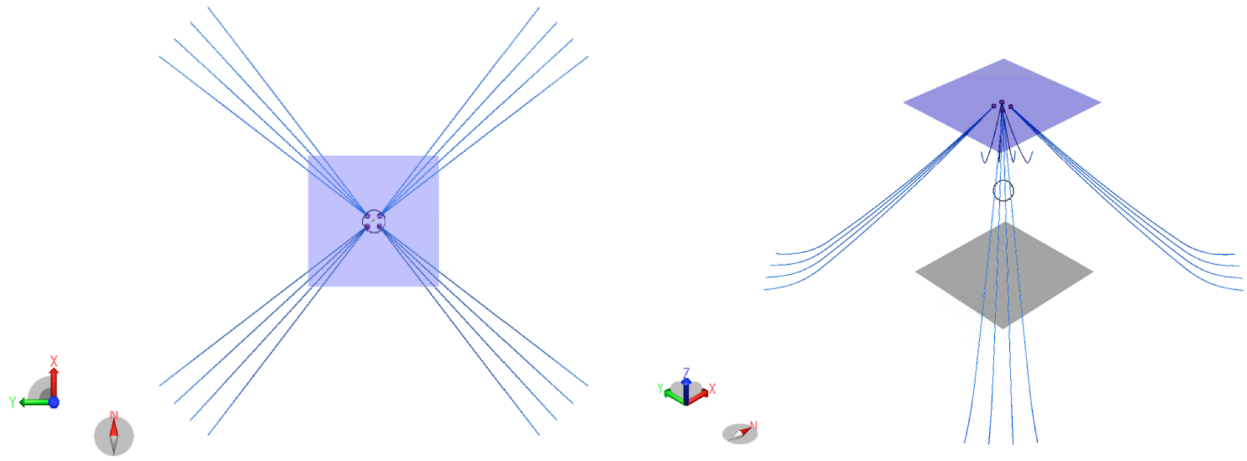

(a) Mooring system viewed diagonally

(b) Mooring system view from above

Figure 7.42: Optimized steel wire rope and chain mooring system.

Comparing this mooring system to the mooring system presented in Table 7.7 and Table 7.8 in section 7.2.2, it is also here observed that the pretension of the mooring lines are strictly reduced. This low pretension in combination with a relatively short chain segment attached to the anchor increases the risk for contact between the steel wire rope and the seabed as environmental loads are applied. Applying the maximum offset of the vessel to the mooring system in MIMOSA shows that for the least loaded line, the suspended length is about 1890 m. Taking into consideration that the length of segment 2 and segment 3 combined is 1831 m, it is clear that contact between steel wire rope and seabed is close. Contact between the seabed and the steel wire segment is not desirable due to the abrasion characteristics of the steel wire rope. Hence, this rough estimate shows that it would be natural to increase the pretension in further design.

Calculation of Vertical Load on Semisubmersible from Mooring System

A calculation similar to the calculation performed in section 7.5.1 is also performed for this mooring system. The vertical load form the mooring system on the semisubmersible is of special interest for this mooring system as the mooring lines are longer and has a larger weight compared to the mooring lines in the polyester rope and chain mooring system.

In this mooring system the mooring lines have a catenary figuration and there is some uncertainty is associated with the determination of the angle α, as presented in Figure 7.43.

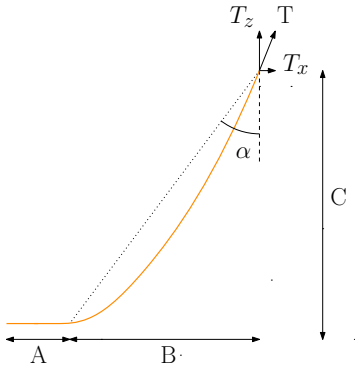

Figure 7.43: Mooring line tension.

The angle α is here found by use the suspended length and the distance to the anchor given from MIMOSA. The length of the mooring line resting on the seafloor, A, is estimated by subtracting the suspended length from the overall length of the mooring line. The distance from the attachment of the mooring line on the semisubmersible to the point where the mooring line touches the seafloor, B, is then estimated. The angle α is then found by

$$\alpha = \tan^{-1}\left(\frac{\mathrm{B}}{\mathrm{C}}\right) \tag{7.10}$$

where C is the water depth and B is distance to touchdown point. This gives α equal 43.5°.

As seen from the figure, the curvature of the mooring line is not accounted for here, which indicates that the angle calculated in somewhat too large. However, this approach provides a rough estimate.

The vertical load for one mooring line is by equation 7.9 estimated to $1.24 \cdot 10^3$ kN. This corresponds to a total vertical load from the mooring system of $1.98 \cdot 10^4$ kN. The remaining buoyancy of the semisubmersible is then $7.23 \cdot 10^5$ kN. Hence, the vertical load of the mooring system corresponds to about 2.7 % of the buoyancy of the semisubmersible. This value should, after personal correspondence with the supervisor, not be much larger than about 2 %. The main reason for this is that the cost of buoyancy is high. It is therefore desirable to keep the loading form the mooring system as low as possible.

Performing this same calculation for the initial steel wire rope and chain mooring system presented in section 7.2.2, it is found that the optimized mooring system applies about 36.1 % less vertical load compared to the initial mooring system. This is as expected as the pretension is much higher for the initial system.

It must here be pointed out that this calculation is just a rough estimate. The calculation overestimates the angle α, which gives a lower value for the vertical load. Hence, the calculation is not conservative. The calculation is carried out this way as either MIMOSA, SIMO or RIFLEX gives the angle of the mooring line.

It is also here assumed that the vertical load of the mooring system increases as environmental loads are applied.

7.5.3 Most Optimal Mooring System for DEMO2000

Observing the costs for the two different mooring systems presented in section 7.5.1 and section 7.5.2 it is seen that the mooring system consisting of polyester rope and chain is significantly cheaper than the steel wire rope and chain mooring system. As the cost of the mooring system is an important factor, this strongly indicates that the polyester rope and chain mooring system should be chosen for DEMO2000.

However, the cost of the mooring system hardware, as studied in this master thesis, does not fully reflect cost of the mooring system. Installation costs shall also be considered. The marine operations associated with the installation, especially for deep water, generates a larger part of the mooring system cost. Generally, the installations cost increases as with the amount of expensive equipment, i.e. number of ships, and the time spent at the installation. This indicates that higher pretension and increased weight of the mooring lines increases the complexity and thus the cost of the installation.

It may therefore be assumed that installation of the polyester rope and chain mooring system will be less complex to install than the steel wire rope and chain mooring system. A reduction in the complexity affects both the cost and the health, safety and environment (HSE) performance (K. Larsen, 2015). Consequently, the installation complexity, and installation cost, also arguments for DEMO2000 having a polyester rope and chain mooring system.

The offset is observed to be less than half for the polyester rope and chain mooring system compared to the steel wire rope and chain mooring system. This is as expected as a catenary system at deep water will impose low restoring force. Smaller offset of the semisubmersible indicates that less complex riser solutions may be installed. This may result in less expensive riser systems.

The vertical load on the semisubmersible from the mooring system, calculated for both mooring systems in section 7.5.1 and section 7.5.2, should also be considered when choosing the mooring system. It is desirable to have a mooring system that provides vertical loads which are as low as possible, in order to increase the payload. A catenary system will impose very large weights at deep water, as seen from the calculations carried out in the previous section. It is seen from these calculations that the polyester rope and chain mooring system provides about 36.9 % less vertical load to DEMO2000 compared to the steel wire rope and chain mooring system.

The polyester rope and chain mooring system will form this argumentation be the most optimal mooring system for DEMO2000.

7.6 Experiences with Optimization in SIMO

Marintek has not commercialized the optimization algorithm in SIMA used in this master thesis. An important part of the work performed in this thesis is thus to share the experiences and potential of improvement for the optimization algorithm.

The experiences are listed in the following:

- As this to a large extent is a pilot study, the access to optimization workflows similar to the one created for this master thesis was limited. A large amount of the time was therefore spent on setting up the optimization workflows for the specific problem in SIMO.
- SIMO do not provide a clear image of the line configuration. It is therefore hard to observe in SIMO which parts of the mooring line that are in contact with the seabed. As a consequence of this, it was necessary to view the optimized mooring system in MIMOSA in order to find the suspended length of the mooring line.
- It was during the optimization desirable to include a constraint on which segments that was allowed to be in contact with the seabed. This was especially a problem for catenary system composed of steel wire rope and chain. However, SIMA lacks an easy way to set constraints on which segments that are allowed to be in contact with the seabed. Thus, in order to avoid the contact between the steel wire rope segment and the seabed the maximum and minimum value of the optimization variables needed to be selected carefully. This selection was performed by using MIMOSA. Several different combinations of segment lengths, segment diameters and pretension were tested in combination with the maximum offset in MIMOSA to determine the range for the optimization variables. Due to the large number of variables, this was a very time demanding process. The optimized mooring system presented in Chapter 7.5.2 is, despite of the testing in MIMOSA, close to having contact between the steel wire rope segment and the seabed at maximum offset.
- The sensitivity studies show that small changes in the optimization problem may affect the results quite a bit. This is logic as changing the constraint or the variables results in a new mathematical formulation, and the search direction will therefore be different. However, the offset sensitivity study performed for the polyester rope and chain mooring system gave relatively large variation in cost, even though the offset was way below the constraint. Such large variations was not as expected, and a good explanation for this behavior is not found.
- During the thesis work, a too large value for the breaking strength for the polyester rope segment was by a mistake included in the optimization. As the safety factor constraint dominates the optimization of the polyester rope and chain mooring system, this affected the optimization results greatly. The mooring lines segments were for the optimization of Case 1 and Case 3 reduced to minimum value, resulting in a mooring line of about 1600 m. This gave an unrealistic small seabed footprint of the mooring system. Inserting the correct breaking strength, gave totally different results. As the correct breaking strength was lower than the incorrect one, the mathematical formulation was affected with respect to the safety factor constraint and the pretension. Hence, the optimization results turn out very different for these to cases.
- A repeating problem when optimizing the steel wire rope and chain mooring system was that SIMO

was not able to statically configure the catenary lines. This problem occurred due to too small minimum values of the variables, and showed the importance of selecting realistic ranges for the variables.

- The convergence parameter *desired final accuracy* was not described in the optimization help content in SIMO. The information about this parameter was also limited from Marintek, except for that this is a convergence parameter both effecting the cost function and the constraints. The default value for this parameter, corresponding to 0.01, was used throughout all the work with the optimization. Reducing this parameter to 0.0001 in order to observe how this would affect the optimization in Case 1 compared to the sensitivity study of finding the global minimum for the polyester rope and chain mooring system was performed. It was conceivable that reducing this parameter would have the same affect as running several optimizations with the results from the previous as input to the next. However, this was not what was observed in from the results. The optimized cost with reduced convergence parameter was somewhat lower than the cost found with the default value, but larger than the cost found from the global minimum sensitivity. However, SIMA states that the *desired final accuracy* should not be much smaller than the accuracy by which the gradients are computed. As the delta value of the optimization variables in fact were not changed, thus larger than the convergence parameter, this may have affected the results.

Chapter 8

Dynamic Analysis of Mooring Line Tension

The mooring line top end tension is in SIMO calculated quasi-statically, as described in section 4.4.1. As stated in section 4.3.1 a quasi-static calculation of the mooring line tension is not sufficient unless the effects form the mooing line dynamics are demonstrated neglectable according to (DNV GL, 2013). Dynamic calculation of the top end tension, described in section 4.3.2, is therefore applied in most cases.

This chapter investigates the difference in top end tension calculated by quasi-static and dynamic analyzes. The mooring systems presented in section 7.5.1 and section 7.5.2 are both studied. Dynamic analyzes in the time domain is carried out in RIFLEX, presented in section 4.4.2. Dynamic and quasi-static analyzes in the frequency domain using MIMOSA are also included in the comparison. The theory concerning frequency domain analysis and MIMOSA was covered in detail in the project thesis and is not described in detail in this thesis.

8.1 RIFLEX Model in SIMA

A RIFLEX model is composed in order to perform time domain dynamic calculation of the top end tension present in the most loaded mooring line. The setup of the RIFLEX model is in the following described.

8.1.1 Global Coordinate System

The coordinate system in RIFLEX is similar to the coordinate system applied in SIMO. The x-y plane of the global coordinate system is placed at the sea surface with the z-axis pointing upwards. The global coordinate system with mooring line configurations are presented in Figure 8.1.

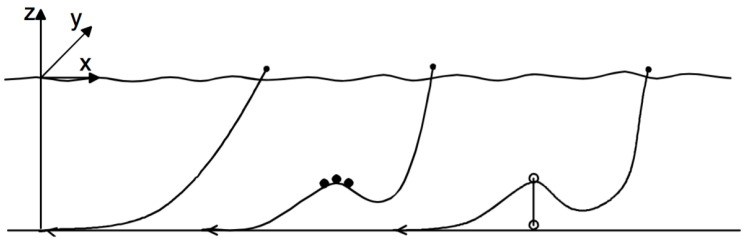

Figure 8.1: Examples of mooring line configurations with global coordinate system (Marintek, 2012).

8.1.2 Arrangement of RIFLEX Model

The RIFLEX model is limited to only consist of the most loaded mooring line. This reduces the computational time compared to model consisting of all mooring lines, and provides a good basis for comparing the different analysis methods. In addition, the most loaded mooring line will be of interest for the safety factor of the mooring system.

The model is composed by converting the catenary system of the SIMO model into RIFLEX. Default settings for all necessary parameters are then provided. A brief description of the RIFLEX model is presented in the following.

Catenary system

The mooring line is composed of bar elements. Bar elements are only deformed in axial directions, and are therefore often used to model cables, chains and ropes (C. A. Felippa, 2004).

The length of the elements is chosen to approximately 30 m. This element size is decided from correspondence with the supervisor, in order to minimize the computational time. A sensitivity on the mesh size was carried out in order to verify convergence of the results from the dynamic analyzes. This sensitivity proved reasonable results at this mesh.

The top end tension and displacement are studied for the top end node of the mooring line. However, the mooring line segments are numbered differently in RIFLEX than in SIMO. Figure 8.2 presents the mooring line with mooring line segments in RIFLEX.

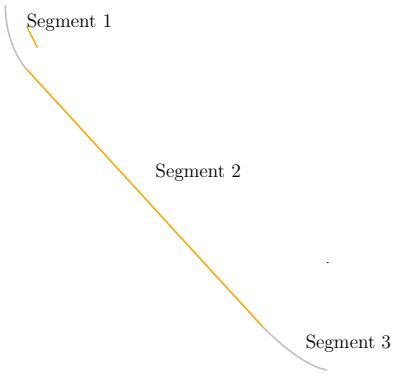

Figure 8.2: Composition of mooring line in RIFLEX.

The segment attached to the fairlead is in RIFLEX segment 1, while the segment attached to the anchor is segment 3. Hence, tension and displacement is studied for the first node in segment 1.

In order to reduce artificial vibrations in the springs attaching the nodes, the global stiffness proportional damping factor is set to 0.03.

Forced irregular motions from file

The irregular motions obtained from the simulations of the semisubmersible with mooring system in SIMO are included in the RIFLEX model by file. The file includes motions in all six degrees of freedom for the specific time step.

The simulation time step is set to 0.01 s, while the desired data is stored each 50 time step.

8.1.3 Comparison of Displacement in SIMO and RIFLEX

The displacement is for SIMO given for the semisubmerible in the center of gravity, corresponding to the origin. However, for RIFLEX the displacement is given for the top end of the most loaded mooring line. The most loaded line in mooring line number 10, which is attached to the fairlead with coordinates (38 m, -46 m, -31 m). As SIMO provides the time series of surge, sway, heave, roll, pitch and yaw at origin of the global coordinate system, and the mooring line is attached to the semisubmersible at a known position in this coordinate system, it is possible to use a simplified approach to verify the motion at this point, assuming rigid body motion and small rotations. The motion is found by equation 8.1 (O. M. Faltinsen, 1990)

$$s = (\eta_1 + z\eta_5 - y\eta_6)\,i + (\eta_2 - z\eta_4 + x\eta_6)\,j + (\eta_3 + y\eta_4 - x\eta_5)\,k \tag{8.1}$$

where η_1 η_2, η_3, η_4, η_5 and η_6 is surge, sway, heave, roll, pitch and yaw, respectively. x, y and z refers to the coordinates in the global coordinate system.

A comparison of the motion calculated with equation 8.1 based on SIMO and motion in RIFLEX, with mean values removed, is presented in the following.

Polyester Rope and Chain Mooring System

For the polyester rope and chain system, the comparison of motion in x-, y- and z-direction is presented in Figure 8.3. The figures include the whole time series and a cut out of the time series. A transient phase of 1200 s is removed from the time series, and the time period for the cut out is arbitrary.

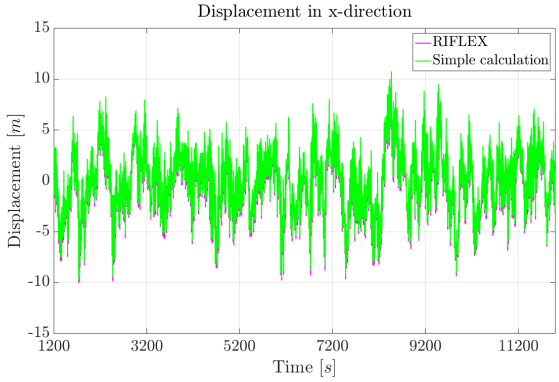

(a) Displacement in x-direction

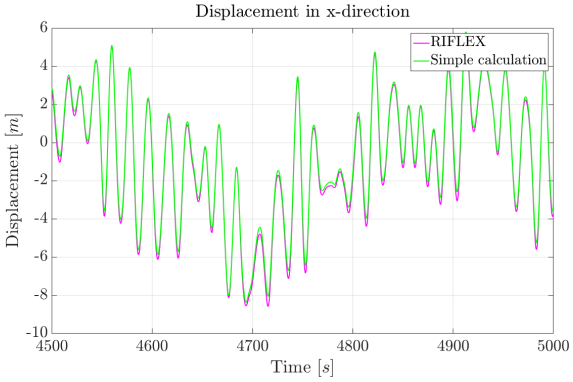

(b) Cut out of displacement in x-direction

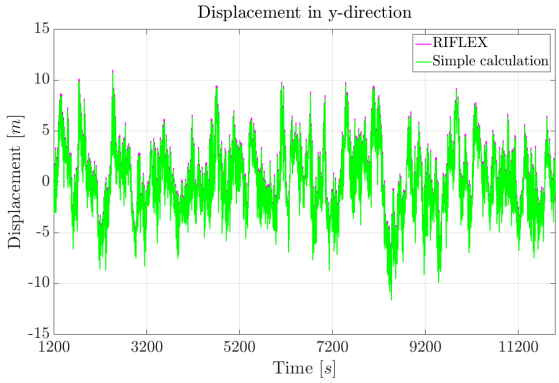

(c) Displacement in y-direction

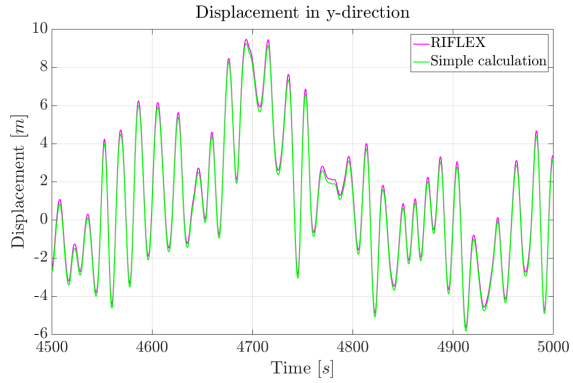

(d) Cut out of displacement in y-direction

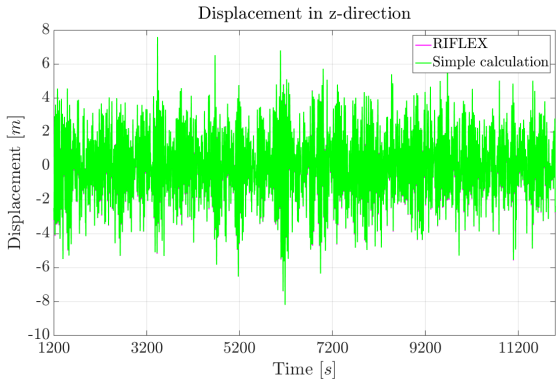

(e) Displacement in z-direction

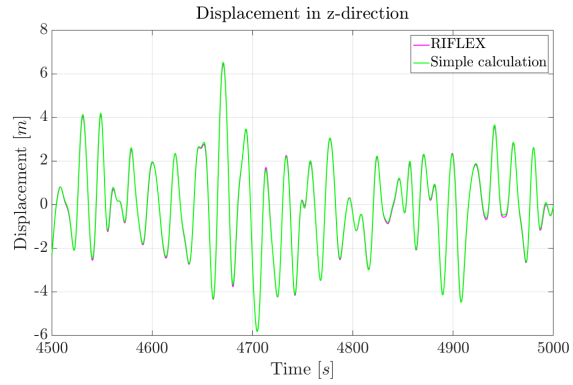

(f) Cut out of displacement in z-direction

Figure 8.3: Displacement in x-, y- and z-direction for RIFLEX and simple calculation based on SIMO.

Small deviations are seen at the largest motion responses, probably because the assumption of small rota-

tions are less valid at these points. Hence, it may be concluded that the motion provided directly by RIFLEX at the fairled point is correct. This output may therefore be utilized as prescribed top end motion of the mooring line for further analysis in RIFLEX.

Observing the time series in x- and y-direction, clear LF and WF motions are observed. As described in section 4.1.3 the LF motions are important in the horizontal plane, as restoring force in this plane only are present due to the mooring system. The response specter in x- and y-direction is presented in Figure 8.4.

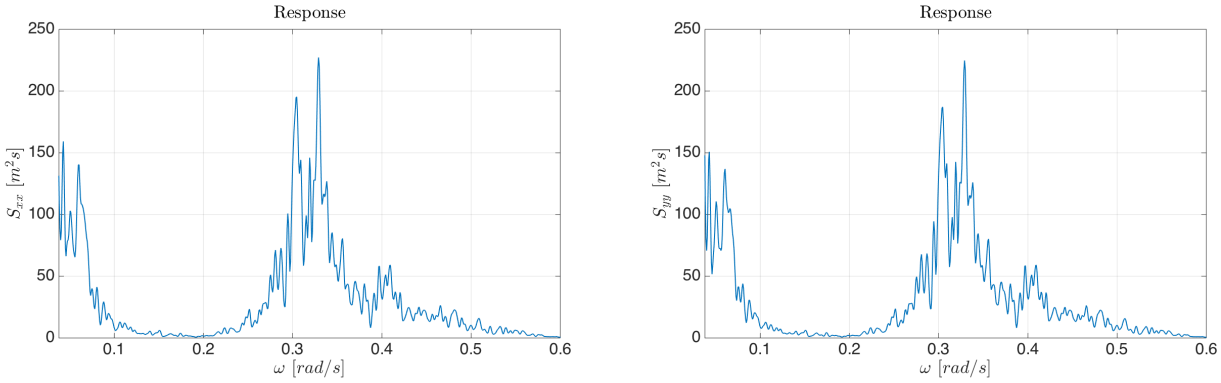

(a) y-direction (b) x-direction

Figure 8.4: Response specter.

As seen in both spectra, two peaks are present. The first peak is located at about ω equal 0.05 rad/s, which corresponds to the natural frequency of the semisubmersible in surge and sway, as presented in Table 6.3 in section 6.2.3. Excitation around this frequency will generate large response. However, the waves applied to semisubmersible has a peak period of 19.8 s corresponding to ω about 0.3 rad/s. The excitation is therefore high at this frequency, as observed from the response spectra.

For lower frequencies than presented in these spectra, quasi-static response due to wind and wave drift will dominate. Hence, for observing the dynamic effects this part is not of interest.

For the motion in the z-direction, only clear WF motions are observed. As described in section 4.1.3, large hydrostatic restoring forces will be present in the vertical plane. The low frequency motions will therefore not be of significant importance here.

Steel Wire Rope and Chain Mooring System

A comparison of the motions calculated by equation 8.1 based on SIMO and the motions from RIFLEX are presented for the x-, y- and z-direction in Figure 8.5. Also here the whole time series and a cut out of the time series are included in the figures. A transient phase of 1200 s is removed, and the cut out of the time series is

arbitrary.

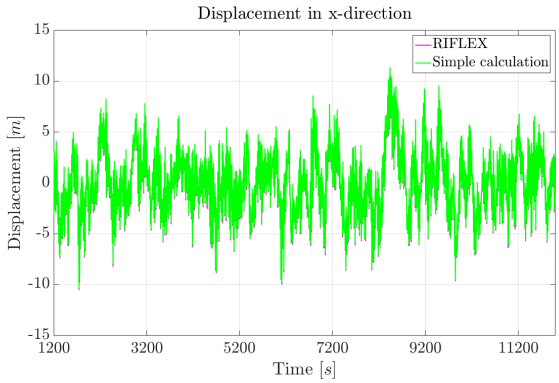

(a) Displacement in x-direction

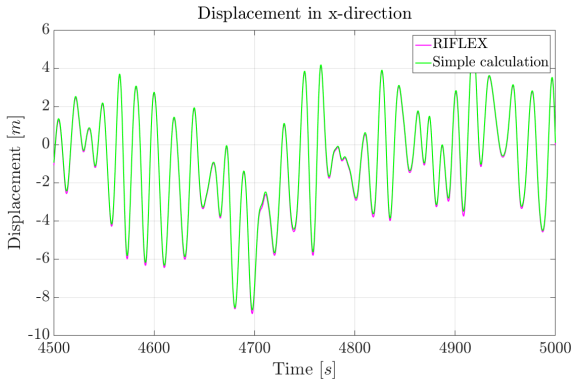

(b) Cut out of displacement in x-direction

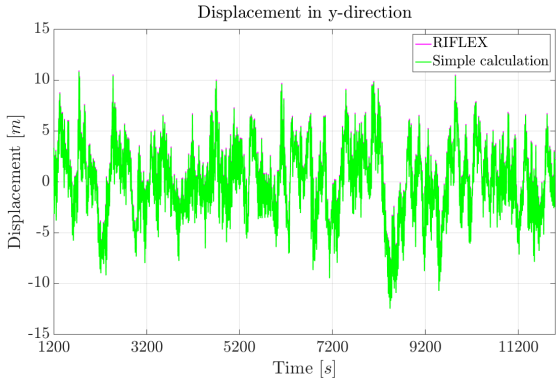

(c) Displacement in y-direction

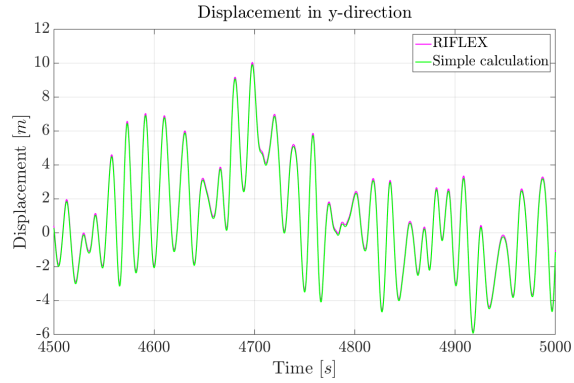

(d) Cut out of displacement in y-direction

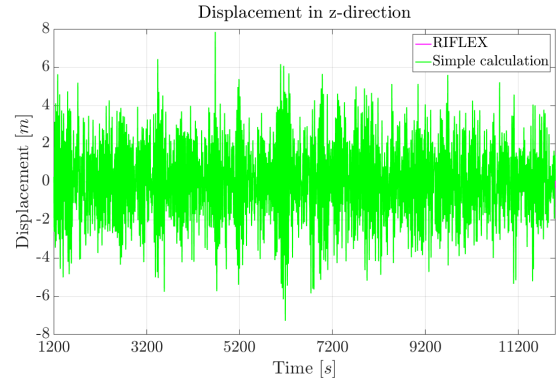

(e) Displacement in z-direction

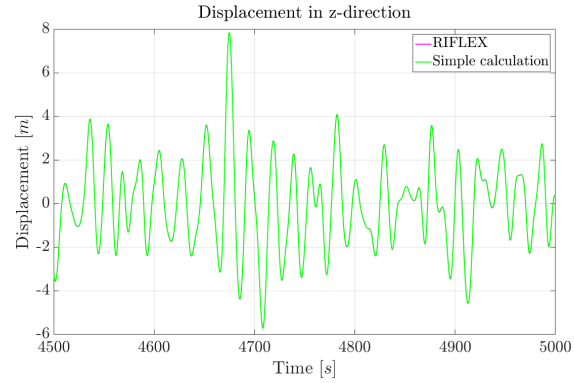

(f) Cut out of displacement in z-direction

Figure 8.5: Displacement in x-, y- and z-direction for RIFLEX and simple calculation based on SIMO.

The simple calculation based on SIMO corresponds well with the motions given by RIFLEX also for this system. Hence, it may be concluded that the motion provided directly by RIFLEX at the fairlead point is correct, and may be used in further analysis.

LF and WF motions are clearly present for the motion in the x- and y- direction. Observing the spectrum for these two directions, presented in Figure 8.6, the same trend as for the polyester rope and chain system is present.

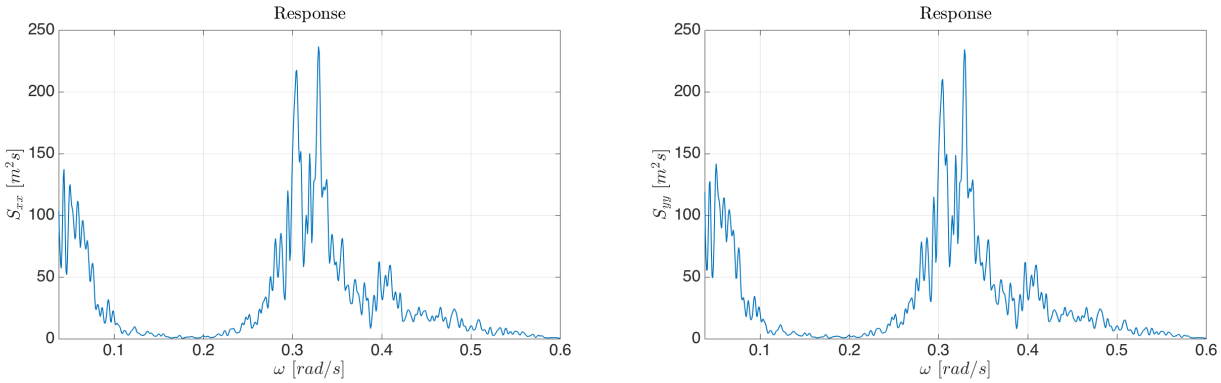

(a) y-direction

(b) x-direction

Figure 8.6: Response specter.

One response peak is located around the natural frequency of semisubmersible, and an other response peak is located around the peak period of the applied waves.

In z-direction the motion is observed to be dominated by WF.

8.2 Top End Tension of Most Loaded Line

The main focus of this section is to compare and discuss the top end tension calculated by a quasi-static analysis using SIMO and a dynamic analysis using RIFLEX. However, results from MIMOSA are here also included.

The analyzes performed in the TD are all based on one realization of three hours. The maximum tensions presented below for the analyzes carried out in SIMO and RIFLEX is therefore not the most probable maximum tension described in section 4.3.3. This provides some uncertainty in the comparison of the results from the TD analyzes and the FD analyzes.

8.2.1 Comparing Frequency Domain and Time Domain

MIMOSA performs the mooring line analysis in FD. In order to compare the analysis performed in FD and in TD, the main differences of these methods should be mentioned. A brief introduction to FD and TD analysis was presented at the beginning of Chapter 4. However, the differences are described more in detail in the following, based on (C. M. Larsen, 1992).

The key difference of these methods are connected to the statistics. Linearization is required in the FD model. Hence, with a Gaussian distributed wave load, the predicted response in FD will also be Gaussian. The non-linear load process is however, correctly represented in the TD procedure, which gives a response that is non-Gaussian. The FD result gives a complete description of the statistics of the response process, while the TD result is a sample of an unknown stochastic process. The statistical properties are therefore estimated based on this sample. This provides some statistical uncertainty that is not present in the FD analysis. However, the model uncertainty is larger in the FD method compared to the TD method due to linearization. The statistical uncertainty in the TD may be overcome by performing many or very long simulations. The model uncertainty in the FD cannot be overcome as some kind of linearization always will be present, and as the spectrum representation of the response process always is linked to the Gaussian distribution. The question is therefore how large the model uncertainty connected to the FD method is, and to what extent the non-linear load process gives non-Gaussian response.

8.2.2 Polyester Rope and Chain Mooring System

Top End Motion

In order to the discuss the top end tensions for the most loaded line, the top end motions calculated in SIMO, RIFLEX and MIMOSA needs to be considered. As described in section 8.1.3, the motion at the top end of the most loaded mooring line will be the same for the calculation performed in SIMO and in RIFLEX. However, the calculation of the top end motion in the FD using MIMOSA is different from the calculation performed in SIMO.

MIMOSA estimates the total motion by separately calculating the WF motion and the LF motion. Significant motion and extreme motion for both LF and WF are estimated, and the extreme total maximum motion is found by combining the LF motion and the WF motion with the mean offset in accordance with the a combination rule. This procedure is described in the project thesis, and can be found in MIMOSA User's Manual (K. E. Kaasen, H. Lie and K. Mo, 2012). As stated in section 6.1.2 the motion equation is solved in SIMO by use of the method separation of motions. This method is described in section 4.4.1 and involves separating the WF and LF motions. However, the LF and WF motions estimated in SIMO are taken from the same realizations and is therefore correlated.

The extreme motions are presented in Table 8.1 and are given for the vessel origin. Due to different coordinate systems in MIMOSA and SIMO, the motions are given as absolute values. The load is applied from Northeast.

	Total maximum motion $[m]$		
	x	y	z
SIMO/RIFLEX	43.43	45.35	7.16
MIMOSA	39.90	40.84	4.91

Table 8.1: Motion of vessel in SIMO/RIFLEX and MIMOSA.

As seen from the table, the motions calculated in SIMO are slightly higher compared to MIMOSA for all three directions. However, the motions are very similar, due to the fact that SIMO and MIMOSA uses the same RAOs.

Top End Tension

The top end tension of the most loaded line in SIMO and RIFLEX is presented in Figure 8.7. As seen from the figure, a transient phase of 1200 s is removed from the time series in order to get reliable results.

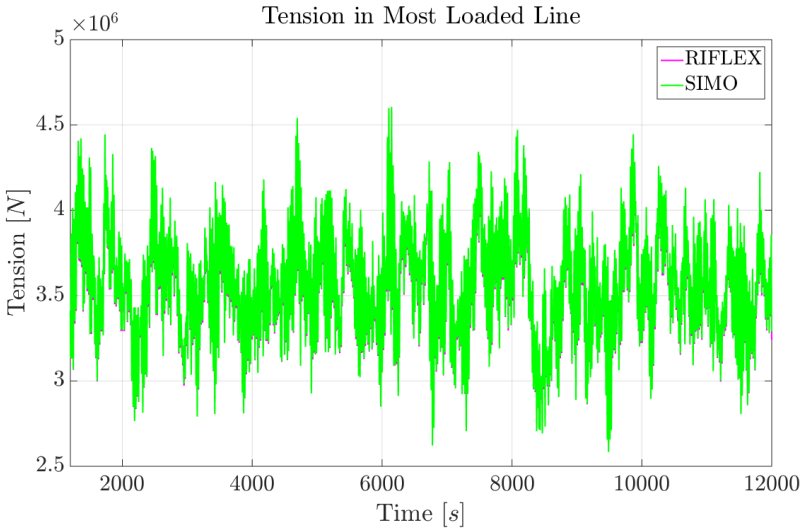

Figure 8.7: Time series of top end tension in most loaded line.

The tension maxima present for the quasi-static analysis performed in SIMO are generally larger than the tension maxima present for the dynamic calculation performed in RIFLEX. However, the dynamic and quasi-static analysis results are very similar. This trend is even more clear from observing a cut out of the time series as presented in Figure 8.8.

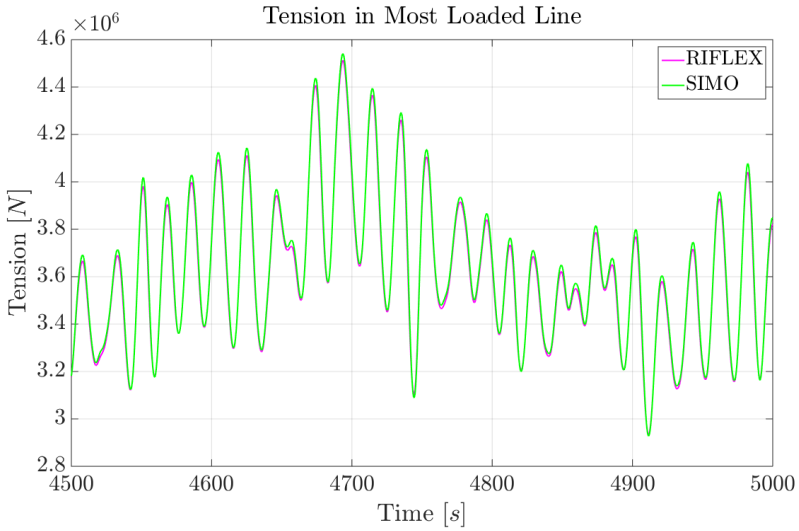

Figure 8.8: Cut out of time series of top end tension in most loaded line.

Table 8.2 presents a comparison of the mean, minimum, maximum and standard deviation of the top end tension in the most loaded line calculated by SIMO and RIFLEX. Calculation performed in MIMOSA, both quasi-static and dynamic analysis, is also included in the comparison.

	Tension [N]			
	Mean	Minimum	Maximum	Std
SIMO	$3.5651 \cdot 10^6$	$2.5840 \cdot 10^6$	$4.6063 \cdot 10^6$	$3.0016 \cdot 10^5$
RIFLEX	$3.5480 \cdot 10^6$	$2.5944 \cdot 10^6$	$4.5669 \cdot 10^6$	$2.9550 \cdot 10^5$
MIMOSA QS	$3.4376 \cdot 10^6$	-	$4.5258 \cdot 10^6$	-
MIMOSA FEM	$3.4376 \cdot 10^6$	-	$4.4689 \cdot 10^6$	-

Table 8.2: Tension in most loaded line for polyester rope and chain mooring system calculated in SIMO, RIFLEX and MIMOSA.

The quasi-static analysis is, as described in section 4.3.1, performed by statically offsetting the structure in accordance with the wave-induced motions. The dynamic actions of the mooring line associated with mass, damping and fluid acceleration is in this approach neglected. The dynamic analysis, described in section 4.3.2, accounts for the time-varying effects due to mass, damping and fluid acceleration. Hence, drag forces caused by the displacement of the mooring line and inertia forces introduced by the weight of the mooring line are included in this analysis method.

As observed Table 8.2, the analysis performed in the TD provides approximately the same values for mean, minimum, maximum and standard deviation. Hence, the importance of the dynamic effects is neglectable for this mooring system. This is as expected as the mooring system is a taut-leg system with restoring force

dominated by elastic stiffness. As described in section 4.1.1 the mooring line can be here be described by a spring as presented in Figure 8.9.

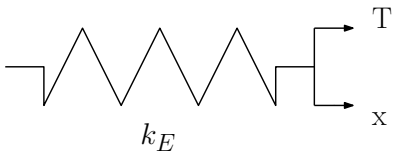

Figure 8.9: Schematic of restoring force for polyester rope and chain mooring line.

The elongation of the line dominates the restoring force of the mooring line, and the tension will only depend on the position of the top end. The influence of velocity and acceleration in the horizontal and vertical plane is therefore neglectable. Consequently, a quasi-static analysis will provide a good approximation of the top end tension for this mooring system.

Nevertheless, it is observed that the quasi-static analysis performed in SIMO provides somewhat larger values than the dynamic analysis performed in RIFLEX. As described in section 4.4.1, the tension calculated in the quasi-static analysis is in SIMO a function of displacement in the horizontal and vertical plane. The SIMO model in this thesis uses five points of offset variations in the vertical plane, with maximum and minimum z-position given as -10 and 10, respectively. As observed from Figure 8.3(e), the vertical displacements of the semisubmersible is within this offset variation. However, between these five points interpolation occurs. This interpolation may introduce some inaccuracies, which may cause these small differences.

Comparing the quasi-static analysis of the mooring line performed in SIMO and MIMOSA, the results are very similar. The tension computed in SIMO is somewhat higher than the tension calculated in MIMOSA. However, MIMOSA computes lower extreme motions in x- and y-direction compared to the motions used in SIMO. As described in section 8.2.1, the FD method requires linearity. The stiffness is thus linearized in MIMOSA. SIMO however, updates the line characteristics throughout the calculation and non-linearities in the stiffness will therefore be taken into account. Linearizing the stiffness is here observed to not influence the results greatly for this mooring line.

The same trend is also present for the dynamic analysis of the mooring line tension. RIFLEX provides somewhat larger tensions than MIMOSA. As the same motions are applied in RIFLEX as in SIMO, larger extreme motions are present for RIFLEX compared to MIMOSA. The calculation method for the dynamic calculation used in RIFLEX and MIMOSA are different. Both programs divide the mooring line into elements (H. Lie, Z. Gao and T. Moan, 2007). However, MIMOSA performed the dynamic calculation by use of the catenary equations, while RIFLEX uses finite element method. In addition, MIMOSA only accounts for the dynamic effects in a simplified manner, as stochastic linearization of the non-linear drag forces is required in the frequency domain (C. M. Larsen, 1992). However, as the tension is dominated by the position of the top end for this mooring line, the dynamic effects will not be of great importance. The main reason for the difference is therefore most probably the difference in calculation method.

Sensitivity Study: Safety Factor

One of the constraints applied to the optimization carried out in Chapter 7 was to fulfill the requirement to safety factor stated by ISO. The safety factors for the calculations performed in SIMO, RIFLEX and MIMOSA are presented in Table 8.3.

	SIMO	RIFLEX	MIMOSA QS	MIMOSA FEM
Safety factor [-]	2.2004	2.2142	2.2343	2.2627

Table 8.3: Safety factor for calculations performed in SIMO, RIFLEX and MIMOSA.

All safety factors are for this mooring system above the requirement of 2.2 as SIMO provides the larges maximum tension in the most loaded mooring line.

Sensitivity Study: Dynamic Amplification Factor

The tension is in the above compared for one realization, which introduces some uncertainties to the results. In order to verify that the trend in these results is realistic, three more time series is here analyzed in both SIMO and RIFLEX. These realizations, including the realization used for the optimization in Chapter 7 and the comparison above, are presented in Table 8.4.

	Realization 1	Realization 2	Realization 3	Realization 4
Wave seed	1	5	7	11
Wind seed	1	20	26	35

Table 8.4: Realizations used for calculation of dynamic amplification.

The analysis results obtained for these four realizations are here used to calculate the relationship between tensions including dynamic effects and the tensions excluding dynamic effects. A dynamic amplification factor (DAF) is here defined as in equation 8.2

$$\text{DAF} = \frac{(T_{max} - T_{mean})_{\text{RIFLEX}}}{(T_{max} - T_{mean})_{\text{SIMO}}} \tag{8.2}$$

The results for these calculations are presented in Table 8.5.

	Realization 1	Realization 2	Realization 3	Realization 4
DAF [-]	0.9786	0.9798	0.9835	0.9791

Table 8.5: DAF calculated for four realizations.

As seen form the table, the differences in DAF for these four realizations are small. This verifies that the trend observed earlier in this section, with neglectable influence of the dynamic effects for this mooring system.

A quasi-static analysis provides realistic values of the mooring line tension for this mooring system.

8.2.3 Steel Wire Rope and Chain Mooring System

Top End Motion

The extreme motions for the vessel with the steel wire rope and chain mooring system is also compared for SIMO, and RIFLEX, and MIMOSA. These extreme motions are presented in Table 8.6.

	Total maximum motion [m]		
	x	y	z
SIMO/RIFLEX	104.61	108.20	7.20
MIMOSA	104.36	108.52	5.65

Table 8.6: Motion of vessel in SIMO/RIFLEX and MIMOSA.

The motions calculated in SIMO and MIMOSA is observed to be very similar, despite the difference in calculation method of the extreme motion for this two simulations tools.

Top End Tension

The top end tension in the most loaded line calculated by quasi-static analysis in SIMO and by dynamic analysis in RIFLEX is presented in Figure 8.10.

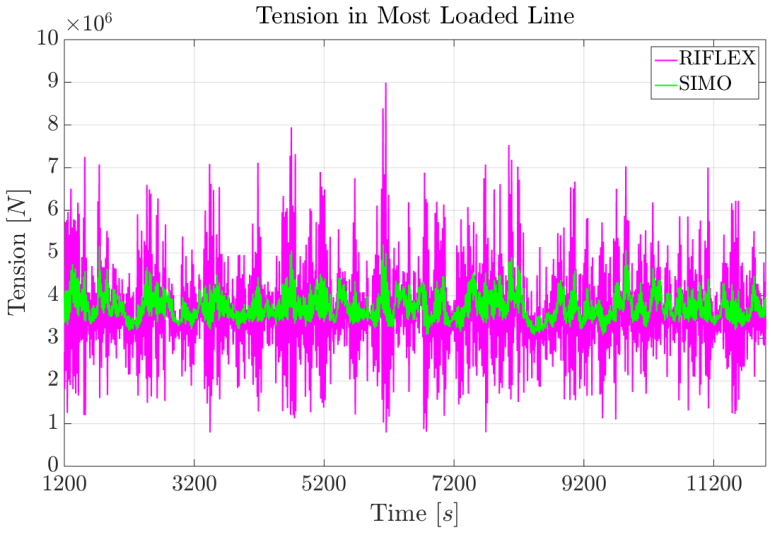

Figure 8.10: Time series of top end tension in most loaded line.

As seen from the figure, the calculation from RIFLEX results in much larger tensions than for the calculation performed in SIMO. An arbitrary cut out of the time series is presented in Figure 8.11.

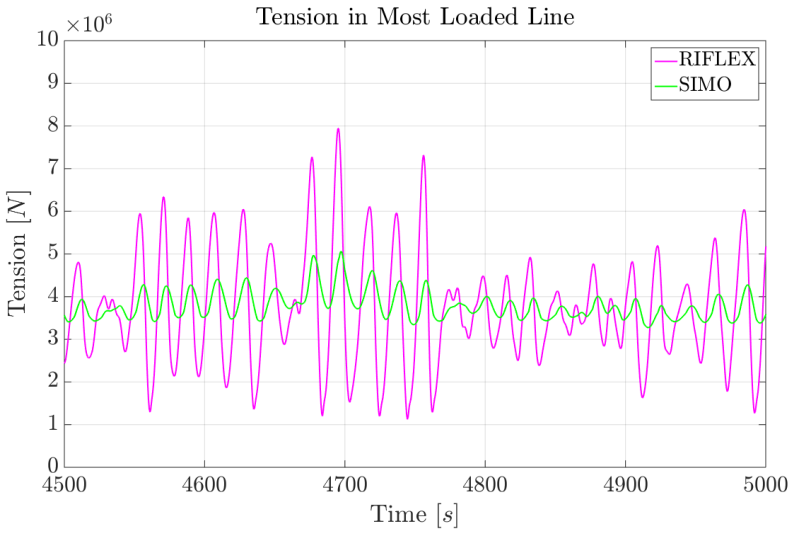

Figure 8.11: Cut out of time series of top end tension in most loaded line.

The mean, minimum, maximum and standard deviation of the time series are presented in Table 8.7.

	Tension [N]			
	Mean	Minimum	Maximum	Std
SIMO	$3.7132 \cdot 10^6$	$3.0740 \cdot 10^6$	$5.2009 \cdot 10^6$	$3.0238 \cdot 10^5$
RIFLEX	$3.6351 \cdot 10^6$	$7.9128 \cdot 10^5$	$8.9925 \cdot 10^6$	$9.3703 \cdot 10^5$
MIMOSA QS	$3.6616 \cdot 10^6$	-	$5.6248 \cdot 10^6$	-
MIMOSA FEM	$3.6616 \cdot 10^6$	-	$1.0532 \cdot 10^7$	-

Table 8.7: Tension in most loaded line for steel wire rope and chain mooring system calculated in SIMO, RIFLEX and MIMOSA.

Comparing the analysis performed in the TD, presented in the table and figures above, large differences in the maximum and minimum tensions are observed. These large differences are caused by the calculation method as discussed in section 8.2.2, which is of great importance to the result for this mooring system.
The mooring lines do here have a catenary configuration, and the restoring force will be a combination geometric and elastic stiffness. As geometric stiffness, as described in section 4.1.1, arises through the change of line geometry, the lateral movements of the mooring line will be significant. A simple schematic of the mooring line is presented in Figure 8.12.

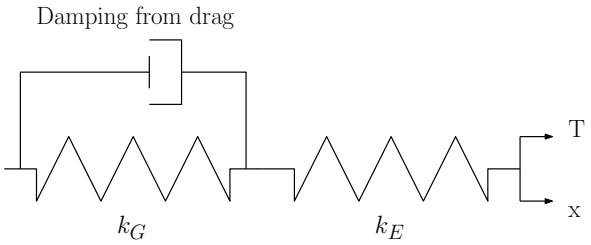

Figure 8.12: Schematic of steel wire rope and chain mooring line.

Drag forces will act as damping forces on the mooring line as it moves laterally. This, in addition to the dynamic effects from inertia forces, will prevent the mooring line from following the motion of the semisubmersible. This results in the large span between the maxima and the minima of the tension calculated in RIFLEX, seen from Figure 8.10.

Even though the motions of the semisubmersible are very similar for SIMO and MIMOSA, there are some difference in the quasi-static analyzes performed in these two simulation tools. The maximum tension from MIMOSA is observed to be somewhat higher than the maximum tension calculated in SIMO. As described in section 8.2.1, and as discussed for the polyester rope and chain mooring system, linearization of all non-linearities is required in order to calculate tension in the FD. The geometric stiffness present for this mooring system will contribute to a non-linear restoring force. SIMO is able to account for this non-linear stiffness as the line characteristics are updated during the calculation. MIMOSA however, linearized the stiffness. The geometric stiffness is thus not properly accounted for in MIMOSA, which will have an influence on the results. The linearizations performed in MIMOSA is in Table 8.7 observed to provide a somewhat larger tension compared to the calculation in SIMO where the non-linearites are taken into account.

Difference in the maximum tension calculated by dynamic analyzes performed in MIMOSA and RIFLEX are also observed, despite the similarity in the offset of the semisubmersible. The linearization of the geometric stiffness in MIMOSA will also be present here. In addition, the calculation method used in MIMOSA and RIFLEX are different as discussed in section 8.2.2. MIMOSA uses the catenary equation for the elements, while RIFLEX uses finite element method. The dynamic effects are, as discussed in Chapter 8.2.2, only included in a simplified way as the drag model is linearized. RIFLEX, on the other hand, properly accounts for the dynamic effects. It should also be mentioned that the linearization performed in MIMOSA also includes linearization of the touch down point. This means that the bottom node is kept fixed. The variation in seafloor contact is hence neglected in MIMOSA. The simplifications carried out in MIMOSA compared to RIFLEX are expected to provide in some deviation of the results. As seen from Table 8.7, MIMOSA provides larger values for the maximum tension compared to RIFLEX. The linearizations performed in MIMOSA are therefore also here seen to overestimate the maximum tension.

Sensitivity Study: Safety Factor

The large differences observed for the maximum tensions in Table 8.7 will influence the safety factor. Safety factors estimated based on the maximum tensions calculated in SIMO, RIFLEX and MIMOSA are presented in Table 8.8.

	SIMO	RIFLEX	MIMOSA QS	MIMOSA FEM
Safety factor [-]	2.1993	1.2250	2.0065	1.0716

Table 8.8: Safety factor for calculations performed in SIMO, RIFLEX and MIMOSA.

As seen from the table, the dynamic analysis performed in RIFLEX and MIMOSA result in safety factors which are far below the requirements for the NCS. This indicates that the design of this mooring system is not feasible. Several changes need to be performed in further design in order for this catenary system to have sufficient strength.

Sensitivity Study: Dynamic Amplification Factor

A sensitivity study of the relationship between the tensions estimated including dynamic effects compared to excluding the dynamic effects are also for this mooring system carried out. Equation 8.2 is used in order to calculate the DAF for four realizations, based on the same wave and wind seeds as presented in Table 8.4. The calculated DAF for each realization is presented in Table 8.9.

	Realization 1	Realization 2	Realization 3	Realization 4
DAF [-]	3.6011	3.9215	3.3143	3.8515

Table 8.9: DAF calculated for four realizations.

As seen from the table, the dynamic amplification is large for this mooring system. The dynamic effects amplifies the quasi-static analysis results up to about four times for the largest calculated DAF. However, there is some deviation in the DAF for the four different realizations. The DAF calculated for realization 2 is 15.5 % larger than the DAF calculated for realization 3.

These large DAF values may be explained by the large water depth. The water depth affects both the amount of steel in water span and the lateral motions. The amount of steel creates large weight which introduce inertia forces connected to the acceleration, while the large lateral motions results in a large amount of drag forces on the mooring lines connected to the velocity.

As stated in the beginning of this chapter, a quasi-static calculation of the mooring line tensions are not sufficient unless mooring line dynamics are demonstrated as neglectable according to (DNV GL, 2013). The mooring line dynamics are definitely not neglectable for this system, and changes need to be included in order for the mooring system to fulfill the requirements for NCS.

Chapter 9

Summary and Recommendations for Further Work

9.1 Summary and Conclusions

In this master thesis, automated optimization of mooring systems has been addressed. Chapter 2 gave a brief introduction to station keeping principles in terms of moored systems. The main mooring hardware components including mooring line, mooring line components and anchor types was also introduced here. Chapter 3 introduced the design limit states of which mooring system analyzes shall be performed in accordance with. Definition of the maximum design condition and maximum operation condition was also presented in this chapter.

Chapter 4 gave an introduction to time domain simulation. The equation of motion was here presented, and each part of the equation was described. The definition of separated and coupled approach was presented, and the two approaches were compared. Mooring line response including quasi-static and dynamic analysis was also described. A brief description of extreme value statistics was also included. Last, this chapter gave a description of how time domain simulations in SIMO and RIFLEX are performed.

The theory concerning automated optimization algorithms was presented in Chapter 5. Basic optimization theory including sequential quadratic programming and the optimization algorithm NLPQLP was here briefly described. Specification of the optimization problem for mooring lines in terms of objective function, variables and constraints was also presented. The last part of this chapter addressed how automated optimization of mooring systems may be performed in SIMA workbench.

The semisubmersible used for the optimization in this master thesis was presented in Chapter 6. Calculation of hydrostatic stiffness, natural periods and damping was performed. A verification of the force coefficients and transfer functions describing waves, wind and current was also carried out. The mooring system was presented, and the setup of the model in SIMO was described. The last part of this chapter contained comparison of analyzes performed in MIMOSA, as part of the project thesis, and analyzes performed in SIMO.

The optimization of the mooring system for the semisubmersible was presented in Chapter 7. The optimization problem was here defined in terms of the cost function, variables and constraints, and three optimiza-

tion cases were defined. Two different mooring systems, one constructed of steel wire rope and chain and the other of polyester rope and chain, were studied. A description of the arrangement of the optimization in SIMA workbench was also given. The optimization results were through the rest of this chapter presented and discussed. An evaluation of the optimized mooring system was also included.

Dynamic analysis of the mooring line tension was performed in RIFLEX in Chapter 8. The simulation in RIFLEX was performed for the most loaded mooring line using the separated approach, importing top end motions calculated in SIMO into RIFLEX. A comparison of the top end tension calculated in SIMO, RIFLEX and MIMOSA was in this chapter presented and discussed.

From the optimization and analyzes performed in Chapter 7 and Chapter 8 the following may be concluded:

- Automated optimization in SIMA may contribute to a significant reduction in cost of the mooring system. The polyester rope and chain mooring system gave the lowest cost at $53.2 \cdot 10^6$ NOK, which corresponded to a reduction compared to the initial polyester rope and chain mooring system of 29.4 %. The optimization of the steel wire rope and chain mooring system gave a cost reduction of 19.3 % compared to the initial mooring system of this type, ending up at the cost $1.23 \cdot 10^7$ NOK.
- The setup of the optimization problem in SIMA is crucial in order for the optimized mooring system to be realistic. Especially, defining the maximum and minimum value for the optimization variables are important. As a consequence of too large span in the optimization variables, the pretension of the mooring lines in both mooring systems ended up very low and the chain segments short. Polyester rope and steel wire rope is therefore close to having contact with seafloor for the optimized mooring systems at maximum offset.
- SIMO, RIFLEX and MIMOSA show good correspondence in the tension of the most loaded line for the polyester rope and mooring system. The dynamic effects are here observed to be neglectable, with a dynamic amplification approximately equal to one. Nor the linearization carried out in the frequency domain in MIMOSA affects the top end tension of the mooring line significantly.
- For the catenary system, constructed of steel wire rope and chain, dynamic effects are seen to affect the top end tension greatly. As the restoring force for this mooring system is non-linear, the linearization performed in the frequency domain influences the calculated top end tension remarkably. Hence, for the dynamic analysis the safety factor ends up far below the requirement.

9.2 Recommendations for Further Work

The work performed in this master thesis can be seen as the first step in the optimization of the mooring system of DEMO2000. Based on the result obtained in this work, choosing the polyester rope and chain mooring system for further optimization is natural as this provides the lowest cost with respect to hardware components.

Two different maximum offsets were studied in the optimization cases carried out in this thesis. The allowed maximum offset will strongly depend on the riser solution chosen for the semisubmersible. As seen from the

results, large allowed maximum offset gives lower mooring line cost. However, the opposite will be the case for the riser system cost. Expanding the optimization to include both the mooring system and riser system would therefore be interesting.

The range of the variables was observed to be somewhat large in the optimizations performed in this thesis. As the focus of the optimization algorithm is to find the lowest possible cost, the input provided by the user in terms of ranges for the variables must be considered carefully. For further optimization of the mooring system, or the riser system and mooring system combined, evaluating and reducing the range of the variables would most likely result in a more realistic system.

Installation cost is only mentioned briefly in this report. For deep water installations this represents a large cost and should be included to a larger extent in further design of the mooring system.

Bibliography

A. Næss and T. Moan (2013). Stochastic Dynamics of Marine Structures.

Aker Solutions. Engineering.

API Recommended Practice (2005). Design and Analysis of Stationkeeping Systems for Floating Structures.

B. Leira (2010). Stochastic Dynamics of Marine Structures [Lecture Notes].

B. Pettersen (2004). Hydrodynamics.

Bridon. Structural Systems Brochure.

Bridon (2013). Oil and Gas Catalogue.

C. A. Felippa (2004). Introduction to Finite Element Method.

C. M. Larsen (1992). Use of Stochastic Dynamic Analysis in Marine Riser Design. *NSF Workshop on Riser Mechanics*.

C. M. Larsen (2014). Marine Dynamics.

Deep Sea Anchors. DPA Concepts.

DNV GL (2012). DNV-OS-H203: Transit and Positioning of Offshore Units.

DNV GL (2013). DNV-OS-E301: Offshore Standard.

G. T. Houlsby and B. W. Byrne (2004). Design Procedures for Installation of Suction Caissons in Clay and Other Soils.

H. Lie, Z. Gao and T. Moan (2007). Mooring Line Damping Estimation by a Simplified Dynamic Model. *OMAE*.

H. Ormberg and K. Larsen (1998). Coupled Analysis of Floater Motion and Mooring Dynamics for a Turrent Moored Ship.

H. Ormberg, I. J. Fylling, K. Larsen and N. Sødahl (1997). Coupled Analysis of Vessel Motions and Mooring and Riser System Dynamics. *OMAE*.

I. J. Fylling. Optimisation of Mooring and Riser Systems Including Fatigue Life Requirements [PowerPoint Slides].

I. J. Fylling (2013). Optimisation of Mooring and Riser System for Deep Water Floating Production Systems Including Fatigue Life Requirements.

ISO Standards (2013). ISO 19901-7: Petroleum and Natural Gas Industries - Specific Requirements for Offshore Structures.

J. Nocedal and S. J. Wright (2006). Numerical Optimization.

K. E. Kaasen, H. Lie and K. Mo (2012). MIMOSA User's Documentation.

K. J. Eik and E. Nygaard (2004). Heidrun Metocean Design Basis.

K. Larsen (2014). Static Equilibrium of Mooring Line.

K. Larsen (2015). Mooring and Station Keeping [Lecture Notes].

K. Schittkowski (1986). NLPQL: A Fortran Subroutine for Solving Constrained Nonlinear Programming Problems. *Annals of Operations Research*.

K. Schittkowski (2011). NLPQLP: A Fortran Implementation of a Sequential Quadratic Programming Algorithm with Distributed and Non-Monotone Line Search.

L. Wang (2010). Coupled Analysis of Deepwater Floating Systems. *Environmental Loads and Responses Network Meeting*.

Marintek. SIMA User Guide.

Marintek. Software Offshore Dynamics.

Marintek (2012). RIFLEX User's Manual.

Marintek (2013). SIMO Theory Manual.

O. M. Faltinsen (1990). Sea Loads on Ship and Offshore Structures.

Ramnäs Bruk (2015). Product Catalogue.

S. Chakrabarti (2005). Handbook of Offshore Engineering.

Vryhof Anchors (2015). Anchor Manual.

Y. Inoue, H. Miyabe, X. Weiyi and M. Nakamura (1991). Comparative Study on the Quasi-Static Analysis and Dynamic Simulations for Estimating the Maximum Tensions of Mooring Lines. *International Offshore and Polar Engineering Conference*.

Appendix A

Force Coefficients and Transfer Functions

A.1 Quadratic Current Coefficients

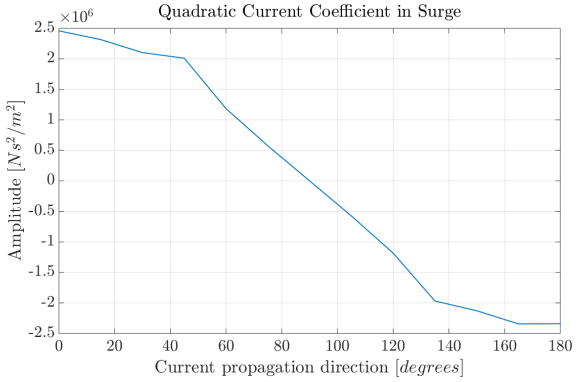

(a) Surge

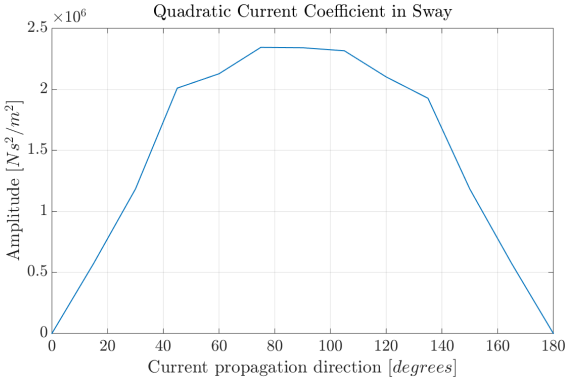

(b) Sway

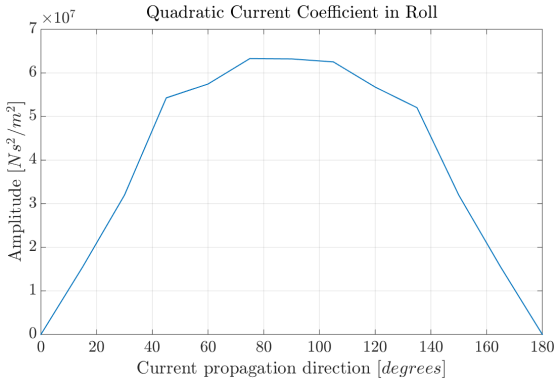

(c) Roll

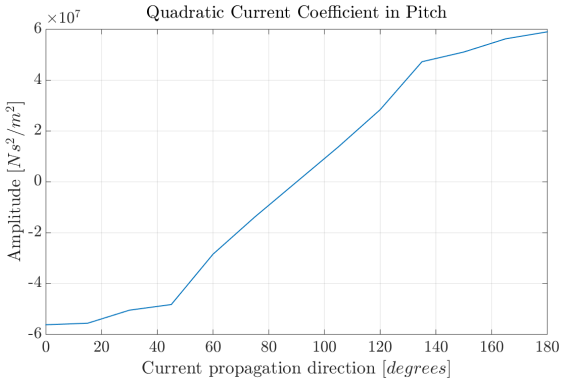

(d) Pitch

Figure A.1: Quadratic current coefficients in surge, sway, roll and pitch.

A.2 Quadratic Wind Coefficients

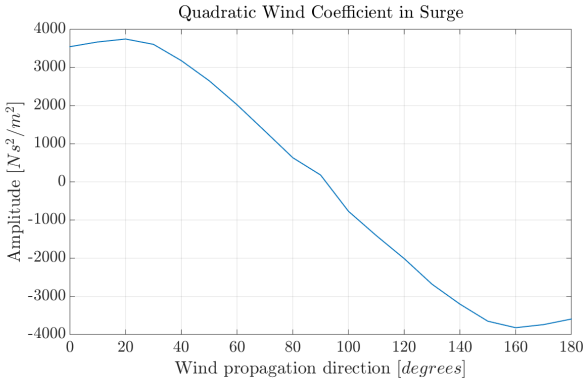

(a) Surge

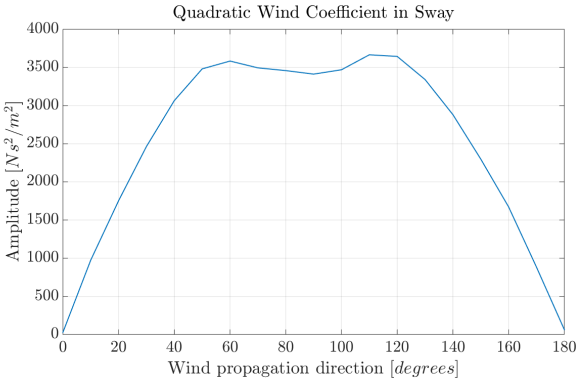

(b) Sway

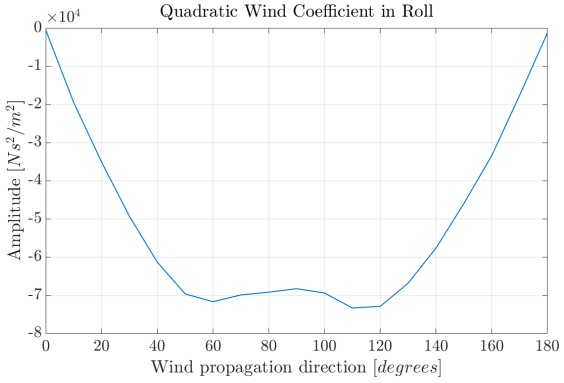

(c) Roll

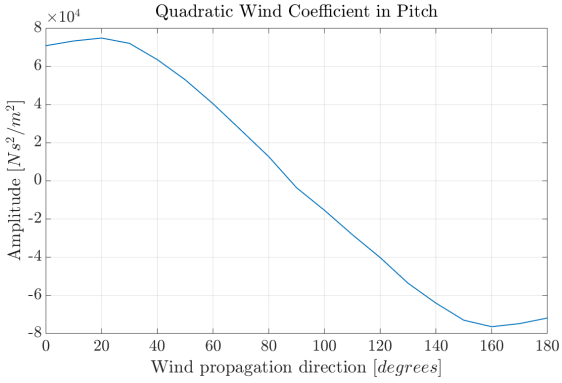

(d) Pitch

Figure A.2: Quadratic wind coefficients in surge, sway, roll and pitch.

A.3 Wave Drift Force Coefficients

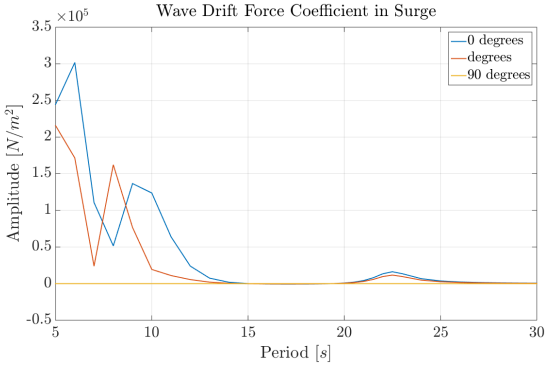

(a) Surge

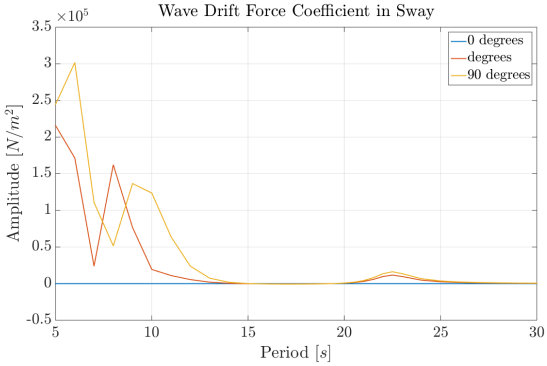

(b) Sway

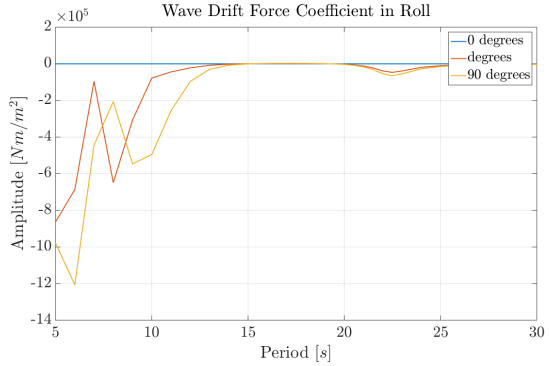

(c) Roll

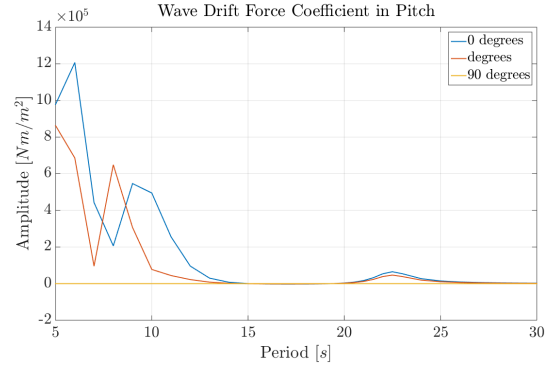

(d) Pitch

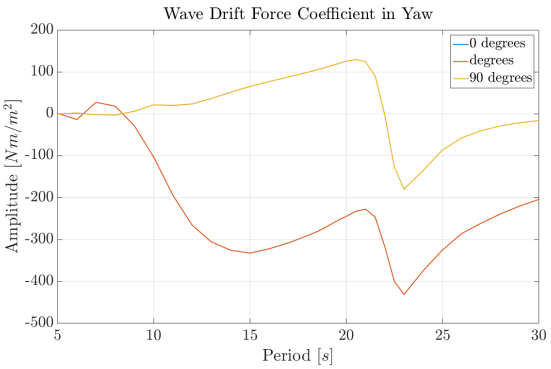

(e) Yaw

Figure A.3: Wave drift force coefficients in surge, sway, roll, pitch and yaw.

A.4 First Order Motion Transfer Functions

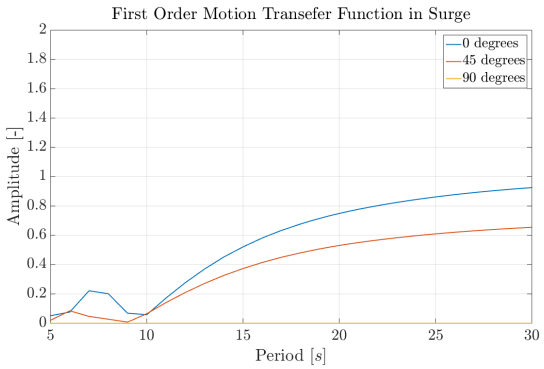

(a) Surge

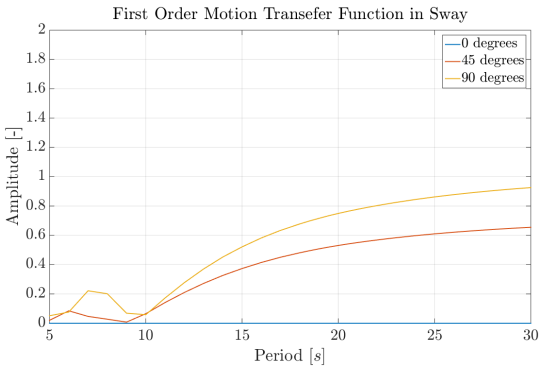

(b) Sway

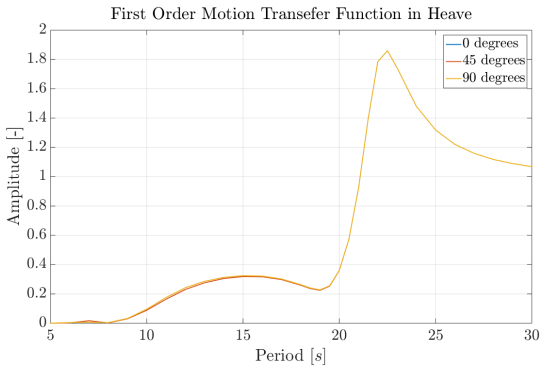

(c) Heave

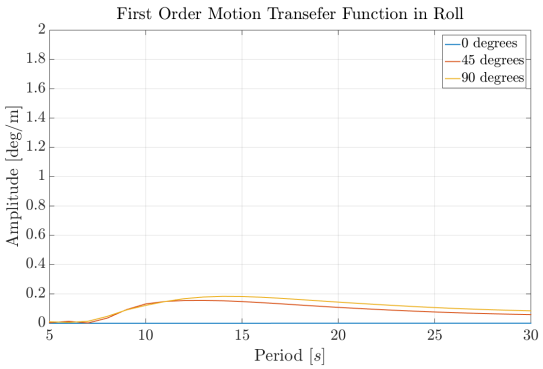

(d) Roll

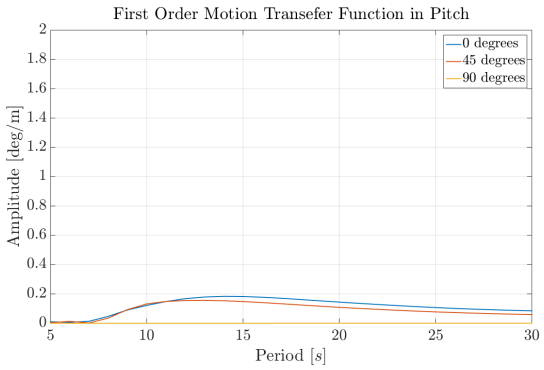

(e) Pitch

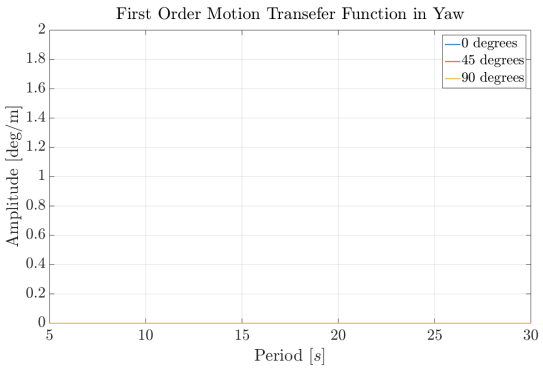

(f) Yaw

Figure A.4: First order motion transfer functions in surge, sway, heave, roll, pitch and yaw.

Appendix B

Optimization Results

B.1 Polyester Rope and Chain Mooring System

B.1.1 Sensitivity Study: Offset Constraint

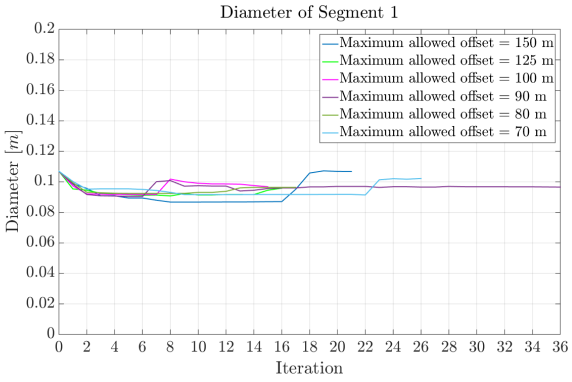

(a) Diameter of segment 1

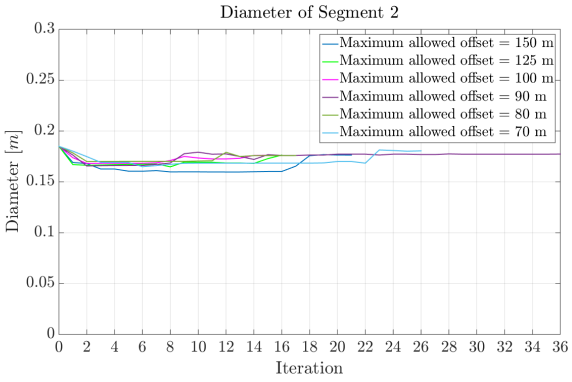

(b) Diameter of segment 2

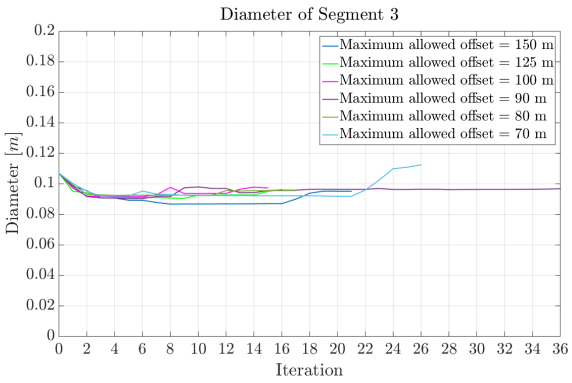

(c) Diameter of segment 3

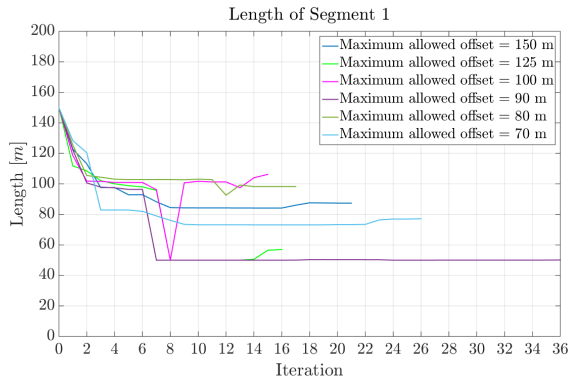

(d) Length of segment 1

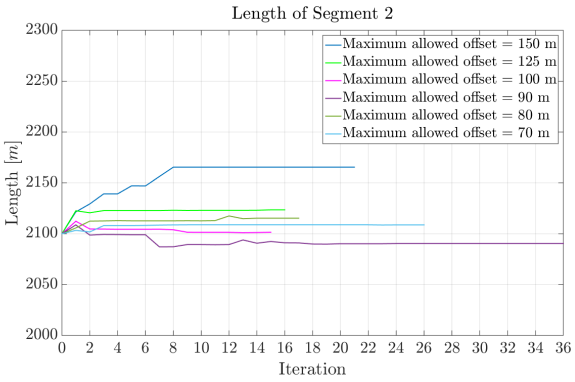

(e) Length of segment 2

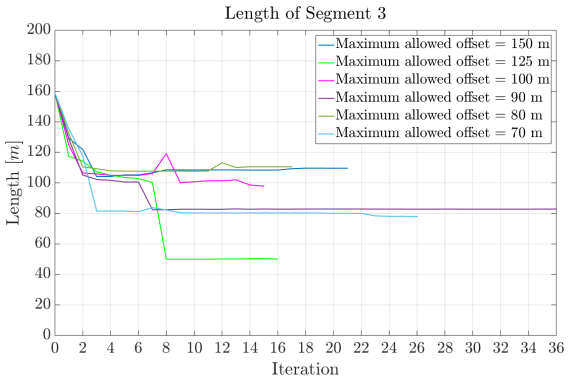

(f) Length of segment 3

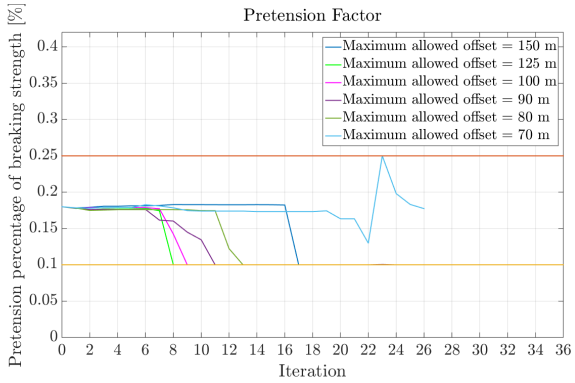

(g) Pretension factor

Figure B.1: Optimization variables.

B.1.2 Sensitivity Study: Global Minimum

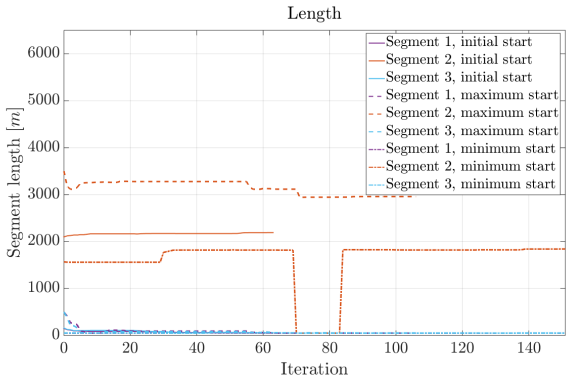

(a) Segment diameters

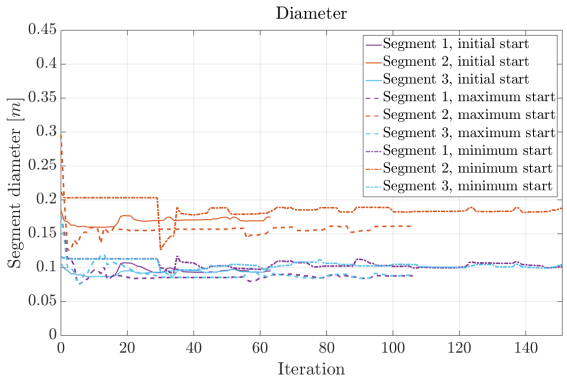

(b) Segment lengths

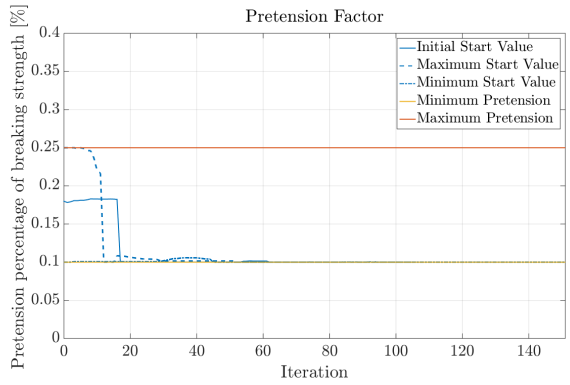

(c) Pretension factor

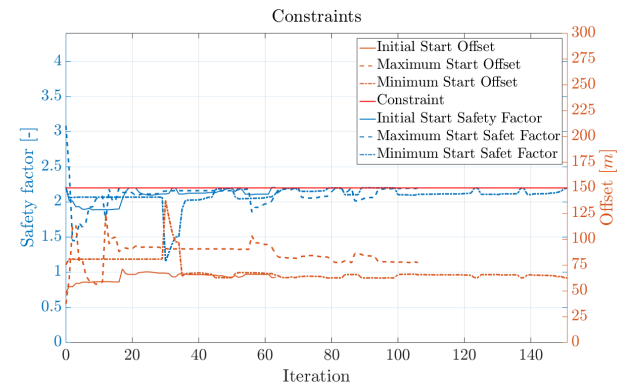

(d) Optimization constraints

Figure B.2: Optimization variables and constraints.

B.2 Steel Wire Rope and Chain Mooring System

B.2.1 Sensitivity Study: Global Minimum

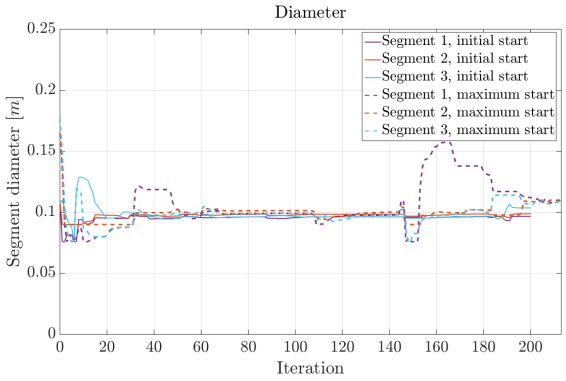

(a) Segment diameters

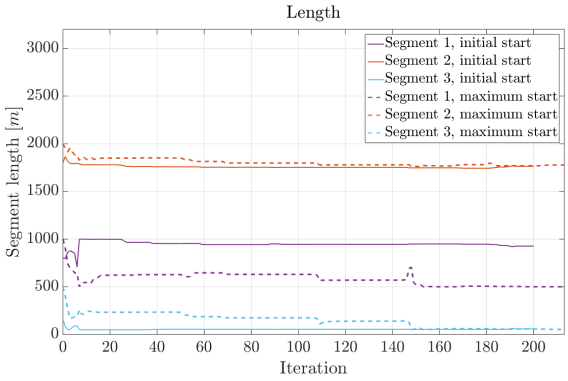

(b) Segment lengths

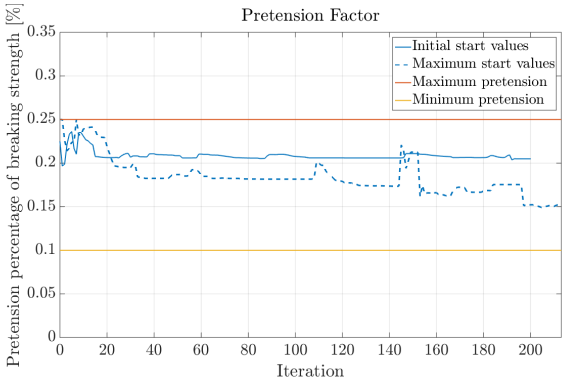

(c) Pretension factor

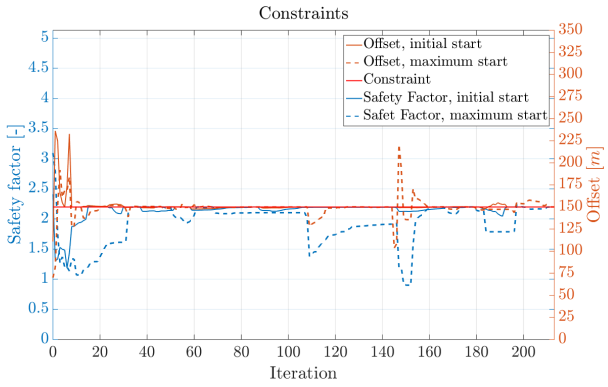

(d) Optimization constraints

Figure B.3: Optimization variables and constraints.